AD NUMBER

AD483640

LIMITATION CHANGES

TO:

Approved for public release; distribution is unlimited.

FROM:

Distribution authorized to U.S. Gov't. agencies and their contractors; Critical Technology; JUN 1966. Other requests shall be referred to Arnold Engineering Development Center, Arnold AFS, TN. This document contains export-controlled technical data.

AUTHORITY

AEDC ltr 23 Jan 1975

EVALUATION OF AN UNCOOLED ROCKET ENGINE OPERATING TECHNIQUE APPLICABLE TO THE EXPERIMENTAL STUDY OF MISSILE BASE HEATING

J. R. Parker and R. J. Christenson
ARO, Inc.

June 1966

ROCKET TEST FACILITY
ARNOLD ENGINEERING DEVELOPMENT CENTER
AIR FORCE SYSTEMS COMMAND
ARNOLD AIR FORCE STATION, TENNESSEE

NOTICES

When U. S. Government drawings specifications, or other data are used for any purpose other than a definitely related Government procurement operation, the Government thereby incurs no responsibility nor any obligation whatsoever, and the fact that the Government may have formulated, furnished, or in any way supplied the said drawings, specifications, or other data, is not to be regarded by implication or otherwise, or in any manner licensing the holder or any other person or corporation, or conveying any rights or permission to manufacture, use, or sell any patented invention that may in any way be related thereto.

Qualified users may obtain copies of this report from the Defense Documentation Center.

References to named commercial products in this report are not to be considered in any sense as an endorsement of the product by the United States Air Force or the Government.

EVALUATION OF AN UNCOOLED ROCKET ENGINE OPERATING TECHNIQUE APPLICABLE TO THE EXPERIMENTAL STUDY OF MISSILE BASE HEATING

J. R. Parker and R. J. Christenson
ARO, Inc.

FOREWORD

The work presented herein was sponsored by the Headquarters, Arnold Engineering Development Center (AEDC), Air Force Systems Command (AFSC), Arnold Air Force Station, Tennessee, under System 921A.

The results of the test were obtained by ARO, Inc. (a subsidiary of Sverdrup & Parcel and Associates, Inc.), contract operator of the AEDC under Contract AF40(600)-1200. The test was conducted in Propulsion Engine Test Cell (T-1) of the Rocket Test Facility (RTF) from November 29 to December 6, 1965, under ARO Project No. RA0417-A02, and the manuscript was submitted for publication on April 21, 1966.

This technical report has been reviewed and is approved.

John W. Hitchcock
Major, USAF
AF Representative, RTF
DCS/Test

Jean A. Jack
Colonel, USAF
DCS/Test

ABSTRACT

A description is given of an uncooled rocket engine operating technique applicable to the experimental study of missile base heating. The primary advantage offered by this technique over those in current use is that it retains the single combustion chamber, uncooled engine concept of the short-duration test technique while providing burn durations of sufficient time to permit use of conventional, steady-state instrumentation. This technique also eliminates the usually complex propellant and control systems associated with conventional liquid-cooled long-duration engines. Uncooled engine operating characteristics are reported for burn durations of 1.2 sec; extrapolation of these data indicate engine burn duration can be extended to 2.5 sec. Base heating data obtained with a 5.47-percent-scale Saturn I-Block II model utilizing the uncooled engine test technique are compared with data from a Saturn I-Block II model which utilized short- and long-duration test techniques.

CONTENTS

ILLUSTRATIONS

TABLES

APPENDIXES

SECTION I
INTRODUCTION

Many test programs have been conducted in ground test facilities to measure the heat flux and pressure on the base of model booster stages of rocket powered vehicles. Early test programs (Refs. 1 through 6) utilized small liquid rocket engines scaled as nearly as practical to the full-scale engines. Typical firing durations for these engines were on the order of 20 sec (long-duration). This burn time was sufficiently long to permit use of conventional steady-state instrumentation to measure and record temperature, heat flux, and pressures on the model base.

Base heating investigations have also been conducted in several ground test facilities utilizing a short-duration shock tube technique developed by the Cornell Aeronautical Laboratory, Inc. (CAL) (Refs. 7 through 9). With this technique, gaseous propellants are used, and steady-state engine operation is usually limited to under 50 msec (short-duration). However, this extremely short burn duration necessitates use of high-response, laboratory-type measuring equipment and complex setup, calibration, and data reduction procedures (Refs. 10 through 15).

During the early planning for a short-duration base heating test on the Saturn I-Block II and SIB booster at AEDC (Refs. 16 and 17), it was recognized that the state-of-the-art of model testing could be advanced if an uncooled engine which did not require the conventional liquid propellant and coolant systems could be designed to operate for burn durations up to 3 sec. This technique would allow use of conventional instrumentation, would retain the operating simplicity of the short-duration model, and would ensure that adequate time is allowed for adjustment toward equilibrium temperatures in separated flow regions on the model base (Ref. 18). The technique would also permit greater flexibility and accuracy in scaling missile base geometrical details such as external engine contours, engine cant angle, and engine gimbal angle.

To evaluate the uncooled engine testing technique, an uncooled combustor and nozzle assembly were designed and fabricated by personnel of the Rocket Test Facility (RTF). The model utilized the previous long- and short-duration Saturn I-Block II, 5.47-percent-scale model configurations to allow comparison of base heating data with previous short- and long-duration data obtained in the same ground test facility. In addition to the external model fairings, the propellant injector and flow measuring venturis and the special fast-action bipropellant valve

were furnished by the George C. Marshall Space Flight Center, NASA, Huntsville, Alabama.

In this report design considerations for the uncooled combustor and nozzles are discussed, and engine operating characteristics and base heating data obtained during five test firings of the uncooled engine model at simulated flight conditions of Mach number 1.63, 38,000-ft altitude are presented.

SECTION II
APPARATUS

2.1 TEST ARTICLE

The uncooled engine consisted of a single copper combustion chamber with an eight-nozzle cluster configuration as shown in Fig. 1a. Propellants were gaseous oxygen and ethylene. The combustor and nozzles were housed in existing 5.47-percent-scale Saturn SI-Block II fairings which included flow deflectors, air scoops, hold-down stubs, and aerodynamic fins (Fig. 1b). The model base heat and flame shields were of a sandwich-type construction, identical to those used with the long-duration test program reported in Ref. 3. The injector, the propellant flow measuring venturis, and the fast-action bipropellant valve were those used in the short-duration test program reported in Refs. 16 and 17.

The full-scale booster propellant pump turbine exhaust gases were simulated by hydrogen gas, which was discharged from exhausterators located circumferentially about each of the four outboard engines and from overboard ducts for each of the four inboard engines (Fig. 1b). The hydrogen was supplied from a common manifold having eight outlets; each outlet incorporated a 0.0025-in.-diam sonic orifice with a flow coefficient of 0.95. The hydrogen flow rate was set for 0.0094 lb_m/sec/eng which simulated the heat content of the full-scale turbine exhaust gases. Further details regarding turbine exhaust simulation using hydrogen gas can be found in Refs. 16 and 17.

Design and operating criteria for the uncooled engine model are compared with long- and short-duration models and the full-scale Saturn booster in Table I.

2.1.1 Design and Description of Nozzles

The uncooled nozzles were designed to operate for burn durations up to 3 sec and to duplicate as nearly as possible both the long- and short-duration nozzle configurations. External nozzle geometry aft of

the heat shield and internal nozzle geometry were duplicated, but it was necessary to make the uncooled nozzle throat section thicker to provide an adequate heat sink. Detailed drawings and photographs of an inboard and an outboard nozzle are presented in Fig. 2.

During initial nozzle design, several materials and combinations of materials were investigated for possible use. These included oxygen-free copper, tantalum-tungsten alloy, copper-beryllium alloy, and copper-zirconium alloy. Although each of these materials possesses certain advantages for use in this particular application, the tantalum-tungsten alloy was selected because of its high melting point and superior strength at elevated temperature. Table II shows thermophysical properties of the 90-percent tantalum, 10-percent tungsten (Ta 10W) alloy from which the nozzles were fabricated. Properties of the other materials investigated during the design were obtained from Refs. 19 and 20.

A bolted flange arrangement was used to attach the nozzles to the combustor. A gas-tight seal was provided by thin, chevron-type Inconel® rings (Figs. 2b and c) located between the nozzles and the combustor. These seals incorporated a spacer to prevent contact between the nozzles and the combustor.

The calculated maximum burn time of the uncooled engine model was based on the time required for the nozzle throat inner wall temperature to reach 75 percent of the TA 10W melting point. Heat transfer calculations used in the design of the nozzles are presented in Appendix I.

2.1.2 Design and Description of Combustor

The combustor design was established using the general configuration of the short-duration, single-chamber combustor (Ref. 17). A sectional view showing the chamber and integral nozzle feed tubes is presented in Fig. 3. Because the combustor was to be uncooled, it was necessary to select a material with high thermal diffusivity so that the chamber inner wall surface would not melt during burn times up to 3 sec. The maximum stagnation temperature in the chamber was estimated to be 6000°F at a chamber pressure of 500 psia based on a combustion efficiency of 95 percent for gaseous oxygen and ethylene (Fig. 4 and Appendix I). Figure 4 presents theoretical performance of O_2-C_2H_4 and LO_2-RP-1 propellants obtained by the method described in Ref. 21. Oxygen-free, high-conductivity (OFHC)® copper was selected as the most suitable material under these conditions. Table II presents thermophysical properties of OFHC copper. The combustor was cast in one piece, radiographically inspected for voids and cracks, and then machined. Photographs of the casting and the finished combustor are shown in Figs. 3b through d.

2.1.3 Design and Description of Propellant System

The uncooled engine gaseous ethylene-oxygen propellant system was designed to satisfy the following criteria:

Maximum chamber pressure rise time	100 msec
Steady-state operating time	5 sec
Ethylene flow rate	3.9 lb_m/sec
Oxygen flow rate	8.6 lb_m/sec

To achieve the desired short starting transient an "infinite volume" reservoir system was used in conjunction with a fast-acting dual-chambered automatic propellant valve (autovalve) capable of opening or closing in 15 msec. A schematic of the propellant system is shown in Fig. 5, and details of the autovalve are shown in Fig. 6. The autovalve consists of two mechanically linked, pneumatically operated piston valves housed in a single body, which was bolted to the combustor. The autovalve had externally mounted cartridge heaters to maintain gas temperature.

Propellant flow rates were controlled by sonic flow metering venturis (Fig. 7) located at the entrance to the autovalve. The venturis were designed by CAL in accordance with Ref. 22. The venturi throat diameters were 0.395 in. for the ethylene and 0.569 in. for the oxygen, and flow coefficients of both were assumed to be 0.99. Propellant flow rates were calculated by the methods given in Appendix II.

The injector (Fig. 8) introduced the gaseous propellants into the chamber in a simple direct-impinging spray pattern. Approximately 20 percent of the fuel flow was injected through film cooling orifices located in the combustor forward face (Fig. 3d) to prevent combustor wall overheating and erosion. Ignition was accomplished with a specially designed spark plug (Fig. 3a) located in the combustor wall.

The gaseous oxygen reservoir consisted of several high-pressure cylinders manifolded to give a capacity of 55,000 scf at 2500 psia. The oxygen was delivered from the reservoir to the model through a 3-in.-diam stainless steel line.

The gaseous ethylene reservoir consisted of a single 182-ft^3, high-pressure cylinder. A 3.5-ft^3 auxiliary tank was installed in series with the primary reservoir near the flow measuring venturi. The ethylene in this tank was pre-heated to 180°F by strip heaters on the tank to ensure that the ethylene remained in a gaseous state while flowing through the

venturi, autovalve, and injector. The auxiliary tank contained enough heated ethylene for one 5-sec run. The ethylene was forced from the top of the tank by the cooler gas which entered through a diffuser plate at the bottom.

2.2 INSTRUMENTATION

Instrumentation was provided to measure nozzle and combustor temperatures, propellant system pressures and temperatures, combustor pressure, and model base pressure and heat flux. A summary of the methods and accuracy of the measuring and recording systems is given in Table III.

2.2.1 Nozzle and Combustor Instrumentation

Outside wall temperatures of one inboard and one outboard nozzle were measured with six surface-attached Chromel®-Alumel® (CA) thermocouples. Locations of these thermocouples are given in Fig. 9.

Combustor temperatures were measured with three CA thermocouples attached to the outside wall and one CA thermocouple recessed in the chamber wall to a depth approximately 0.19 in. from the inner wall. Locations of these thermocouples and details of the thermocouple plug are presented in Fig. 10. Combustor chamber pressure was measured with a strain-gage transducer connected with approximately 2 ft of 0.130-in.-ID line to a pressure tap located in the downstream end of the chamber, as shown in Fig. 10.

2.2.2 Propellant System Instrumentation

Propellant system instrumentation (Fig. 5) consisted of pressure and temperature measurements necessary to set engine operating conditions and provide data for calculation of propellant flow rates. Oxygen and ethylene reservoir pressures were sensed with strain-gage transducers. Propellant line pressures were sensed just upstream of the flow measuring venturis also with strain-gage transducers. Venturi throat pressures and injector pressures were sensed with quartz crystal piezoelectric transducers. Propellant gas temperatures were measured with two sonic, aspirated CA thermocouples, one installed in the oxygen line and the other in the ethylene auxiliary tank. Ethylene temperature was also measured just upstream of the flow measuring venturi with an iron-constantan (IC) thermocouple probe immersed in the gas stream.

2.2.3 Model Base and Flame Shield Instrumentation

Model base and flame shield instrumentation consisted of slug mass calorimeters, commercial membrane-type heat gages, and thin-film dual-element heat gages for measurement of heat flux. This combination of instruments encompassed the types used in the previous long- and short-duration base heating tests. Details of heat gage construction are shown in Fig. 11, and data reduction and other related information are given in Appendix III. Location of instrumentation on the base and flame shield is shown in Fig. 12.

Model base pressures were sensed with strain-gage transducers connected to the pressure orifices on the base heat shield (Fig. 12) with approximately 15 ft of 0.1275-in. -ID tubing.

2.3.4 Tunnel Instrumentation

Tunnel aerodynamic instrumentation consisted of static pressure taps located at various axial stations throughout the plenum, test section, and diffuser. These pressures were sensed with close-coupled strain-gage transducers; selected pressures were also connected to manometers in the control room to monitor pre-fire steady-state tunnel conditions.

Permanent visual records of the firings were provided by two 16-mm high-speed motion-picture cameras mounted at test section camera ports in the exit plane of the nozzles.

2.3 INSTALLATION

Testing was conducted in Propulsion Engine Test Cell (T-1) which is an open-circuit wind tunnel (Ref. 23) equipped with an axisymmetric, supersonic nozzle having a centerbody contoured to conform to the stream surface in the flow field necessary to obtain Mach number 1.63 (Ref. 24). The model and centerbody were cantilever-mounted from a spider arrangement in the plenum chamber (Fig. 13) and extended aft through the nozzle into a 36-in. -diam by 28-in. -long test section. Tunnel airflow and engine exhaust gases discharged into a conical inlet, 72-in. -diam, 50-ft-long, straight cylindrical diffuser (Ref. 24) and were ducted to the facility rotating exhaust machines. Instrumentation leads, propellant system lines, valves, control leads, turbine exhaust lines, etc., are contained in the centerbody. The lines and leads terminate in the inlet plenum, where they pass out of the test cell through a sealed porthole and are connected to the permanent facility system.

SECTION III
PROCEDURE

Prior to each test period, high-pressure pumps were used to charge the propellant reservoirs to the pressure necessary to give the desired propellant flow rates according to Appendix II. The ethylene auxiliary tank and line heaters were then turned on, and the ethylene temperature was allowed to stabilize at 180°F (250°F for Run No. 1). A calibration of all instrumentation systems was obtained with the test cell at sea-level pressure and again at 2.0 psia. After calibrations were complete, tunnel flow was established.

The tunnel test section static pressure was set to correspond to the desired simulated altitude. Inlet total pressure was set to give a pressure ratio corresponding to Mach number 1.63. Inlet air temperature was maintained at 150°F.

After tunnel flow had stabilized, the firing was initiated by a sequencer which automatically controlled the firing events as shown below:

t-5 sec	Instrumentation started manually
t-0 sec	Automatic sequencer initiated and high-speed cameras started
t+2 sec	Signal sent to autovalve to open
t+2.1 sec	Autovalve open and common time signal triggered on all recorders
t+2.4 sec	Turbine exhaust flow initiated
t+3.0 sec	Primary close signal sent to autovalve and to turbine exhaust valve, argon purge initiated
t+3.15 sec	Secondary close signal sent to autovalve
t+13.0 sec	Close signal sent to argon purge valve

The combustor and nozzles were cooled for 10 sec after each firing with an argon purge, which was introduced into the oxygen line just upstream of the injector. The argon flow rate was approximately 8 lb_m/sec Nitrogen was not used for purging because of its incompatibility with hot tantalum.

SECTION IV
RESULTS AND DISCUSSION

The uncooled engine model test technique was evaluated in five firings. The first two firings were conducted primarily for systems checkout and were limited to 0.5- and 1.0-sec burn duration. Base heating data were obtained with and without turbine exhaust simulation during the third, fourth, and fifth firings. The third and fourth firings were of 1.0 sec duration; the fifth was timed for 1.5 sec, but an ignition malfunction resulted in an actual burn time of only 1.2 sec. Although the uncooled engine model test program was planned to extend systematically the engine burn duration from 0.5 to 3.0 sec, testing was terminated after the 1.2 sec firing because of test cell scheduling considerations for a higher priority program.

The following discussion presents combustor and propellant system operating characteristics, combustor and nozzle temperatures, model base and flame shield heat flux measurements, base pressures, and a comparison of uncooled engine model heat flux and base pressure data with previous long- and short-duration data. Typical test cell operating pressures for short- and long-duration tests are compared to those obtained with the uncooled engine technique in Fig. 14. The good agreement shown in test section pressure ratio indicates that all three techniques were tested at essentially the same simulated flight conditions.

4.1 COMBUSTOR AND PROPELLANT SYSTEM OPERATING CHARACTERISTICS

A summary of propellant system operating pressures, temperatures, flow rates, and other pertinent data from the uncooled engine tests are presented in Table IV. A typical combustor pressure history for a 1.0-sec firing is shown in Fig. 15a. Ignition system malfunctions occurred on the first and fifth firings and resulted in a delayed ignition which caused a combustor overpressure during the starting transient (Fig. 15b). The overpressure did not damage the combustor or nozzles.

By using an "infinite-volume" propellant reservoir system and a fast-acting propellant valve, it was anticipated that the uncooled engine starting transient would be on the order of 0.1 sec. The advantages derived from a rapid starting transient are: (1) heat flux to the base approaches a step input, and (2) shorter engine burn times can be used to obtain the desired period of steady-state engine operation.

The recorded chamber pressure (Fig. 15) and propellant line pressure histories (Fig. 16) indicate that, after the autovalve opened, wave

reflections in the propellant system were not completely damped until about 0.6 sec. However, after the first 0.2 sec of burn time the magnitude of the pressure oscillations were less than 5 percent of the propellant line pressure; hence, engine operation after 0.2 sec is considered steady state and is therefore useful for obtaining base heating data.

The short starting transient obtained with the uncooled engine is a significant improvement over the long-duration model which required about 1.5 sec to reach steady-state operation, as shown in Fig. 17. In addition, the inherent problem of triethylaluminum contamination of the model base instrumentation during ignition of the long-duration LO_2-RP-1 engine is alleviated on the uncooled engine model because the gaseous propellants are spark ignited.

During the pre-test procedures for the second test, the ethylene contained in the heated portion of the fuel line (from the top of the auxiliary tank to the autovalve) underwent a decomposition-polymerization reaction which filled a portion of the line with a solid polyethylene-type polymer, as shown in Fig. 18. The exact cause of this reaction was not completely ascertained, but it is surmised that it could have been triggered when cold ethylene gas, probably containing some liquid, was bled into the hot auxiliary tank during the initial propellant system pressurization. Up until this incident, the auxiliary tank and fuel lines were preheated to 250°F; however, because of the uncertainty as to the cause of the reaction, the pre-heat temperature was lowered to 180°F for the remaining tests. No further incidents were encountered.

4.2 COMBUSTOR TEMPERATURES

Combustor temperatures measured with surface-attached thermocouples located at an inboard and outboard combustor-nozzle interface are presented in Fig. 19. The calculated temperature for an inboard interface is also shown for comparison. The calculated temperature was obtained using a computer program for a two-dimensional heat conduction network.

The measured interface temperatures indicate that heating was more severe near the center of the chamber on the combustor center section than in the thicker surrounding section. A variation in temperatures was noted between firings; these differences are discussed in Section 4.3.

Extrapolation of the inboard interface temperature data obtained during the run (No. 5) in which the highest temperatures were recorded

indicates that the melting point of copper would be reached in about 2.8 sec. The highest temperature would probably occur at the aft face of the combustor center section; hence, the copper would have presumably melted in this region before 2.8 sec. In fact, melting and erosion did occur at the rear of the center section (Fig. 20) although the inboard thermocouple indicated less than 1000°F during the longest (1.2 sec) run that was made. Melting of the center section began at approximately 0.5 sec as evidenced by the characteristic green coloration of copper in the exhaust plumes seen in motion pictures of the firings. Modification of the rear face of the center section by addition of a conical section or by flame spraying with a ceramic coating would probably alleviate this problem.

Combustor temperatures measured with a plug thermocouple embedded in the combustor wall to a depth approximately 0.19 in. from the chamber inner wall and with a surface-attached thermocouple at the same approximate location are shown in Fig. 21. The test data represent the average for the five runs since the maximum deviation was less than 17°F. The maximum temperature measured near the inner wall was 210°F. Extrapolation of these temperature data to the 2.5 sec burn time limitation indicates that inner wall temperature should not exceed 450°F.

4.3 NOZZLE TEMPERATURES

Temperature measured with a surface-attached thermocouple located on the outer wall of an outboard nozzle in the plane of the throat is presented in Fig. 22. A corresponding measurement on an inboard nozzle was not obtained because of a faulty thermocouple. These test data represent the average temperature for the five runs since the maximum deviation was less than 20°F. The measured temperatures show good agreement with the calculated temperatures which were obtained using one-dimensional, transient heat conduction theory described in Appendix I.

A calculated temperature curve for the nozzle throat inner wall is also presented in Fig. 22 for reference, although no measurement was made at this location. This curve shows that approximately 80 percent of the inner wall throat temperature rise expected for a 2.5-sec burn duration is attained within the first second of engine operation. Since the nozzle throats did not show any signs of deterioration for run durations up to 1.2 sec, it is presumed that throat overheating would not occur if burn duration was extended to 2.5 sec.

Surface temperatures measured on an outboard and an inboard nozzle skirt are shown in Fig. 23. Data were obtained on the inboard nozzle skirt section during only the second and third firings because of thermocouple malfunction on other firings. The indicated temperatures were much higher than those previously shown for the throat primarily because of the thinner wall thickness at the skirt station. The indicated skirt temperatures were higher than predicted by the one-dimensional theory (Fig. 23). This is attributed to the fact that conduction heat transfer from the hotter throat station to the nozzle skirt is not accounted for in the theoretical calculation. Temperatures on an inboard nozzle skirt were not obtained for the run (No. 5) in which the highest temperatures were recorded; for this run outboard skirt temperatures were estimated by determining the percent increase in temperature of the outboard nozzle between runs 2 and 5 and applying this factor to the indicated temperature of the inboard nozzle for run 2. This procedure was validated by a similar correlation between runs 2 and 3, during which data were available for both nozzles. The results of this procedure indicate that the inboard and outboard nozzles are both capable of operation for burn durations up to 2.5 sec.

A large variation in skirt temperatures between individual firings is shown in Fig. 23. A similar variation was also evident in the combustor temperatures shown in Fig. 19. Examination of the engine operating parameters presented in Table IV, however, does not indicate any significant trends in engine performance between individual firings, which correlate with the trend (with run number) in model temperatures. One explanation for the variation in temperatures might be that in reducing the ethylene pre-heat temperature from 250 to 180°F, liquefaction of the ethylene occurred during the run thereby lowering the combustion efficiency and combustion temperature. However, if this occurred the effect of changes in ethylene flow rate and combustion efficiency would have had to compensate since there was no significant change in chamber pressure. It is also possible that the "hard starts" on the first and fifth runs had an effect on the model temperatures since these two runs produced the highest temperatures.

Nozzle surface temperatures measured at an inboard and outboard combustor interface during the first run are shown in Fig. 24. Data were not obtained on the subsequent four runs because of faulty thermocouples. During design of the nozzle-to-chamber attachment, it was thought that the nozzle interface might become hot enough to cause failure of the Inconel seal and/or possibly cause local melting of the copper combustor interface. However, extrapolation of the nozzle flange temperature data and the combustor temperatures previously shown in Fig. 19 indicates that the burn time can be extended to about 2.5 sec before the hotter inboard interface temperatures approach the melting

point of copper. Furthermore, the extrapolations indicate that the temperatures at 2.5 sec would not be high enough to damage the Inconel seals, which can withstand 1800°F for durations up to 3 min. It should be pointed out, however, that considerable difficulty was encountered in obtaining a leak-tight joint with the Inconel seals. Success in using seals of this type is dependent on having scratch-free, fine surface finishes on both mating surfaces and maintaining a very close tolerance on seal compressive force.

4.4 BASE HEATING

Heat flux to the base heat shield was measured with three types of heat gages. The first type consisted of in-house fabricated slug mass calorimeters, which duplicated those used in the previous long-duration model tests. The second type consisted of commercial, membrane-type heat gages. This type gage had not been used previously in Saturn model tests; however, similar gages have been used with good results in other base heating tests such as reported in Ref. 26. The third type consisted of dual-element thin-film heat gages developed by CAL and used exclusively in all previous short-duration tests.

In the following discussion, typical heat flux measurements obtained with each of the three types of gages are presented, followed by a comparison of uncooled engine base heat flux with short- and long-duration data from Ref. 17.

4.4.1 Slug Mass Calorimeters

Temperature and heat flux histories for a typical slug mass calorimeter are presented in Fig. 25. Heat flux was computed by the method described in Appendix III. For run 3, an average value of total heat flux without turbine exhaust simulation was obtained by arithmetically averaging the data between ignition and shutdown. A corresponding value for run 4 was obtained by averaging the first 0.4 sec of the run. The total heat flux with turbine exhaust simulation was obtained by averaging the data from run 4 between 0.4 sec and shutdown. Base heating data are not reported for run 5 because of the abnormal engine starting transient and inconsistent engine operating temperatures compared with runs 3 and 4.

4.4.2 Membrane-Type Heat Gages

Typical heat flux measurements obtained with the commercial, membrane-type heat gages are presented in Fig. 26. For both runs 3

and 4, data from each of the gages reached a stable level then increased beginning between 0.4 and 0.5 sec. This increase was expected for run 3 since hydrogen, which was initiated at 0.4 sec, could have burned in the base. For normal operation without hydrogen (run 4) however, the rise in heat flux was unexpected. It is believed that this increase in total heat flux was caused by an increase in radiation heating from the vaporized copper present in the inboard engine exhaust plumes (as indicated visually). This supposition is reinforced by the fact that the gages closest to the inboard engines (N8 and N10) showed a larger increase than the outer gage (N13).

4.4.3 Dual-Element Thin-Film Heat Gages

The thin-film heat gages were designed to be used for heating durations of only 0.050 sec; hence a calculation was made to determine the time required for the rear face (radiation gage) temperature to begin increasing due to conduction through the substrate. This calculation indicated that conduction began in about 0.10 sec. Therefore, data obtained after this time with the thin-film gages are invalid for quantitative purposes.

However, the thin-film gages were very effective in showing the qualitative effect of turbine exhaust discharge on base heating. This can be seen in Fig. 27 by comparing convective and total heat flux for run 4, which does not have hydrogen discharge, with run 3, which does. A definite increase in heating occurred immediately upon initiation of hydrogen, indicating recirculation and burning of turbine exhaust gas in the base cavity.

4.4.4 Base Heating Comparison

A comparison of uncooled engine model base heating data with short- and long-duration data (Ref. 17) is presented in Fig. 28. Total heat flux is presented as a function of heat gage azimuth location about the model centerline. The base was divided into an inner and outer region mainly for the sake of clarity of data presentation but also because previous model and flight test data have indicated different levels of heating in these two regions.

For the uncooled engine model, heat flux data from all three types of heat gages are included in the comparison. The slug mass calorimeter heat flux data were obtained by the averaging method given in Section 4.4.1. The membrane-type gage heat flux data were obtained at a burn time of 0.4 sec for the comparison without turbine exhaust simulation; the average difference in heat flux level between runs 3 and 4

was attributed to hydrogen burning and hence was added to the level obtained at 0.4 sec to obtain data for the comparison with turbine exhaust simulation. Thin-film gage heat flux data were obtained at 0.125 sec and are presented only for the comparison without turbine exhaust simulation because of the gage limitation explained in Section 4.4.3.

For the condition of no turbine exhaust simulation (Fig. 28a), the uncooled engine heat flux data were slightly lower than the short- and long-duration data but indicated the same circumferential trend and were generally in good agreement.

The comparison of heat flux data with turbine exhaust simulation is presented in Fig. 28b. Both the uncooled engine heat flux and the long-duration heat flux increased when hydrogen flow was initiated because of recirculation and burning in the base; however, no significant increase was apparent in the short-duration data. Part of the increase in the uncooled engine model heat flux is attributed to the radiation heating from the vaporized copper discharged from the inboard engines. In general, however, valid base heating data can be obtained, and the effect of recirculated turbine exhaust gases can be evaluated using the uncooled engine test technique.

4.5 FLAME SHIELD HEATING

The flame shield on the Saturn vehicle is the plate located between the four inboard engines at the nozzle exit plane. The purpose of the flame shield is to prevent recirculation of hot exhaust gases from the inboard engine cluster into the base region. Uncooled engine model flame shield heat flux data from four slug mass calorimeters with design and location identical to calorimeters used in the long-duration tests are presented in Fig. 29. A comparison of uncooled engine heat flux data with long- and short-duration data are presented in Fig. 30. The short-duration data were obtained with a thin-film heat gage. The trend of the uncooled engine model data is similar to that of the long-duration data, but the magnitude of measured heat flux was nominally 45 percent higher than the long-duration heat flux at the center of the flame shield. This variation is attributed to the higher exhaust gas temperature obtained with the more efficient gaseous engine of the uncooled model. Table I shows that the uncooled engine exhaust gases are about 110 percent hotter than the long-duration LO_2-RP-1 model engine exhaust gases. For the single calorimeter location where data were available from all three testing techniques, the heat flux measurements of the uncooled engine model were 5 and 22 percent higher than long- and short-duration data, respectively.

4.6 BASE PRESSURE

Both the uncooled engine and long-duration models had seven pressure taps located at identical positions on the base heat shield. The short-duration model had sixteen taps located throughout the base; however, the locations did not duplicate those of the other models. Since no trend in pressure could be detected during any individual run, a single base pressure level was obtained for each model by arithmetically averaging the available measurements.

A comparison of uncooled engine model base pressure data with short- and long-duration data is presented in Fig. 31. Excellent agreement is indicated between uncooled engine and short-duration data at the Mach number 1.63, 38,000-ft trajectory condition. On the other hand, the long-duration base pressure data were significantly higher than the short-duration and uncooled engine data although test conditions were identical. This disagreement is presumably due to differences between the single chamber, multiple-nozzle gaseous propellant engine used for the short-duration and uncooled engine models and the LO_2-RP-1, multi-engine, long-duration model. The differences which are probably most significant are: (1) the uncooled engine model and short-duration model inboard engines are canted outward 3 deg from the model centerline, whereas the long-duration inboard engines were not canted, (2) different isentropic exponents of the combustion products, (3) different engine efficiencies, and (4) different nozzle wall temperature. Of these four differences, the inconsistency in geometrical detail is probably more important since it changes the vent area between adjacent inboard engine exhaust plumes and hence the quantity of gas rejected onto the base cavity. It also changes the impingement characteristics of the inboard and outboard engines which in turn probably influence the mixing phenomena between the outboard engine exhaust plumes and the surrounding airflow.

A comparison of intermediate-duration model flame shield pressure data with short- and long-duration data is presented in Fig. 31b. The pressure taps from which these data were obtained were identically located on each model. Essentially the same results were obtained for the flame shield pressure ratio as was shown for the base pressure; namely, that good agreement was obtained between uncooled engine and short-duration model data, and poor agreement between these data and long-duration data. The same possible reasons for disagreement in data will apply here as was previously discussed for the base pressures.

4.7 APPLICATION OF THE UNCOOLED ENGINE MODEL TECHNIQUE TO SUBSONIC TESTING

The uncooled engine model provides a distinct advantage over the short-duration technique for tests which must simulate subsonic flight conditions. Attempts to obtain base heating data with the short-duration model at Mach number 0.8 in Test Cell T-1 of the RTF have been unsuccessful because the engine burn time was shorter than the time required for tunnel airflow to stabilize after engine ignition. Tunnel pressure data obtained during these tests indicate that about 1.6 sec is required for tunnel flow to stabilize after engine ignition; hence, with a nominal burn time of 2.5 sec for the uncooled engine, there remains 0.9 sec of burn time at stabilized engine and tunnel conditions in which valid base heating data can be obtained at subsonic conditions.

SECTION V
SUMMARY OF RESULTS

A description of an uncooled engine model testing technique applicable to the experimental study of missile base heating is presented. The technique utilizes an uncooled, single combustor, multi-nozzle engine which burns gaseous oxygen and ethylene propellants. An evaluation was conducted to determine engine operating characteristics and obtain base heating data for comparison with short- and long-duration 5.47-percent-scale Saturn I-Block II model testing techniques. The significant results of the evaluation are summarized as follows:

1. Five successful firings of the uncooled engine were obtained. Burn durations ranged from 0.5 to 1.2 sec for a cumulative operating time of 4.7 sec.
2. Engine operating temperatures were within design specifications except at one location in the combustor. With a minor modification to correct this problem, engine burn duration can probably be extended to 2.5 sec based on extrapolation of indicated combustor and nozzle temperatures.
3. Base heating data comparable with that from the short- and long-duration model testing techniques were obtained with the uncooled engine model testing technique.
4. Base heating data obtained in these tests indicate that the effects of turbine exhaust gas discharge (recirculation and burning in the base region) can be evaluated with the uncooled engine technique. Moreover, this technique permits a choice of two methods for initiating turbine exhaust gas discharge: one is to

initiate flow prior to or simultaneously with engine ignition, as with the short-duration technique; the other is to initiate flow after engine operation has stabilized, as with the long-duration technique.

5. Features of the uncooled engine technique which make it attractive for base heating investigations are: (1) the model is simple to fabricate and operate, (2) details of the missile base under study can be easily and accurately scaled, (3) conventional steady-state instrumentation can be used to obtain base heat flux and pressure data, and (4) the technique can be used to obtain base heating data at simulated subsonic flight conditions as well as at supersonic conditions.

REFERENCES

1. Parker, Joseph R., Jr. and Gillard, T. J. "An Investigation of Base Heating with a 5.47-percent Saturn SA-1 Booster Model at Mach Number 0.8 and 1.15." AEDC-TN-61-134 (AD226234), November 1961.

2. Dawson, John G., Jr. "An Investigation of Base Heating on a 5.47-percent Scale Model Saturn SA-1 Booster Afterbody at Mach Numbers 1.63 and 3.07." AEDC-TDR-62-9 (AD270501), January 1962.

3. Parker, Joseph R., Jr. "An Investigation of Base Heating on a 5.47-percent Scale Model Saturn SA-5 Booster Afterbody at Mach Numbers 0.8 and 1.2 and Typical Trajectory Altitudes." AEDC-TDR-62-62 (AD274714), April 1962.

4. Gillard, T. J. "A Ground Test Facility for Evaluating Missile Base Flow Phenomena at Simulated Trajectory Conditions." AEDC-TDR-64-264 (AD453981), January 1965.

5. Kennedy, T. L. and Lowry, J. F. "An Investigation of Base Heating on a 5.47-percent Scale Model of the Saturn S-1 Booster at Transonic Mach Numbers." AEDC-TN-61-106 (AD262743), August 1961.

6. Beheim, Milton A., and Obery, Leonard J. "Wind Tunnel Studies of Booster Base Heating." Aeronautics and Aerospace Engineering, February 1963.

7. Bird, K. D., Matthis, C. L., and Reece, J. W. "The Application of Short-Duration Techniques to the Experimental Study of Base Heating." Cornell Aeronautical Laboratory, Inc., Report No. HM-1510-Y-1(I), April 1962.

8. Matthis, C., Muench, R., and Richard, W. "The Design and Development of a Short-Duration Constant Pressure Combustor for Use in Rocket Base Heating Investigations." Cornell Aeronautical Laboratory, Inc., Report No. HM-1510-Y-2, December 1962.

9. Sargeant, R. J. "The Application of Short-Duration Techniques to the Experimental Study of Base Heating." CAL Report No. HM-1510-Y-1(II), April 1965.

10. Bogdan, Leonard. "High-Temperature, Thin-Film, Resistance Thermometers for Heat Transfer Measurement." Cornell Aeronautical Laboratory, Inc., Report No. HM-1510-Y-5, February 1963.

11. Martin, James F., Duryea, George R., and Stevenson, Leroy M. "Instrumentation for Force and Pressure Measurements in a Hypersonic Shock Tunnel." Cornell Aeronautical Laboratory, Inc., Report No. 113, January 1962.

12. Vidal, Robert J. "Transient Surface Temperature Measurements." Cornell Aeronautical Laboratory, Inc., Report No. CAL-114, March 1962.

13. Bogdan, Leonard. "Measurement of Radiative Heat Transfer with Thin-Film Resistance Thermometer." Cornell Aeronautical Laboratory, Inc., Report No. HM-1510-Y-9, July 1963.

14. Vidal, R. J. "Model Instrumentation Techniques for Heat Transfer and Force Measurements in a Hypersonic Shock Tunnel." Cornell Aeronautical Laboratory, Inc., Report No. AD-917-A-1, February 1956.

15. Reiner, A. M. "Reduction of Thin-Film Resistance Thermometer Temperature Histories to Heating Rates." Chrysler Corporation Space Division, Report No. TN-AE-64-48, December 1964.

16. Hutcheson, Lex. "Base Heating on a 5.47-percent Scale Model Saturn 1B Booster Afterbody at Mach Number 1.18 and 1.63 at Trajectory Altitudes." AEDC-TR-66-46 (AD479640), March 1966.

17. Dawson, John G., Jr. "Evaluation of Short Duration Rocket Engine Technique for Base Heating Simulation with External Air Flow." AEDC-TR-66-103, June 1966.

18. Ibrig, H. K., Jr. and Korst, H. H. "Quasi-Steady Aspects of the Adjustment of Separated Flow Regions in Transient External Flows." AIAA Journal, Vol. 1, No. 4, April 1966, pp. 934.

19. Touloukian, Y. S., Editor. "Retrieval Guide to Thermophysical Properties Research Center Literature." Vols. I, II, and III. Thermophysical Properties Research Center, Purdue University, McGraw-Hill Book Company, 1960.

20. Lewis, Henry F. and Horn, Dennis D. "Some Considerations in the Design of Water-Cooled Nozzle Throat Sections for High-Temperature, High-Pressure Operation." AEDC-TDR-64-51 (AD437973), April 1964.

21. Zeleznik, Frank J. and Gordon, Sanford. "A General IBM 704 or 7090 Computer Program for Computation of Chemical Equilibrium Composition, Rocket Performance and Chapman Jouquet Detonations." NASA TN-D-1454, Lewis Research Center, Cleveland, Ohio, October 1962.

22. Smith, Robert E., Jr. and Matz, Roy J. "Verification of a Theoretical Method of Determining Discharge Coefficients for Venturis Operating at Critical Flow Conditions." AEDC-TR-61-8 (AD263714), September 1961.

23. Test Facilities Handbook (5th Edition). "Rocket Test Facility, Vol. 2." Arnold Engineering Development Center, July 1963.

24. Peters, C. E. "Annular Nozzles for Missile Base Flow Testing." AEDC-TN-60-62 (AD236195), April 1960.

25. Peters, C. E. and Wehofer, S. "A General Investigation of Two-Stream Supersonic Diffusers." AEDC-TDR-62-22 (AD273289), January 1962.

26. Dawson, John G., Jr., et al. "Base Recirculation on a 10.7-percent-Scale Model of the Thorad Afterbody at Trajectory Mach Numbers of 0.33 to 3.05." AEDC-TDR-63-136, August 1963.

27. Schneider, P. J. Temperature Response Charts. John Wiley and Sons, Inc., New York, 1963.

28. McAdams, William, H. Heat Transmission. Third Edition. McGraw-Hill Book Company, Inc., New York, 1942.

29. Huff, Vearl N., and Fortini, Anthony. "Theoretical Performance of JP-4 Fuel and Liquid Oxygen as a Rocket Propellant I - Frozen Composition." Lewis Flight Propulsion Laboratory, NACA RM E56A27, April 1956.

30. Tempelmeyer, K. E. and Sheraden, G. H. "Compressible Flow Tables for Gases with Specific Heat Ratios from 1.10 to 1.28." AEDC-TN-58-9 (AD152041), March 1958.

31. Wehofer, S. "Rocket Heat Transfer Measuring Devices and Techniques." AEDC-TDR-63-93 (AD411799), July 1963.

32. Davis, G. L. "Calibration of Thin-Film Resistance Thermometers for Absorptivity Coefficient." Chrysler Corporation Space Division, Report No. TN-AE-65-113, December 1965.

33. Torti, M. C. "Physical Properties and Fabrication Techniques for the Tantalum-10% Tungsten Alloy." National Research Corporation, Newton, Massachusetts.

34. Materials Data Book - Copper Alloys. ARO, Inc., Arnold Engineering Development Center.

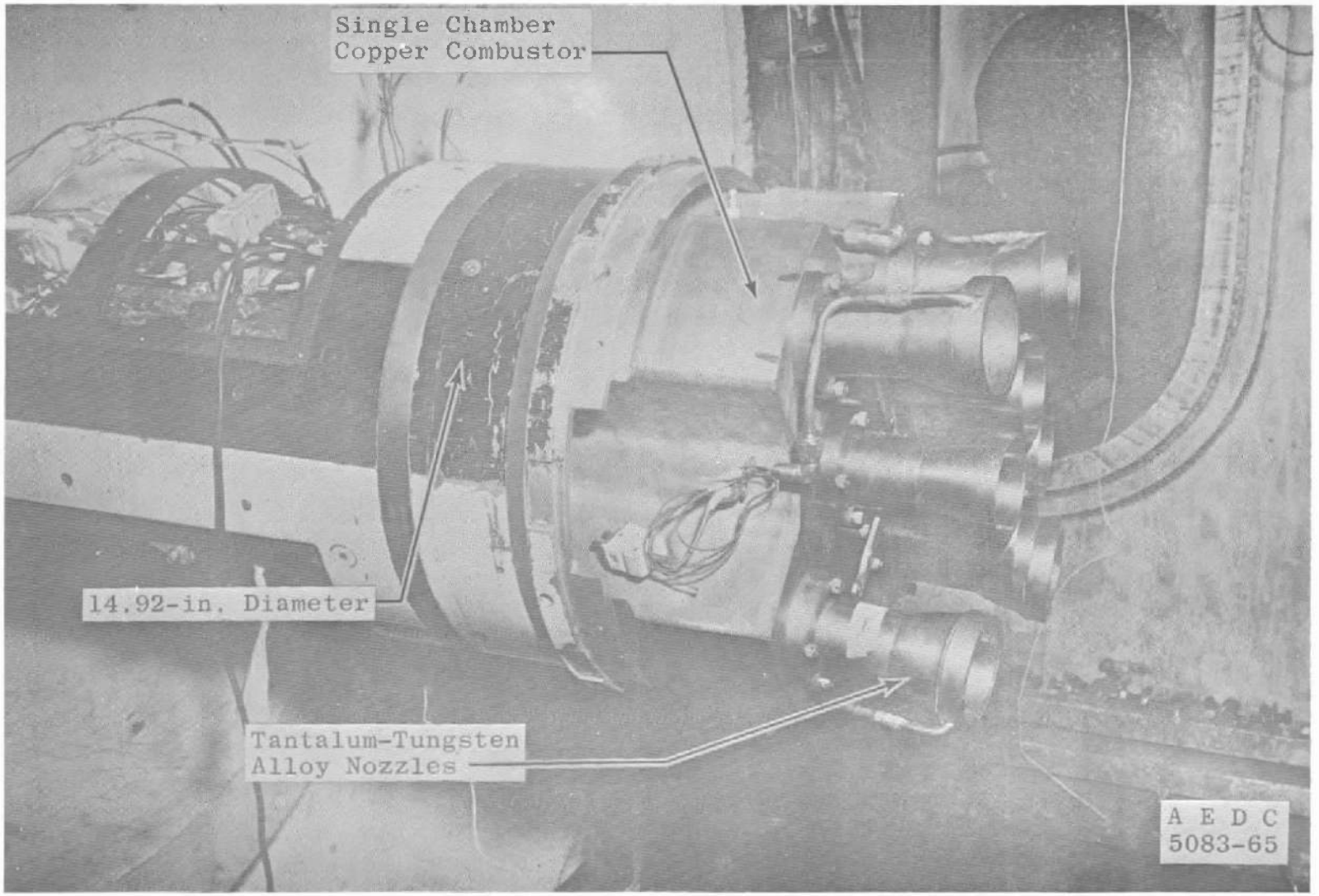

a. Photograph of Combustor and Nozzles

Fig. 1 Uncooled Engine Model

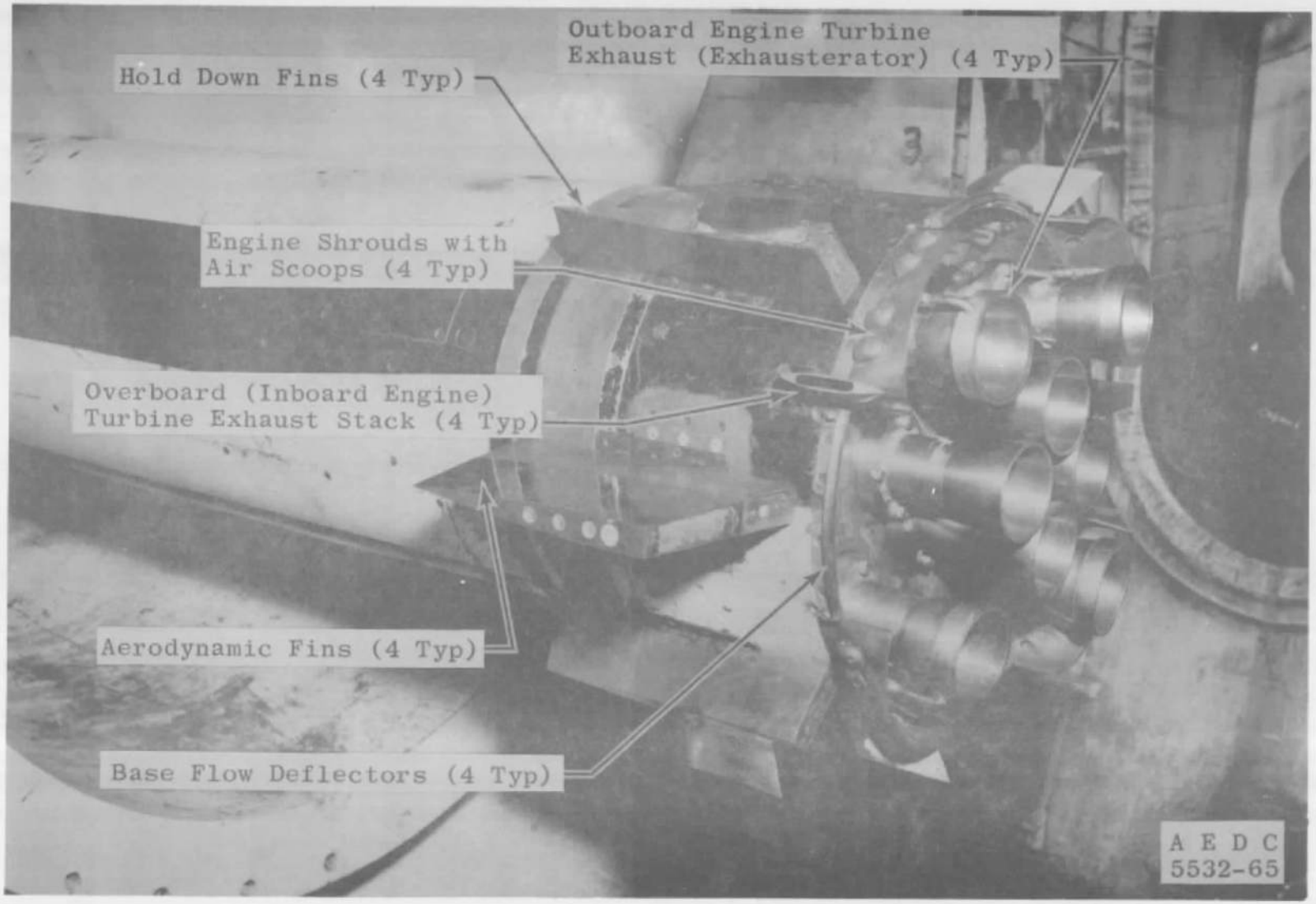

b. Photograph of 5.47-percent-Scale Saturn S1 Block-II Fairings

Fig. 1 Concluded

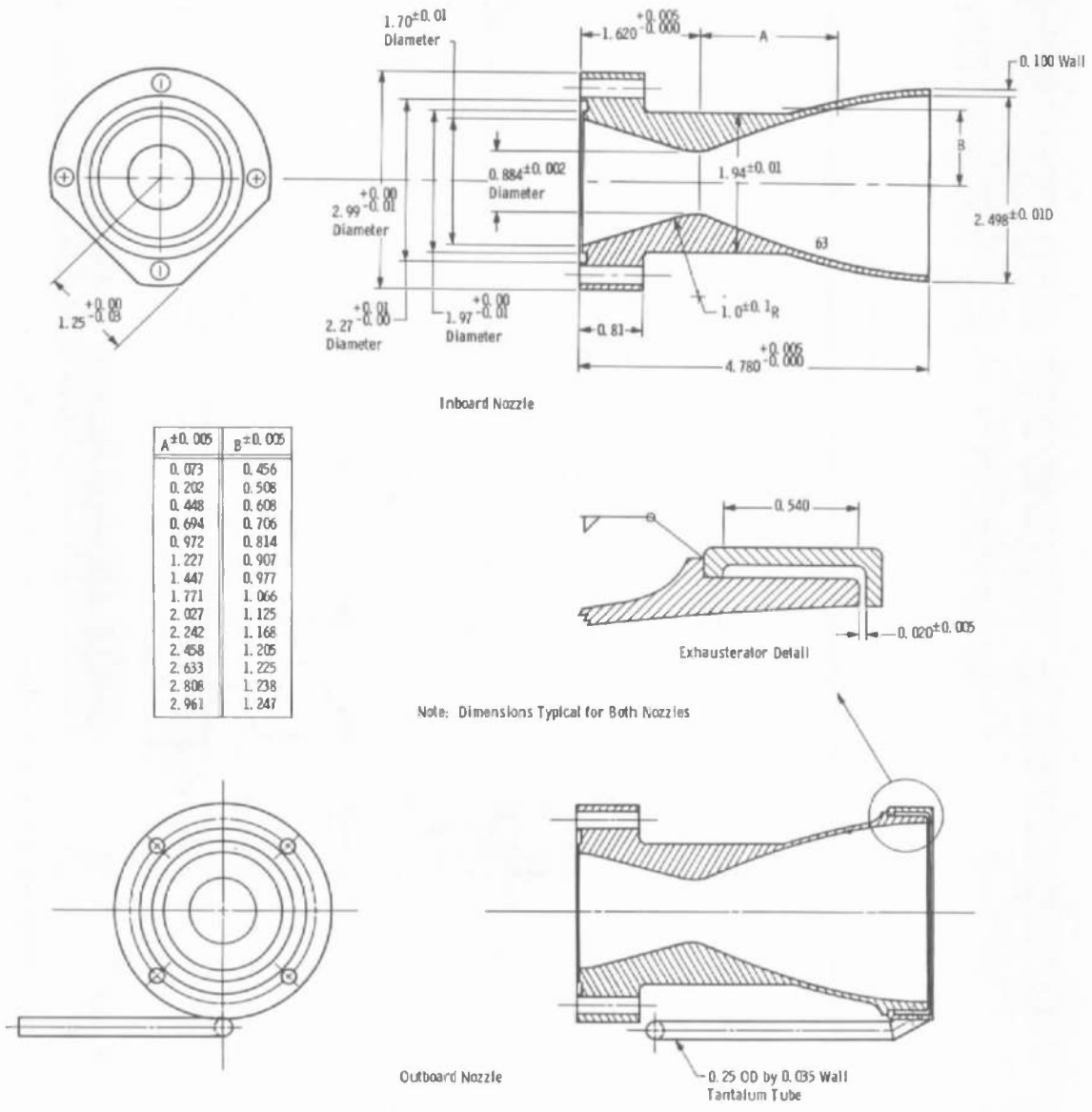

A±0.005	B±0.005
0.073	0.456
0.202	0.508
0.448	0.608
0.694	0.706
0.972	0.814
1.227	0.907
1.447	0.977
1.771	1.066
2.027	1.125
2.242	1.168
2.458	1.205
2.633	1.225
2.808	1.238
2.961	1.247

a. Design Drawing

Fig. 2 Details of Tantalum-Tungsten Nozzles

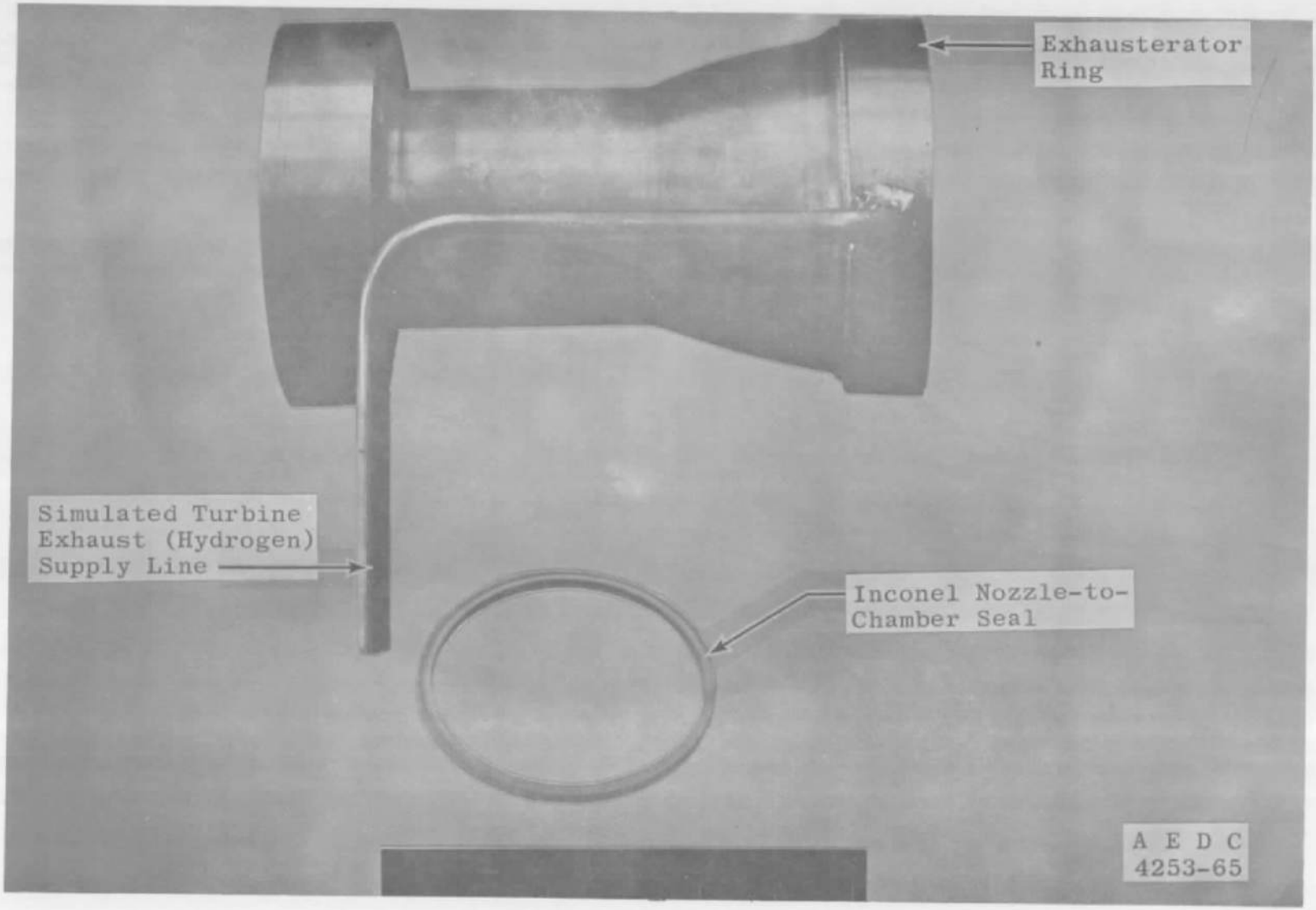

b. Photograph of Outboard Nozzle

Fig. 2 Continued

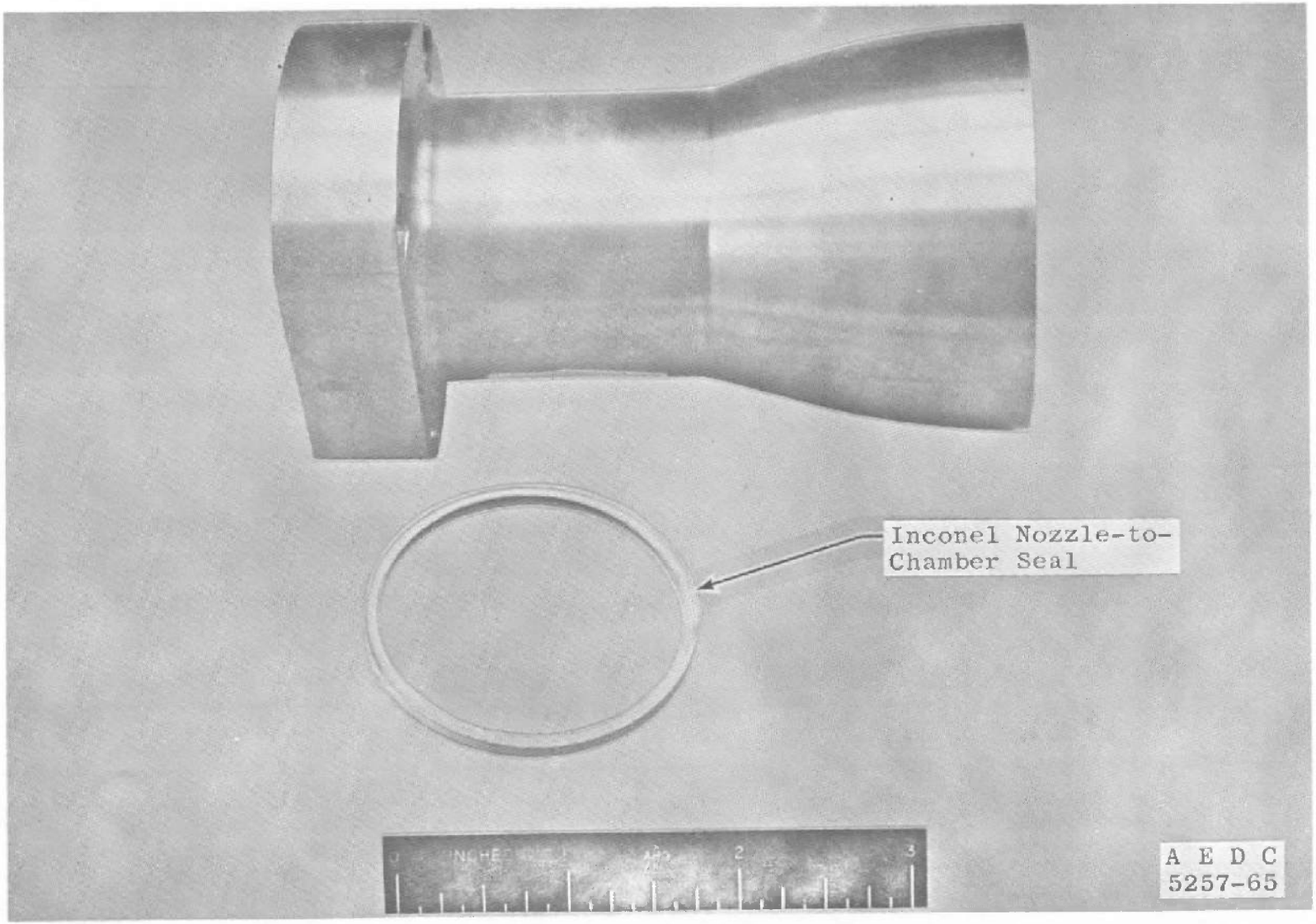

c. Photograph of Inboard Nozzle

Fig. 2 Concluded

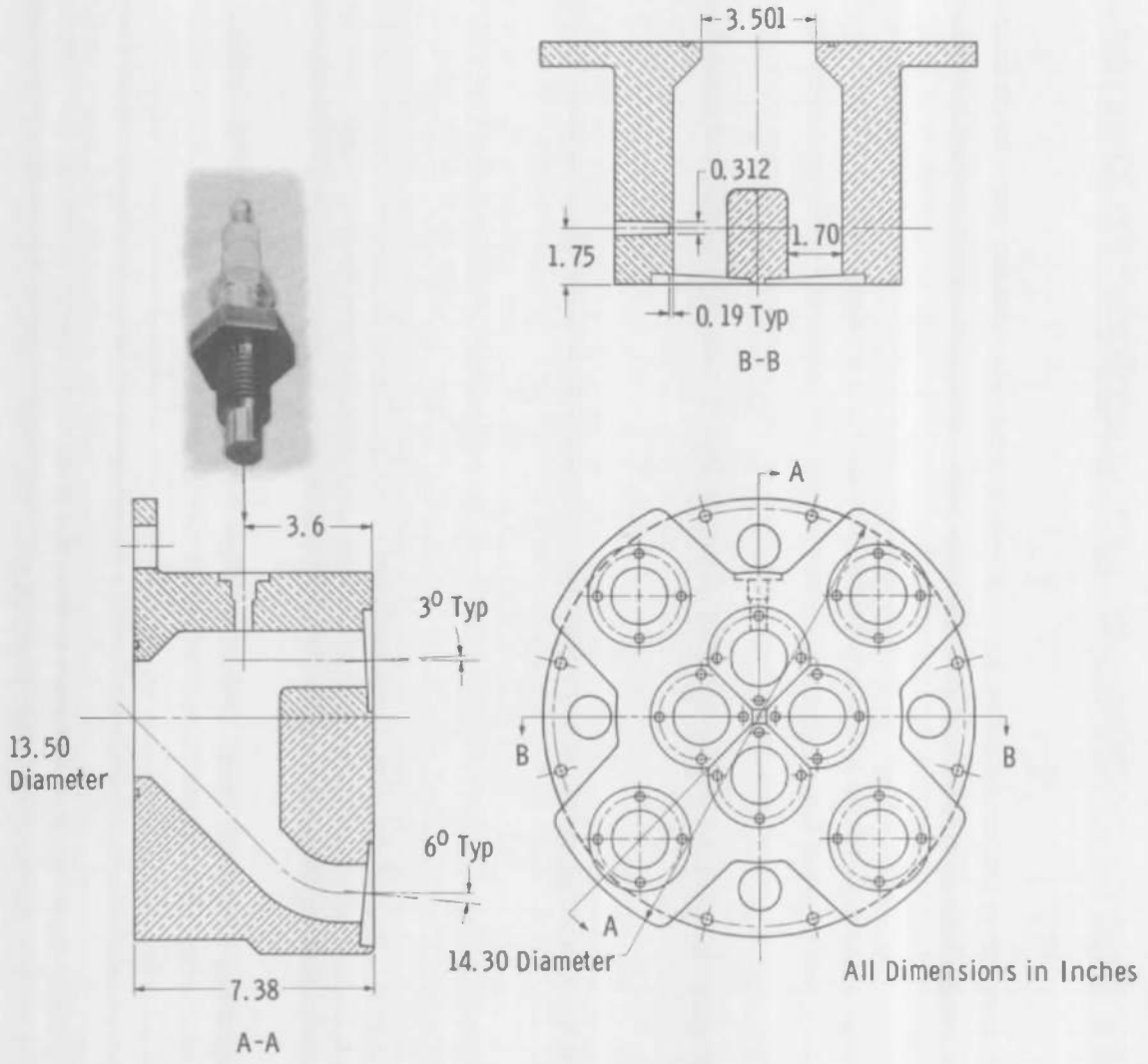

a. Schematic

Fig. 3 Combustor Design Details

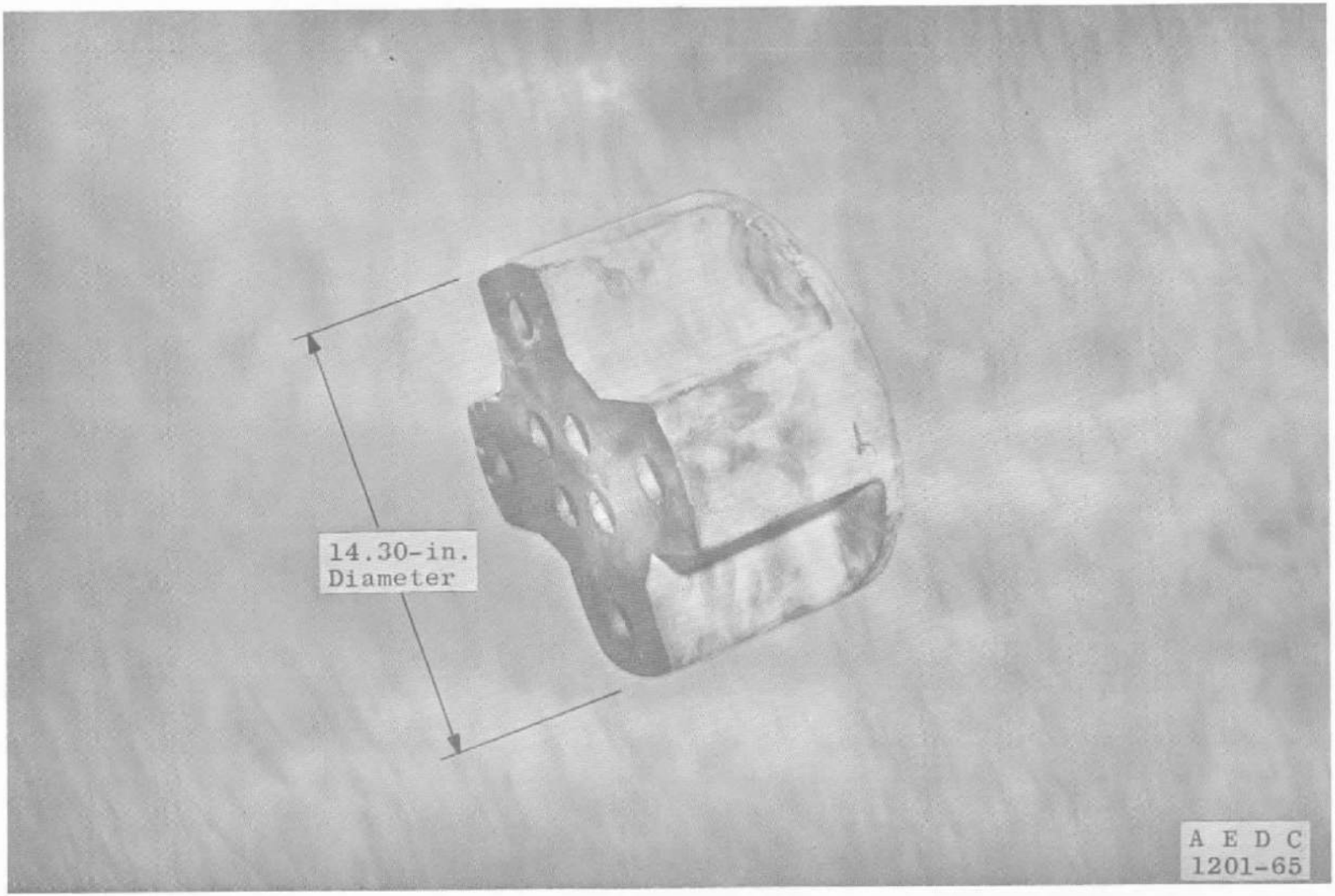

b. View of Combustor prior to Machining

Fig. 3 Continued

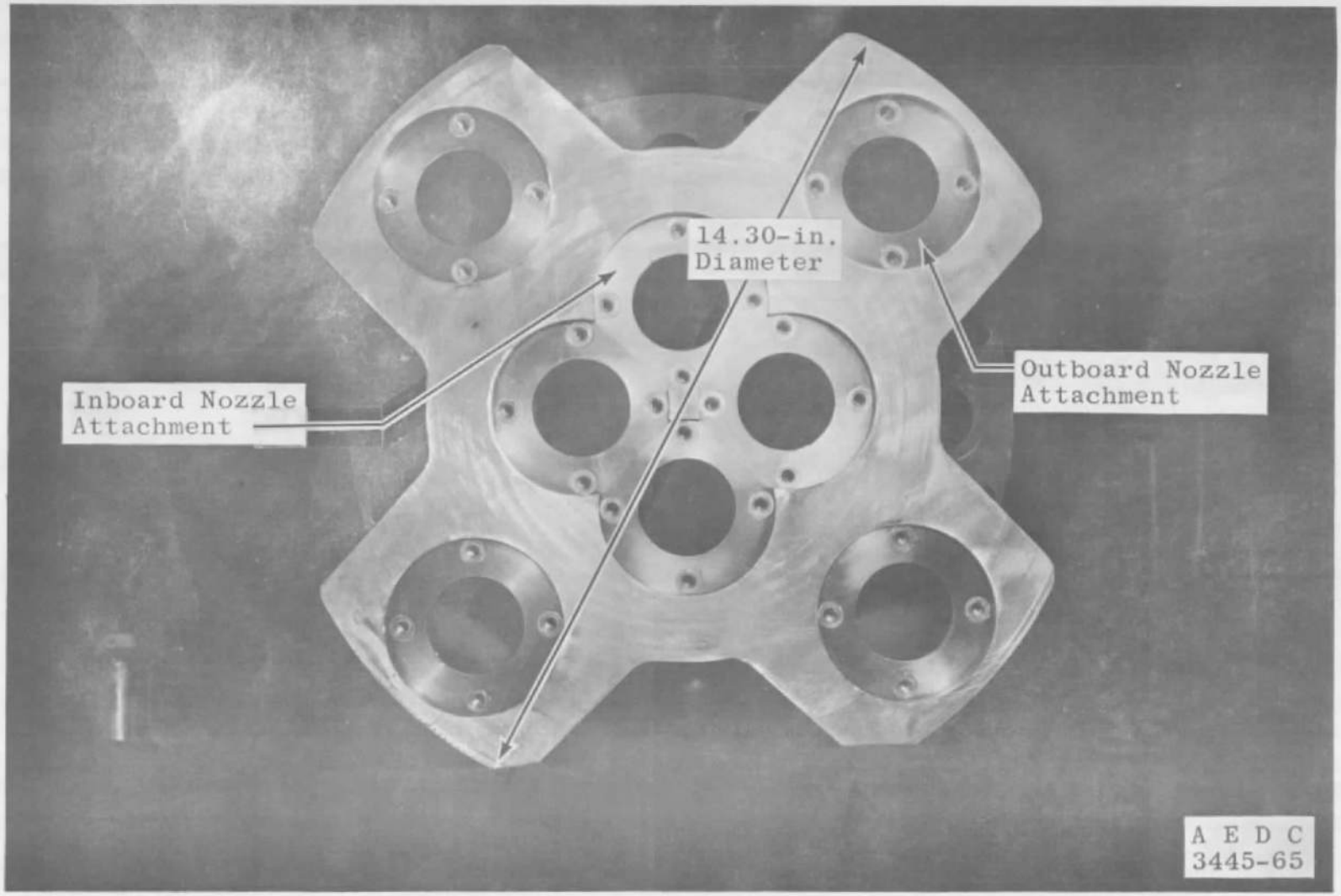

c. View of Combustor after Machining (Looking Upstream)

Fig. 3 Continued

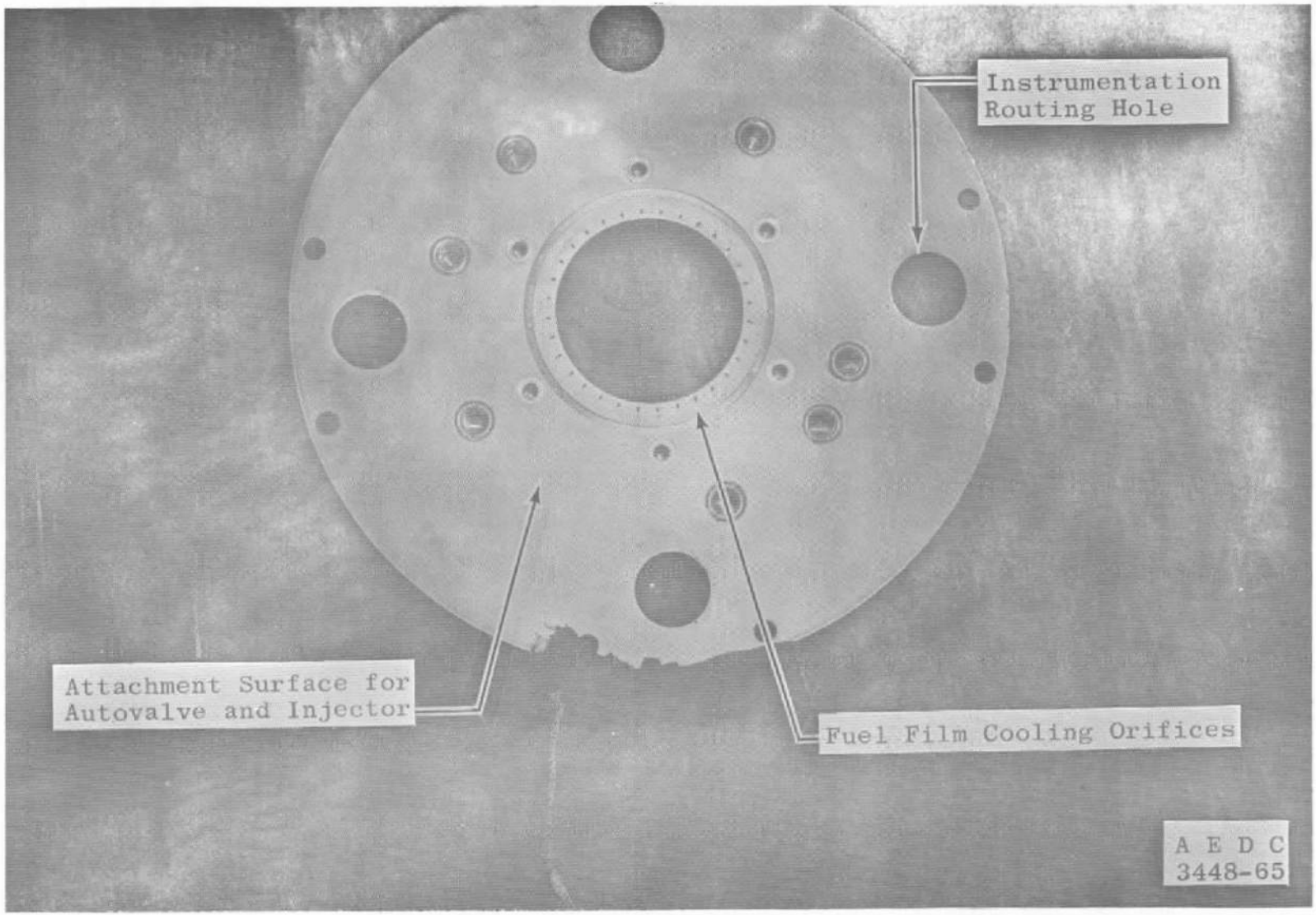

d. View of Combustor after Mochining (Looking Downstream)

Fig. 3 Concluded

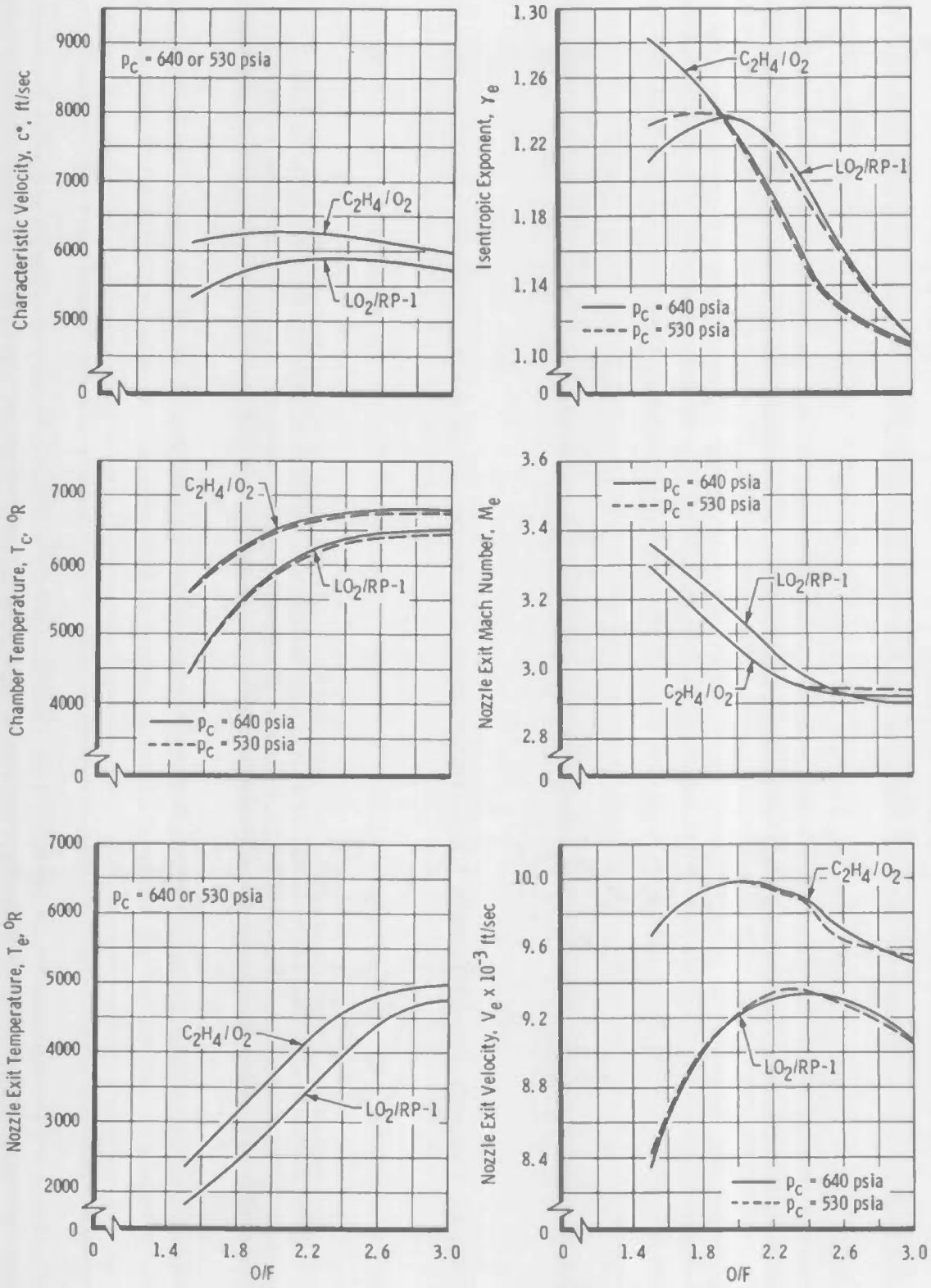

Fig. 4 Theoretical Performance of Gaseous Oxygen with Gaseous Ethylene and Liquid Oxygen with RP-1, Nozzle Area Ratio 8:1, Equilibrium Flow (Ref. 21)

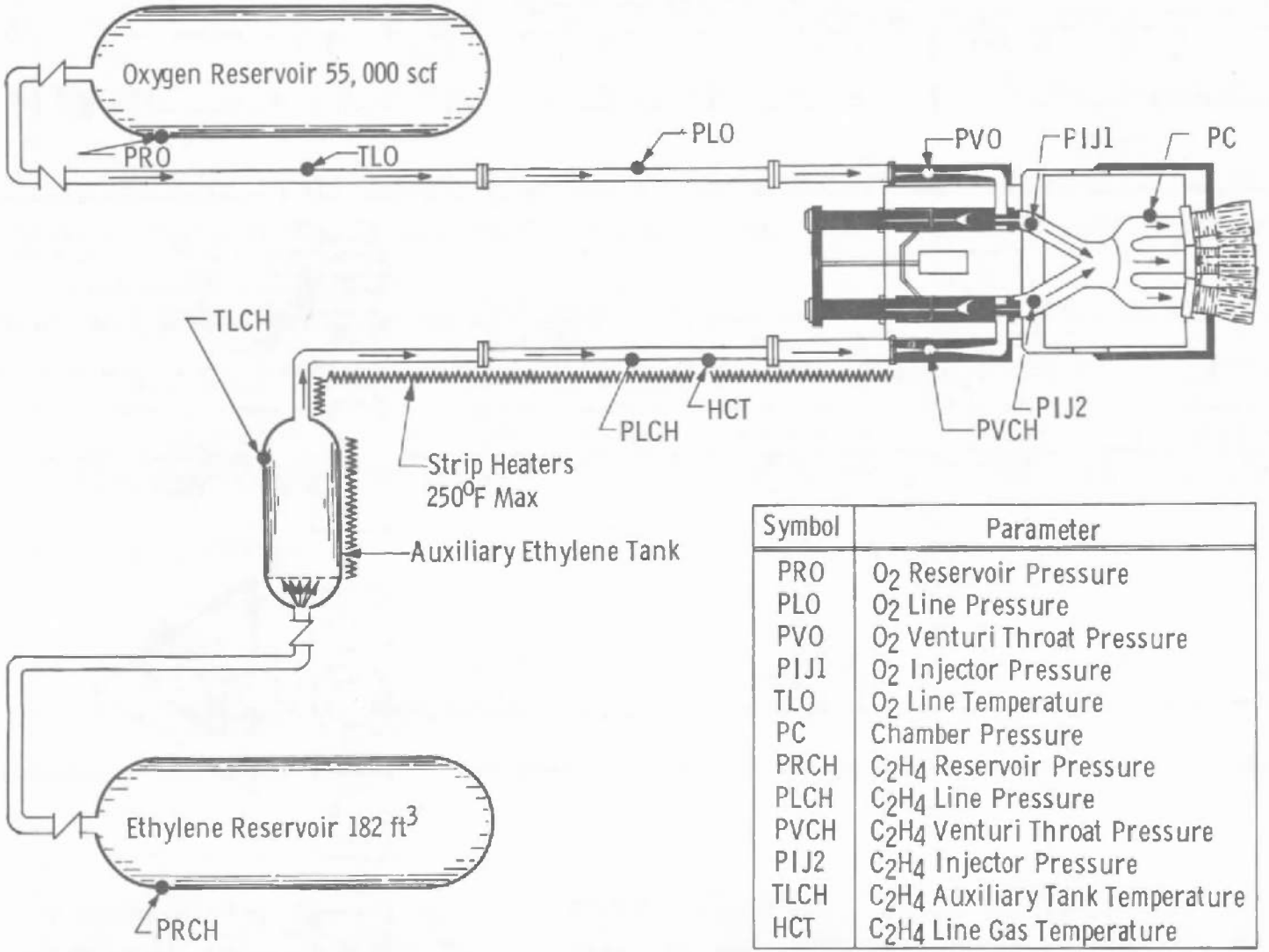

Symbol	Parameter
PRO	O_2 Reservoir Pressure
PLO	O_2 Line Pressure
PVO	O_2 Venturi Throat Pressure
PIJ1	O_2 Injector Pressure
TLO	O_2 Line Temperature
PC	Chamber Pressure
PRCH	C_2H_4 Reservoir Pressure
PLCH	C_2H_4 Line Pressure
PVCH	C_2H_4 Venturi Throat Pressure
PIJ2	C_2H_4 Injector Pressure
TLCH	C_2H_4 Auxiliary Tank Temperature
HCT	C_2H_4 Line Gas Temperature

Fig. 5 Uncooled Engine Model Propellant System Schemotic

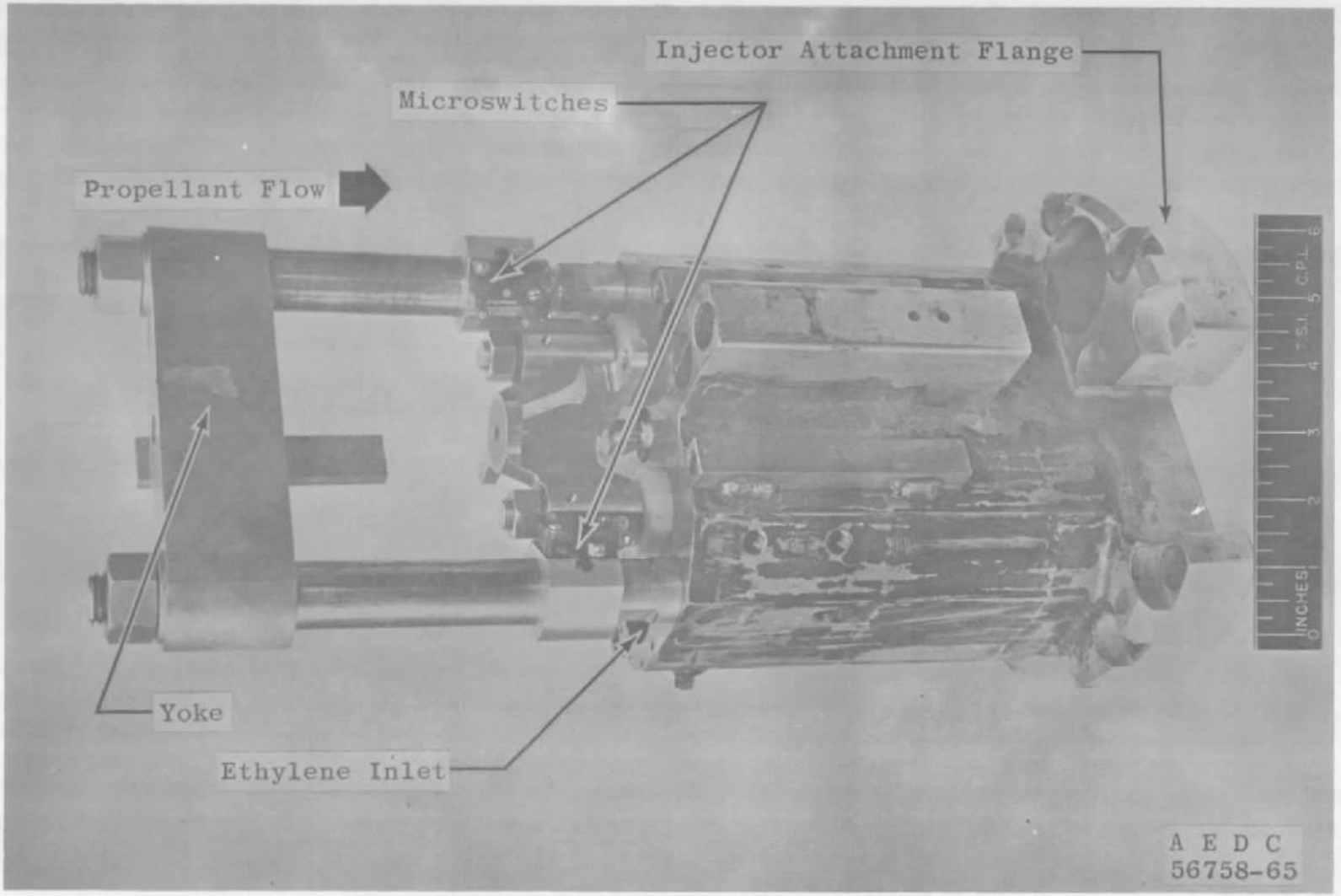

a. Photograph

Fig. 6 Propellant System Autovalve Details

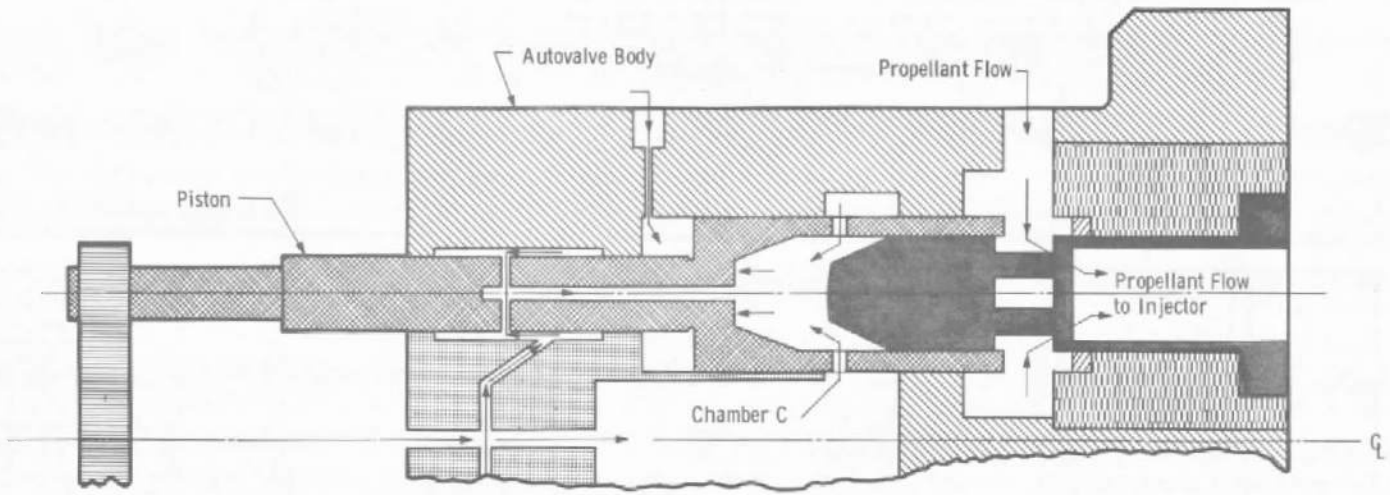

Note: Valve is symmetrical about centerline; only one-half of valve is shown.

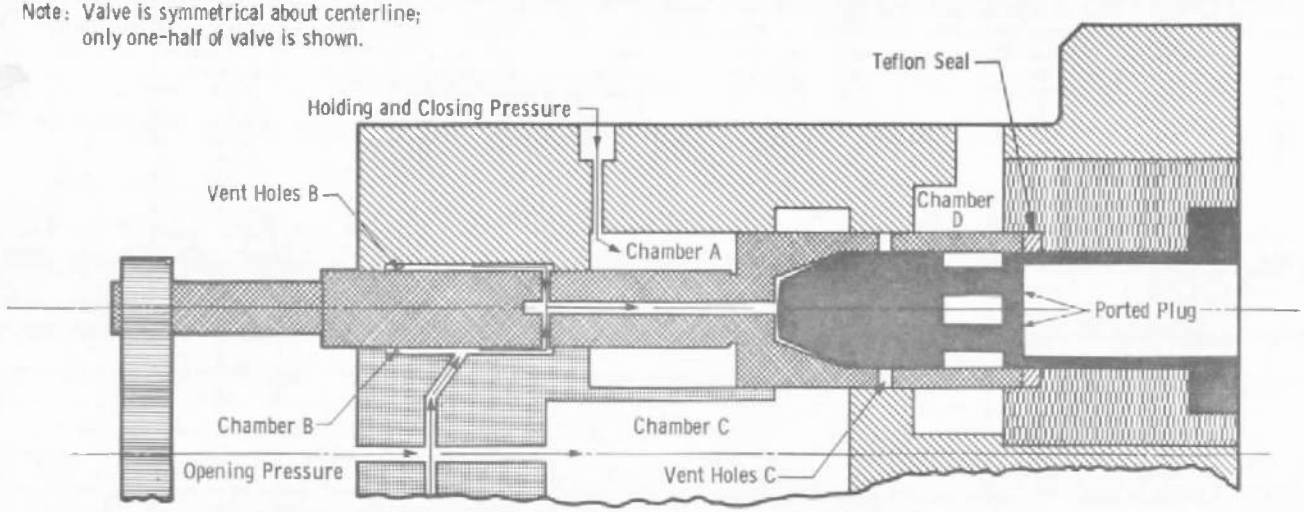

b. Schematic

Fig. 6 Concluded

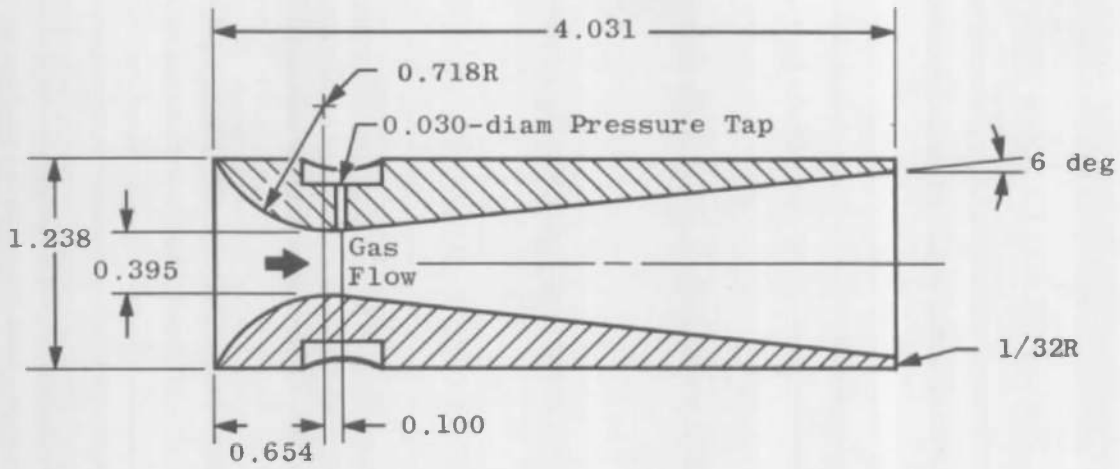

Ethylene Venturi

1. All Dimensions in Inches
2. Material, Brass

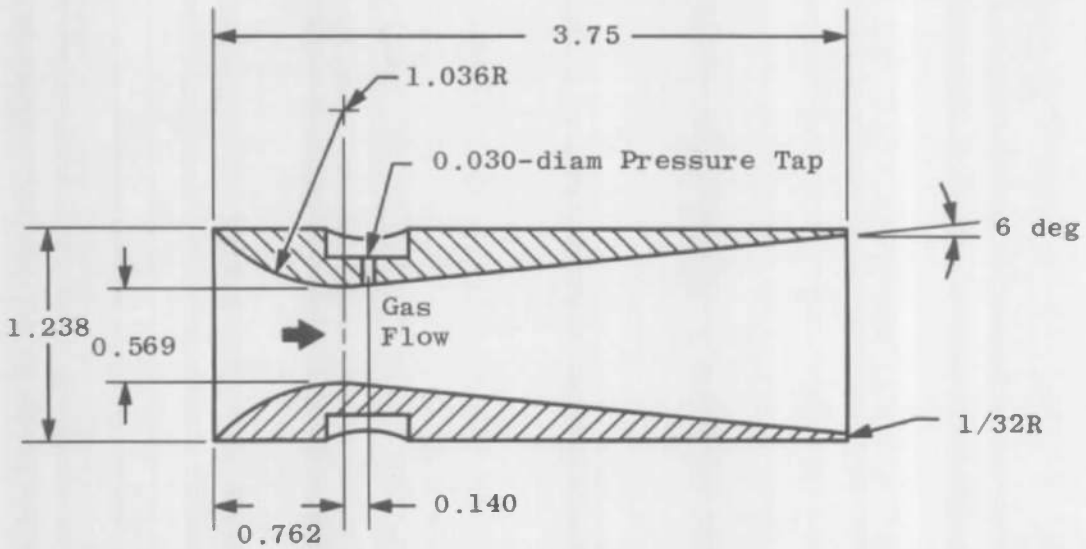

Oxygen Venturi

a. Schematic

Fig. 7 Propellant System Flow-Metering Venturis

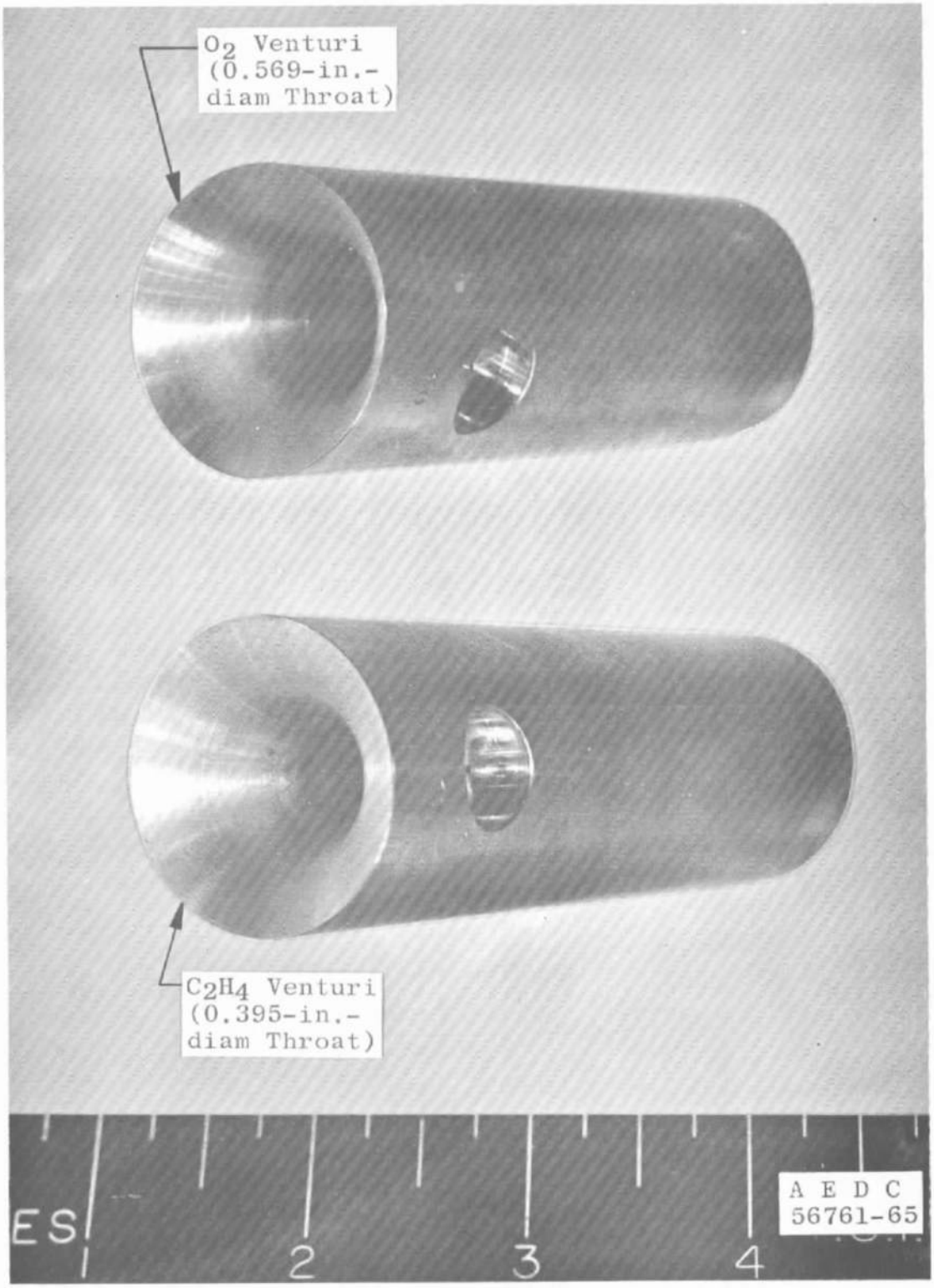

b. Photograph

Fig. 7 Concluded

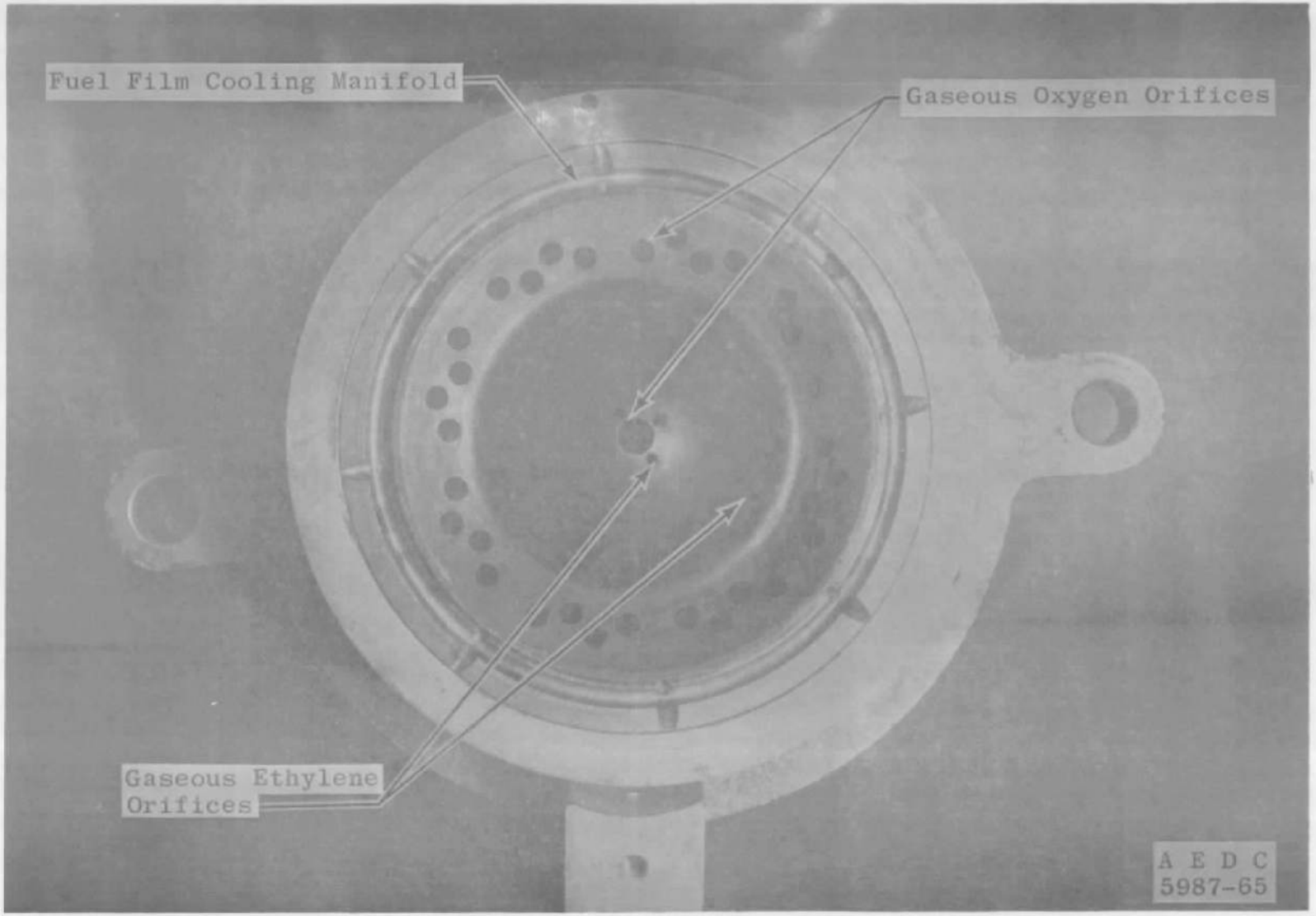

Fig. 8 Photograph of Injector

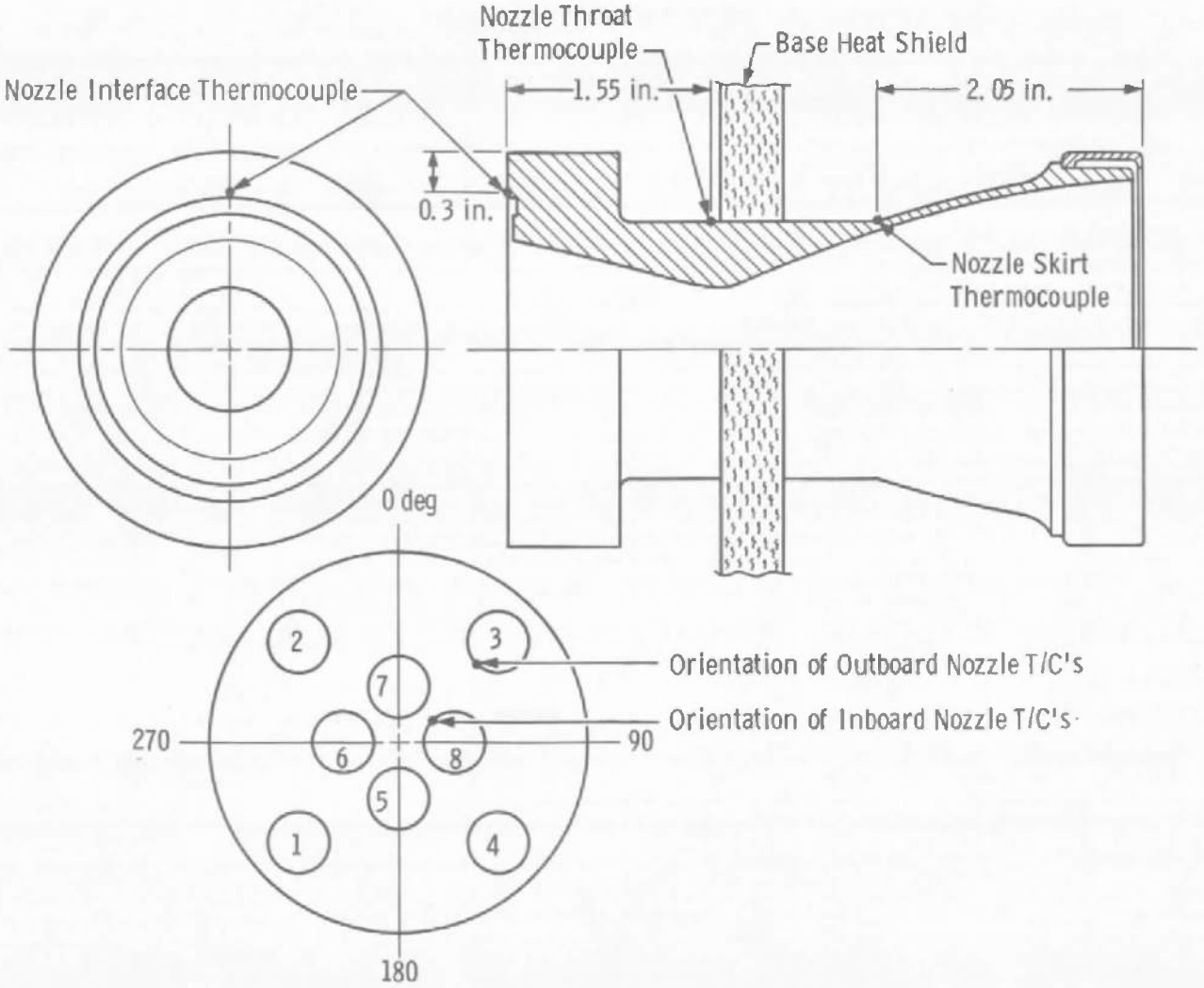

a. Schematic

Fig. 9 Locations of Nozzle Surface Attached Thermocouples

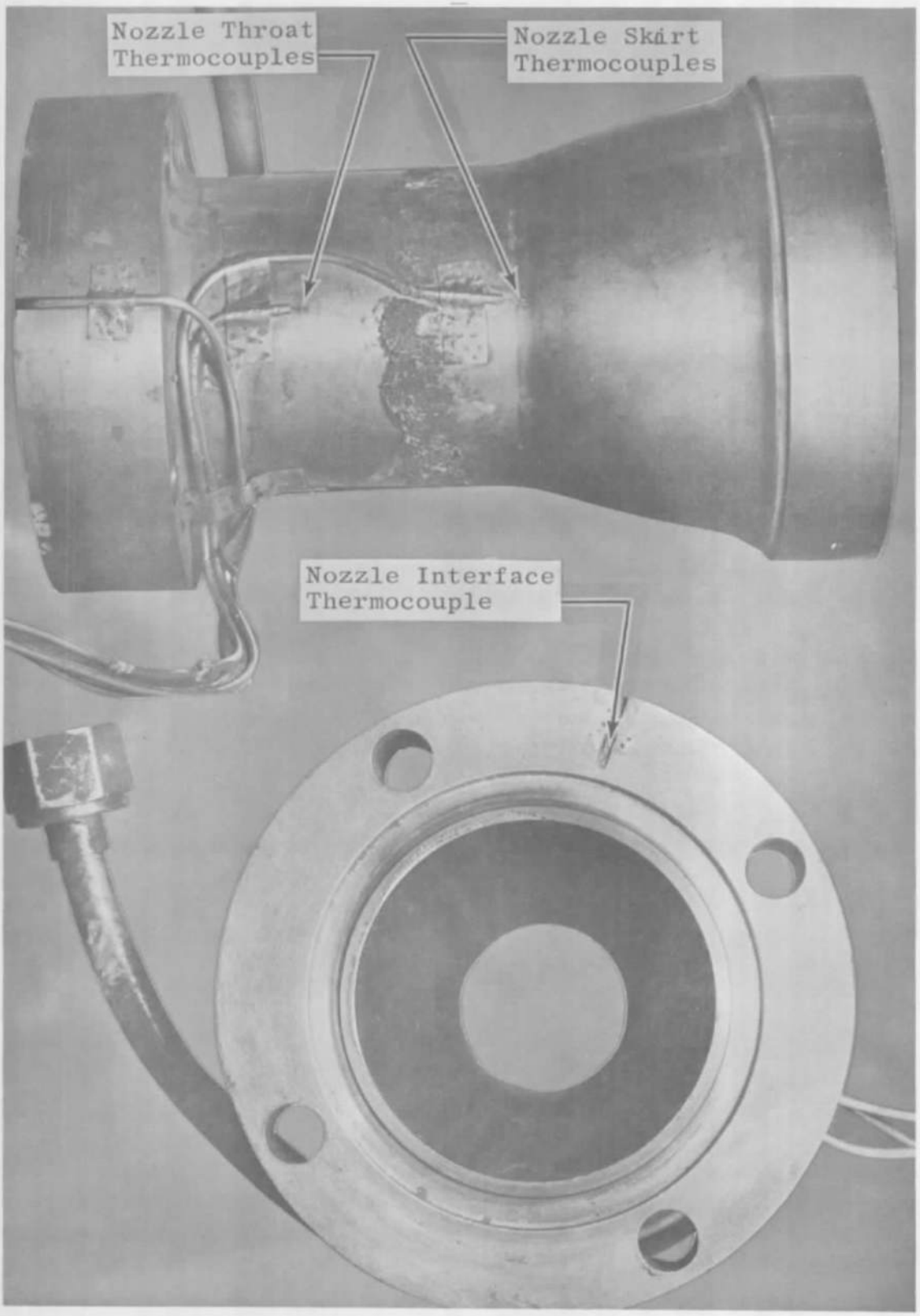

b. Photograph

Fig. 9 Concluded

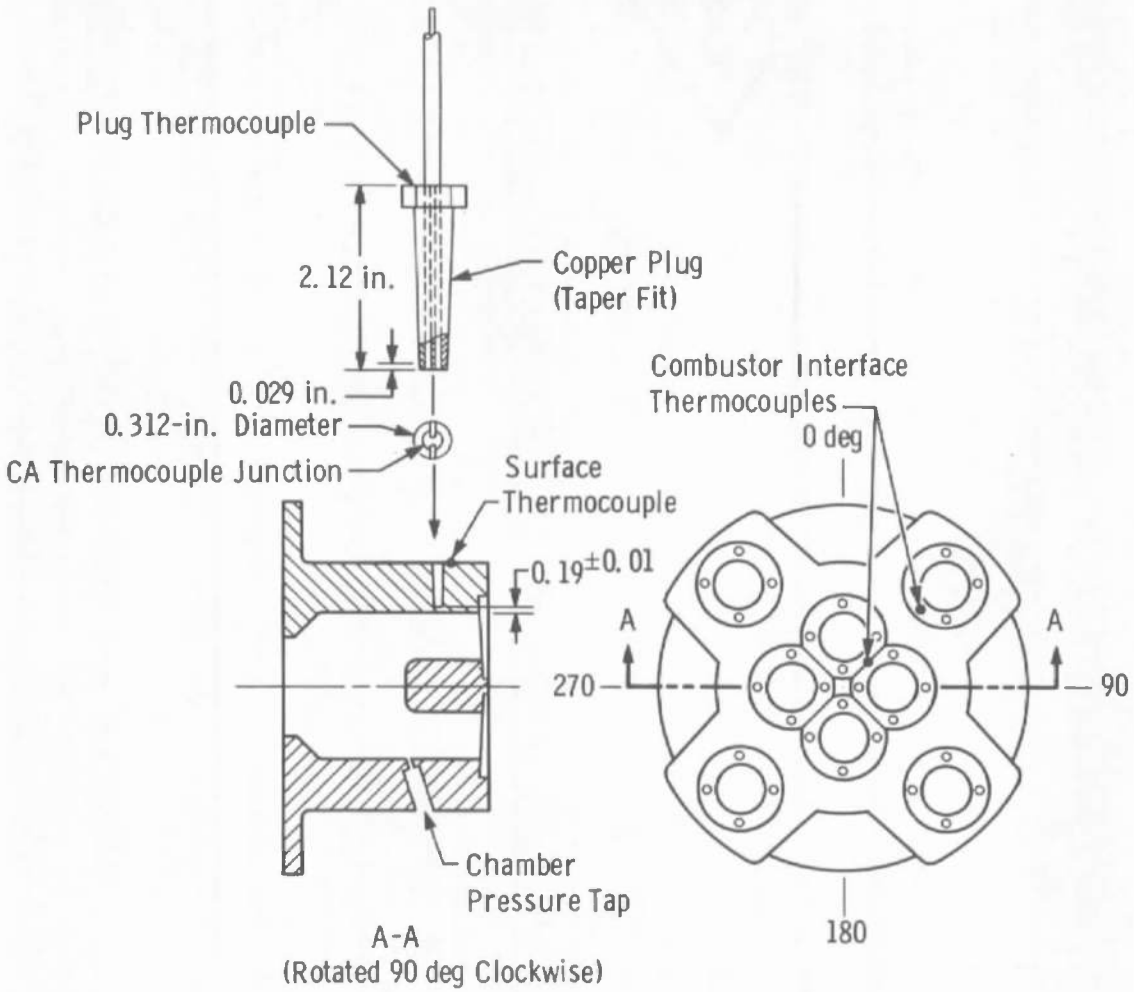

a. Schematic

Fig. 10 Combustor Instrumentation Details

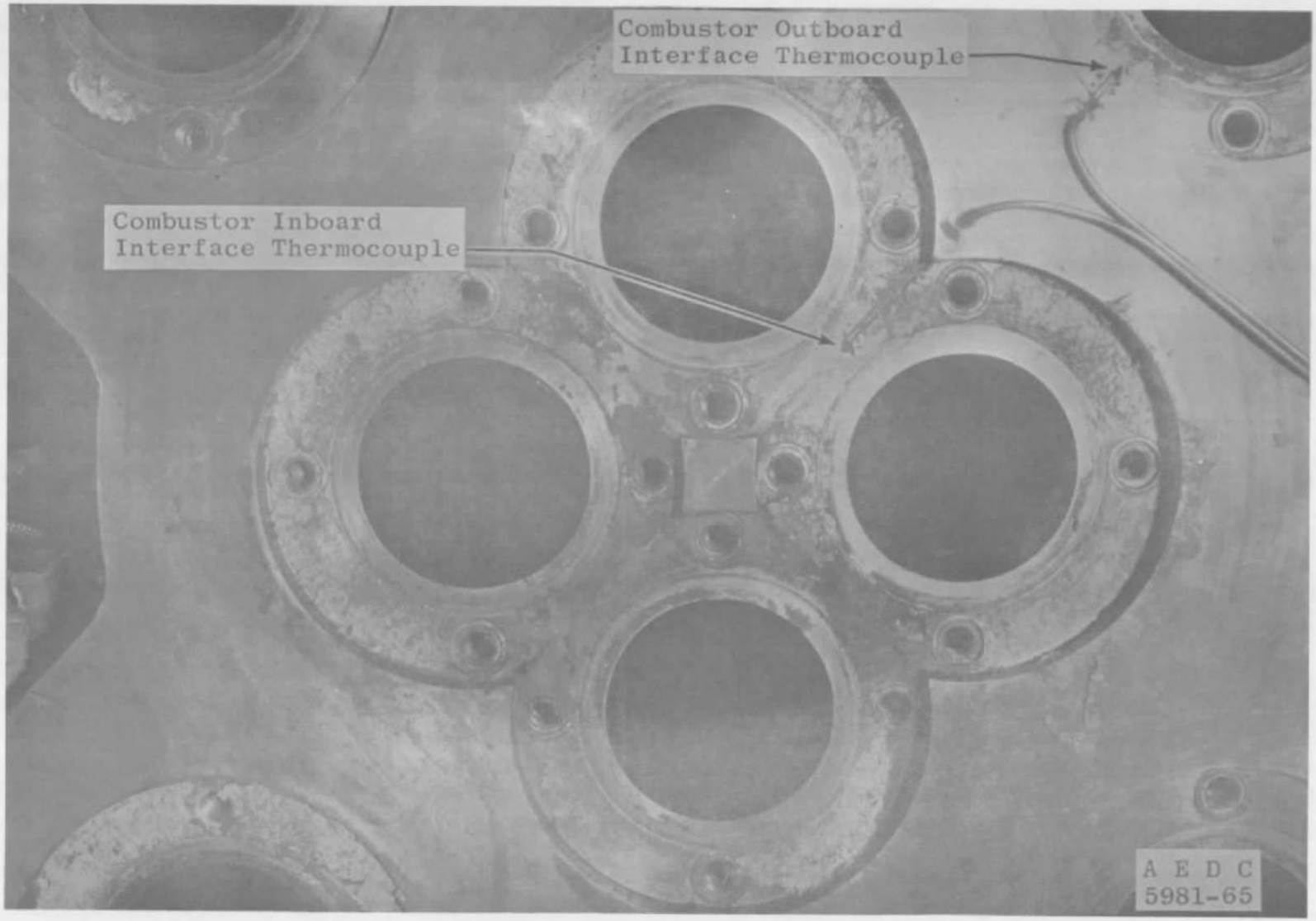

b. Photograph of Combustor Interface Thermocouples

Fig. 10 Concluded

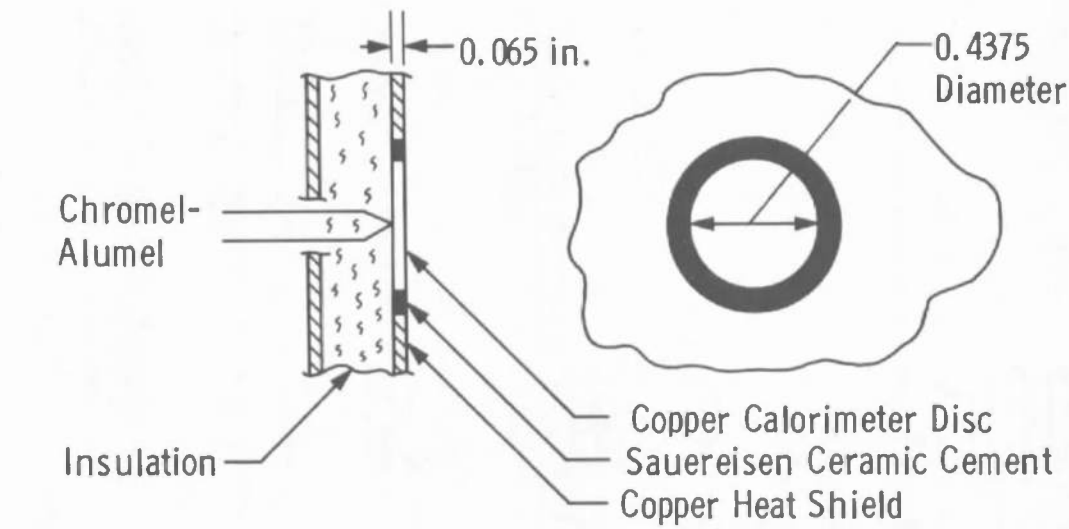

Slug Mass Calorimeter

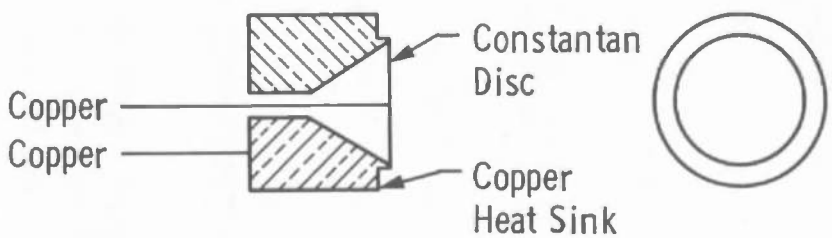

Membrane Heat Gage

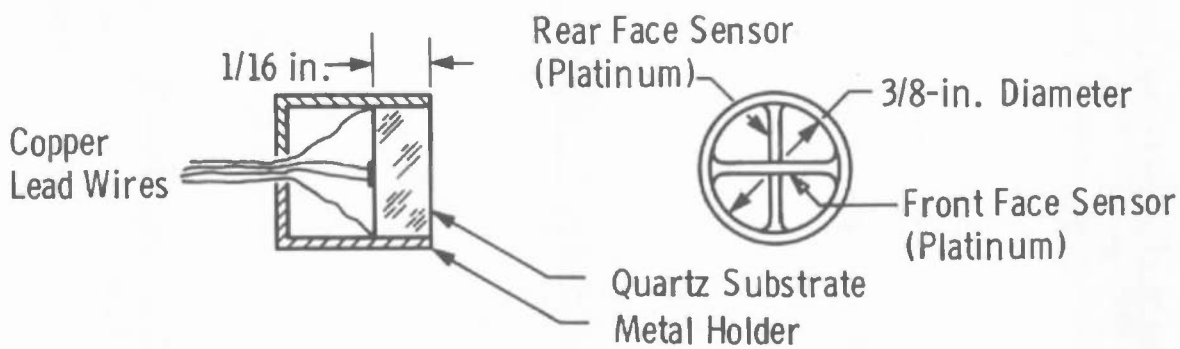

Thin-Film Dual-Element Heat Gage

Fig. 11 Details of Base Heat Flux Gage

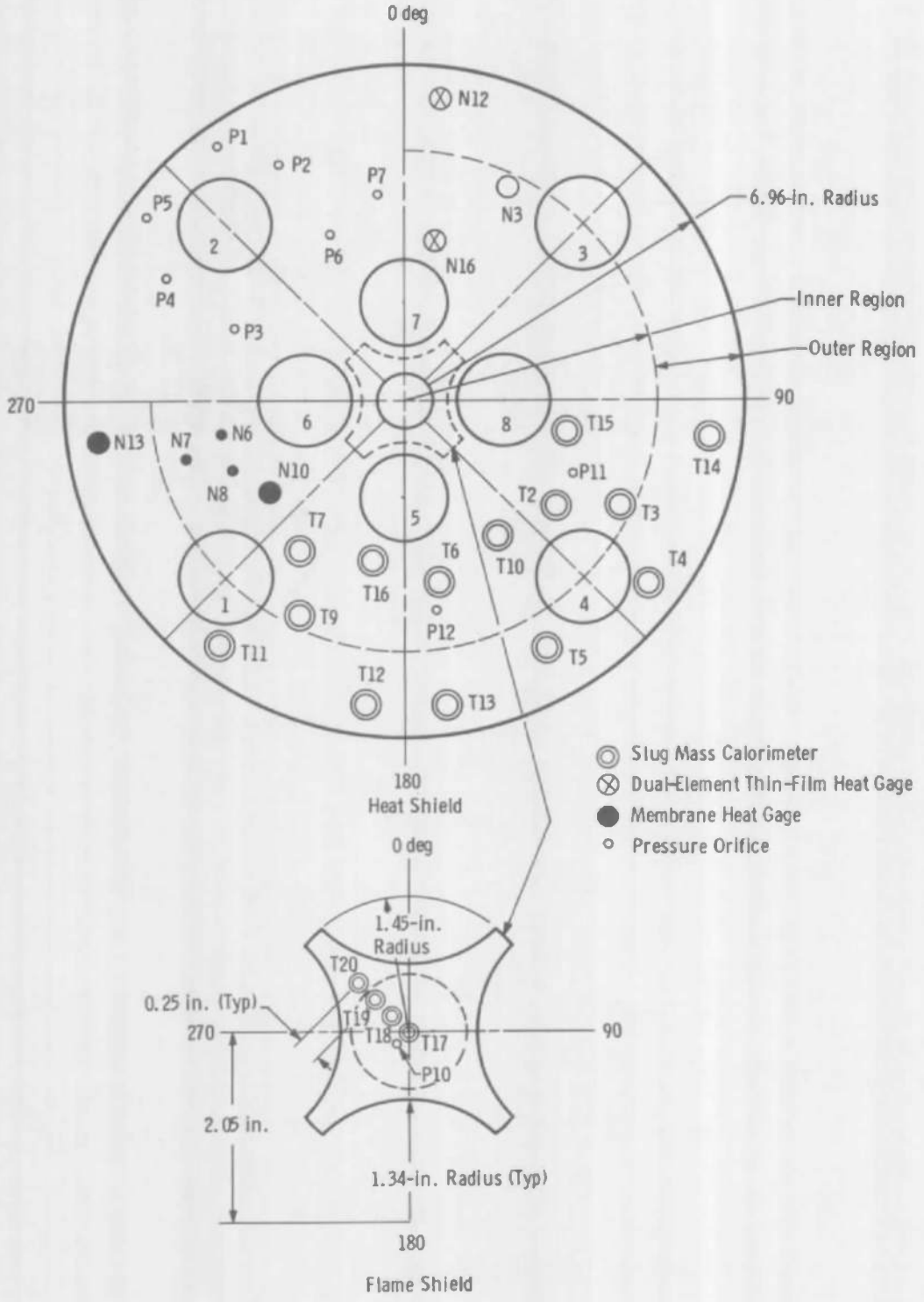

a. Schematic

Fig. 12 Base Heat Shield and Flame Shield Instrumentation Locations

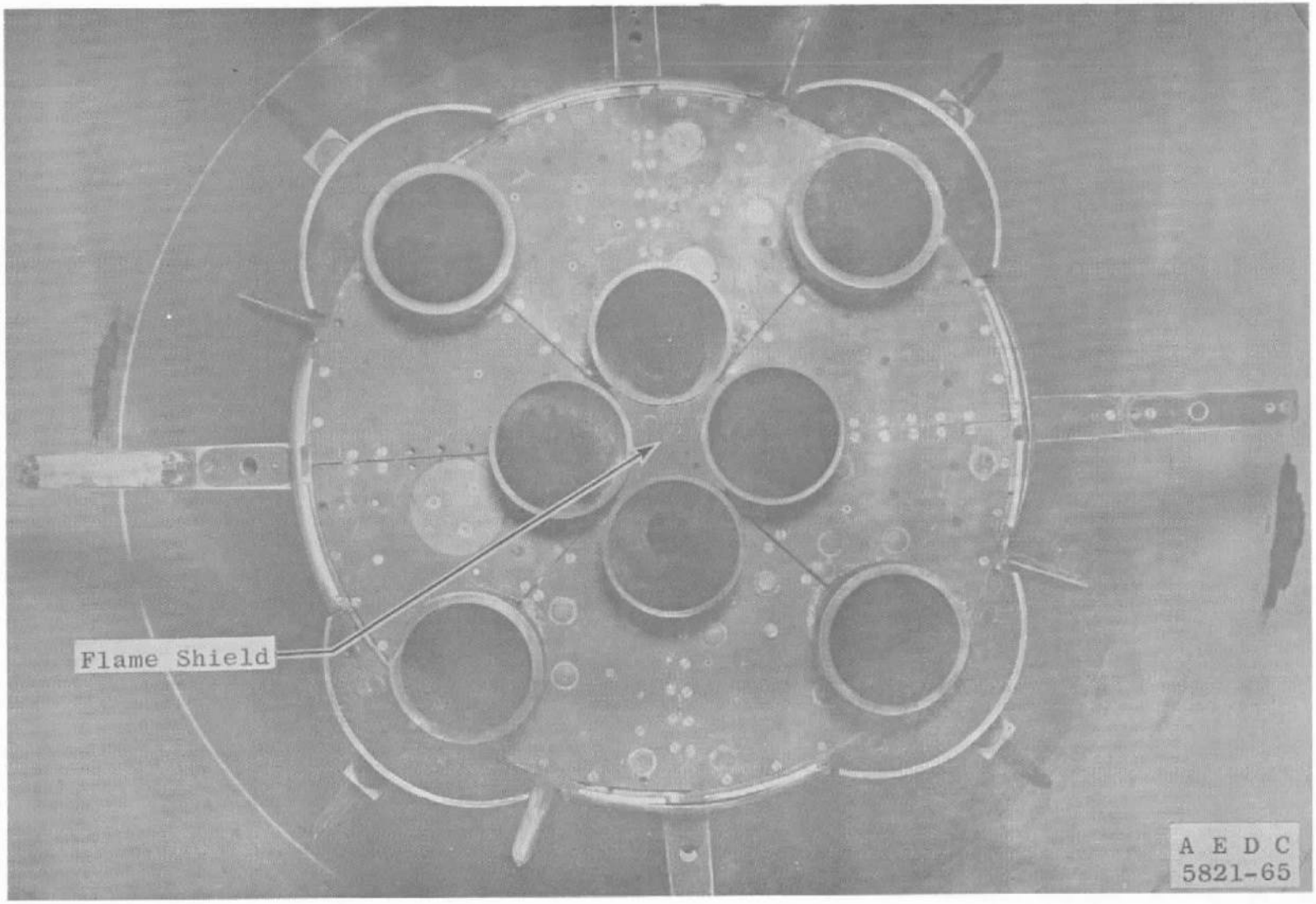

b. Photograph

Fig. 12 Concluded

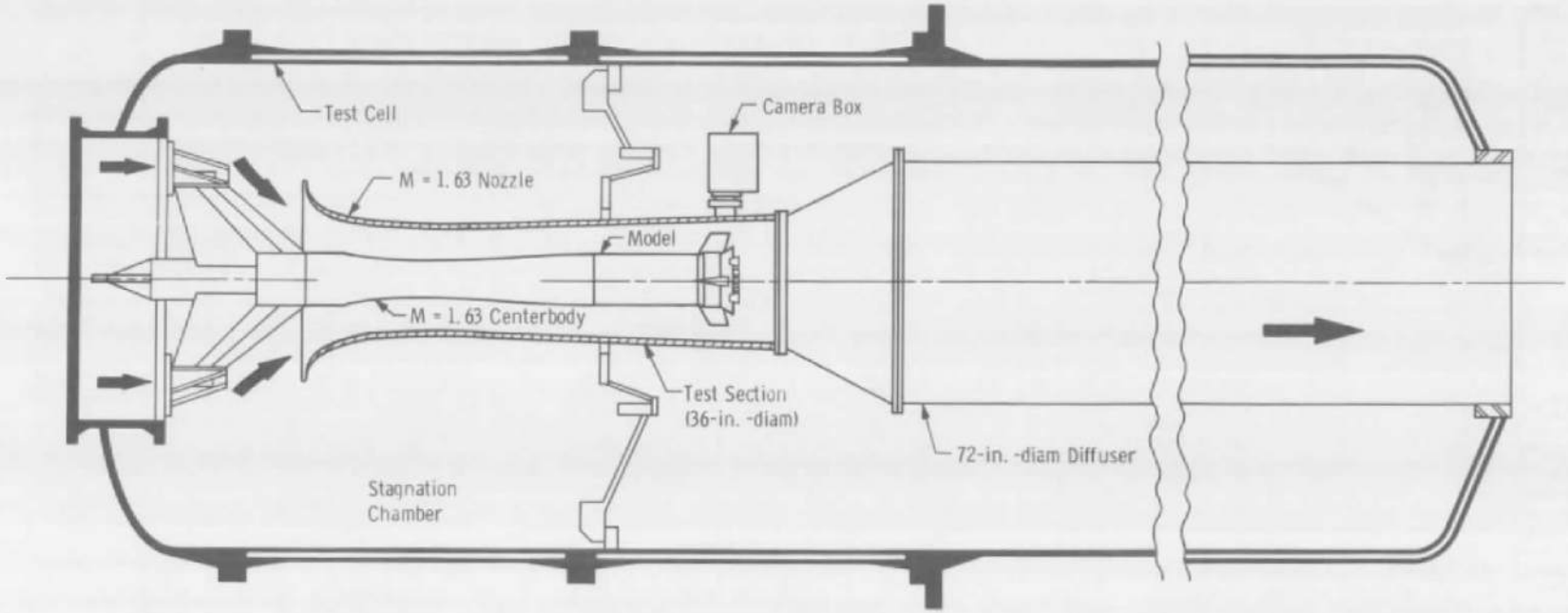

a. Schematic

Fig. 13 Uncooled Engine Model Installation in Propulsion Engine Test Cell (T-1)

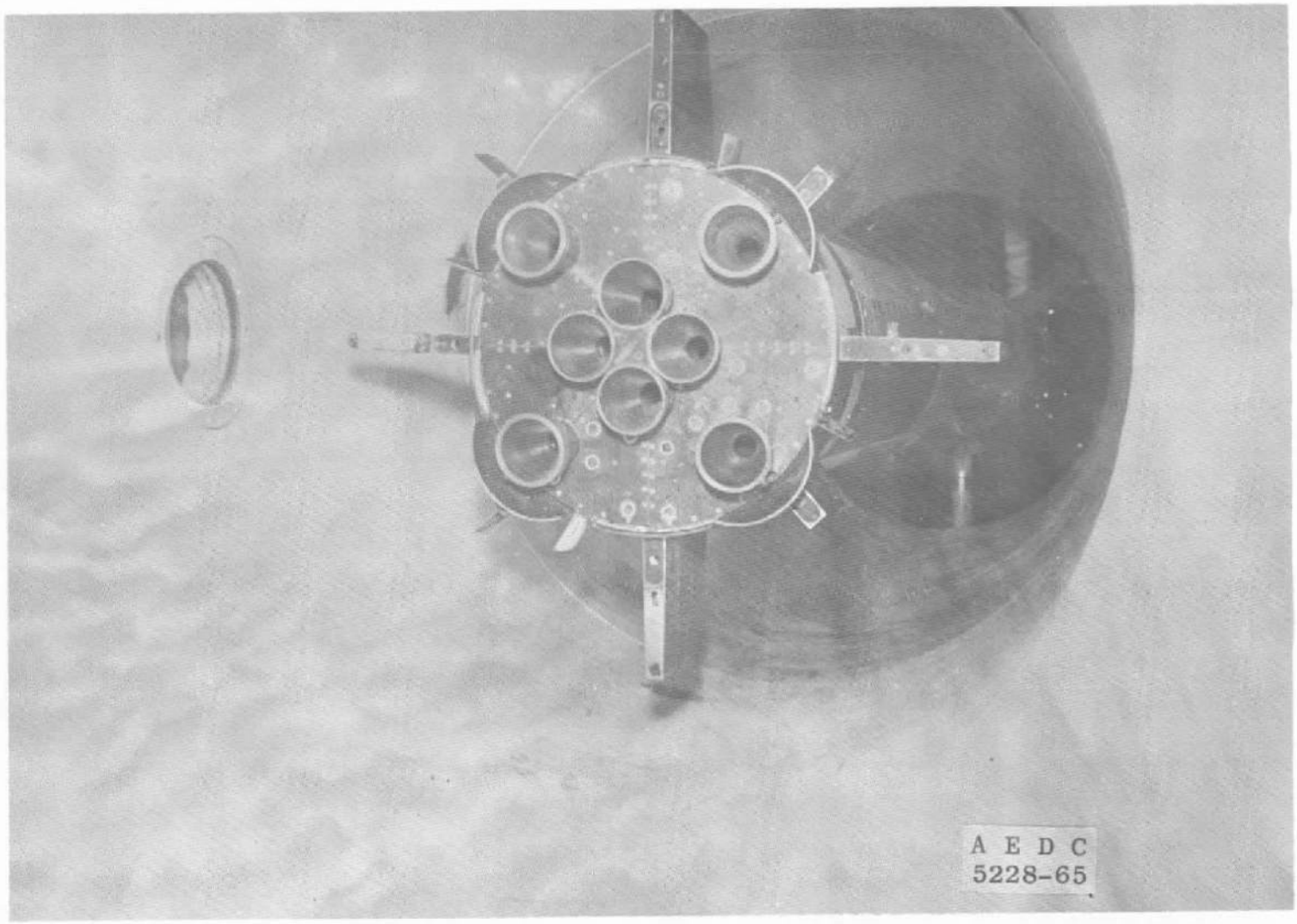

b. Photograph

Fig. 13 Concluded

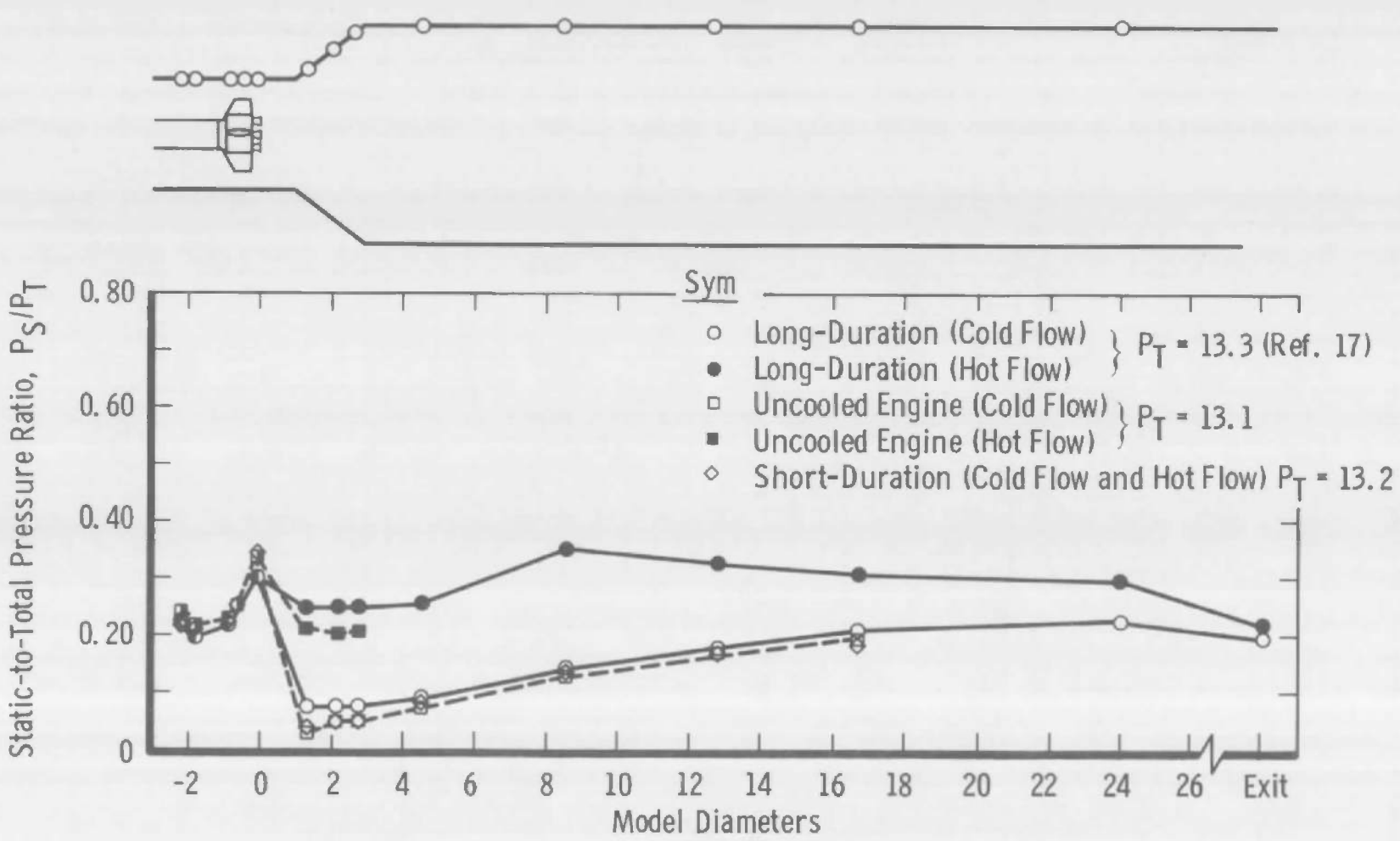

Fig. 14 Typical Operating Pressures for Long- and Short-Duration Tests Compared to Uncooled Engine Tests (Mach 1.63, 38,000 ft)

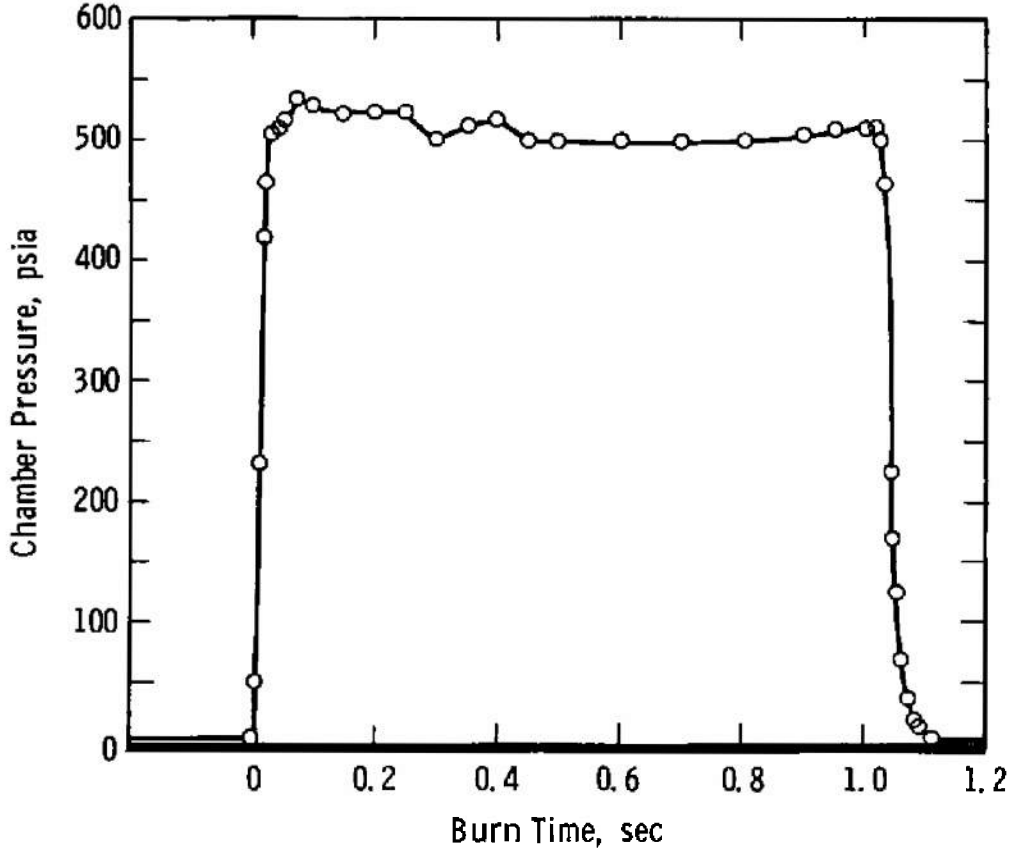

a. Normal Firing

Fig. 15 Typical Combustor Chamber Pressure History

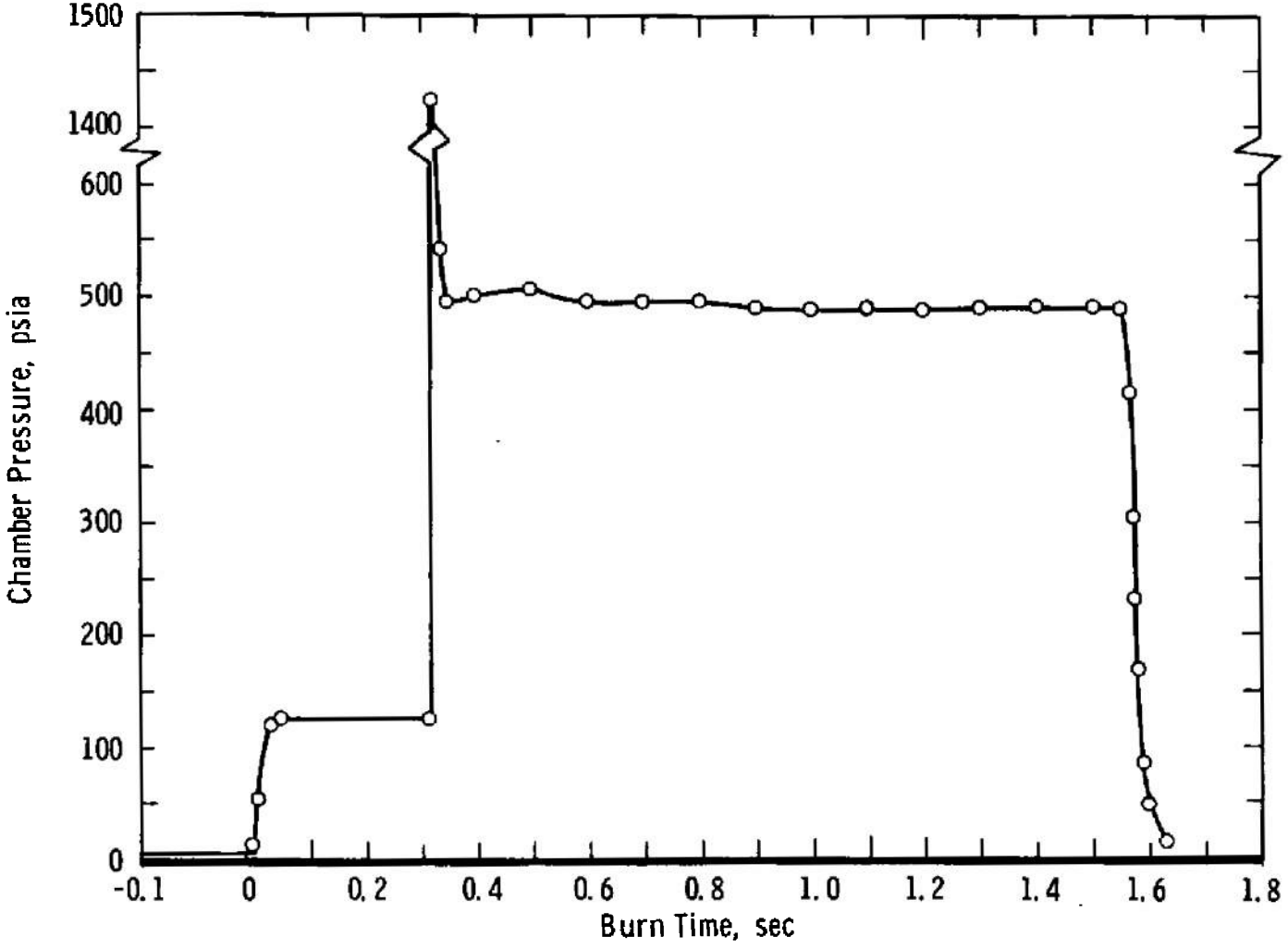

b. Delayed Ignition Firing

Fig. 15 Concluded

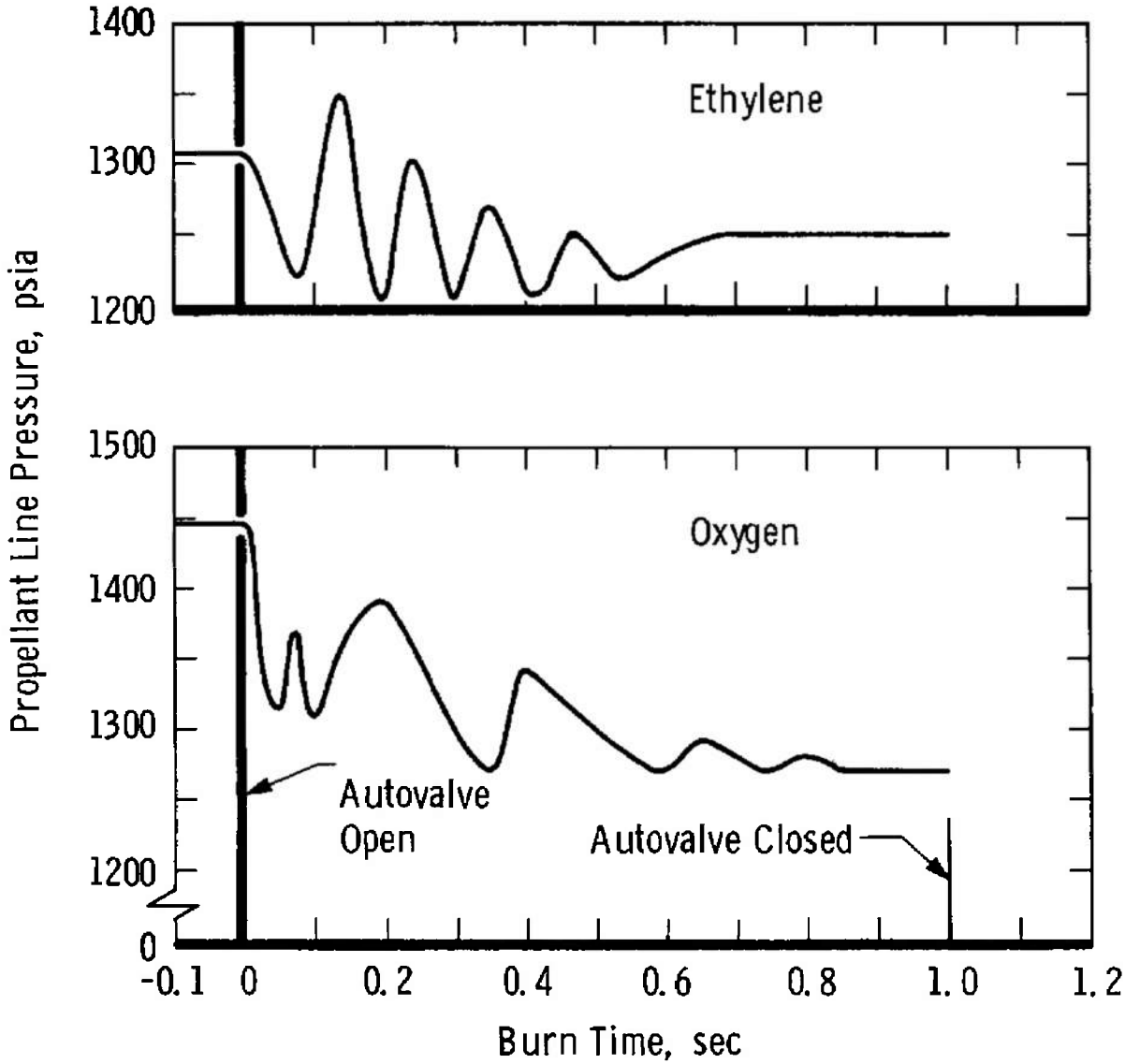

Fig. 16 Propellant Line Pressure-Time Histories

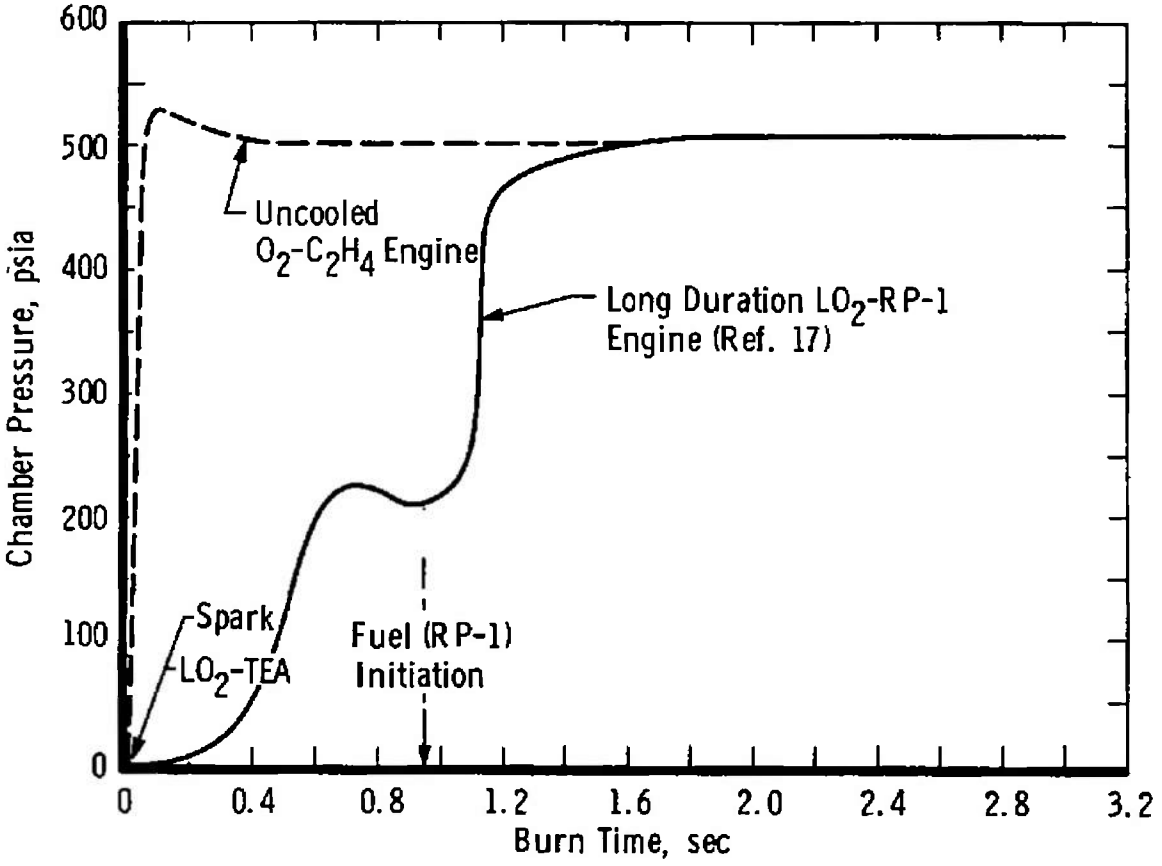

Fig. 17 Comparison of Engine Starting Transient for Uncooled Engine and Long-Duration Models

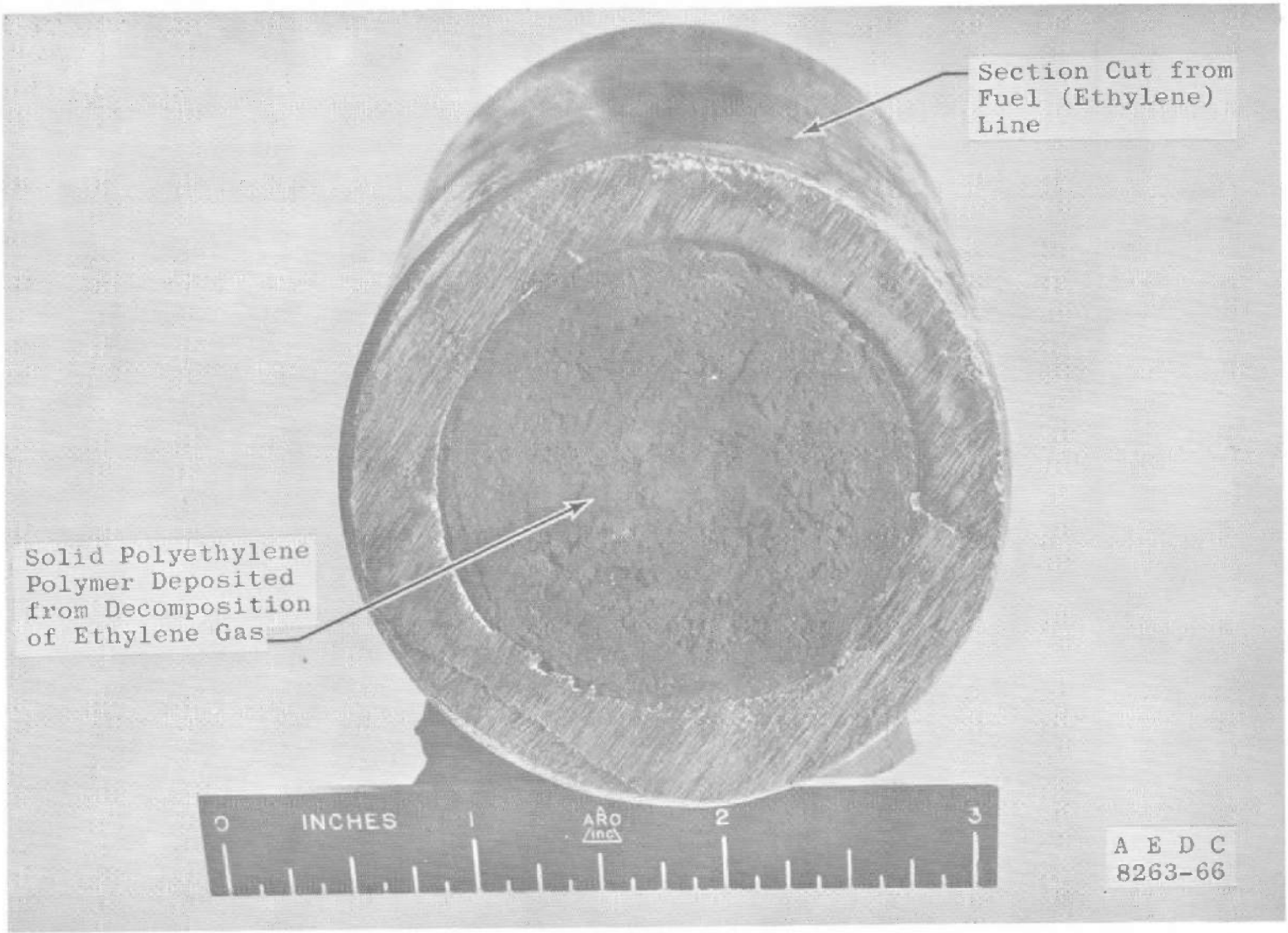

Fig. 18 Photograph of Filled Fuel Line

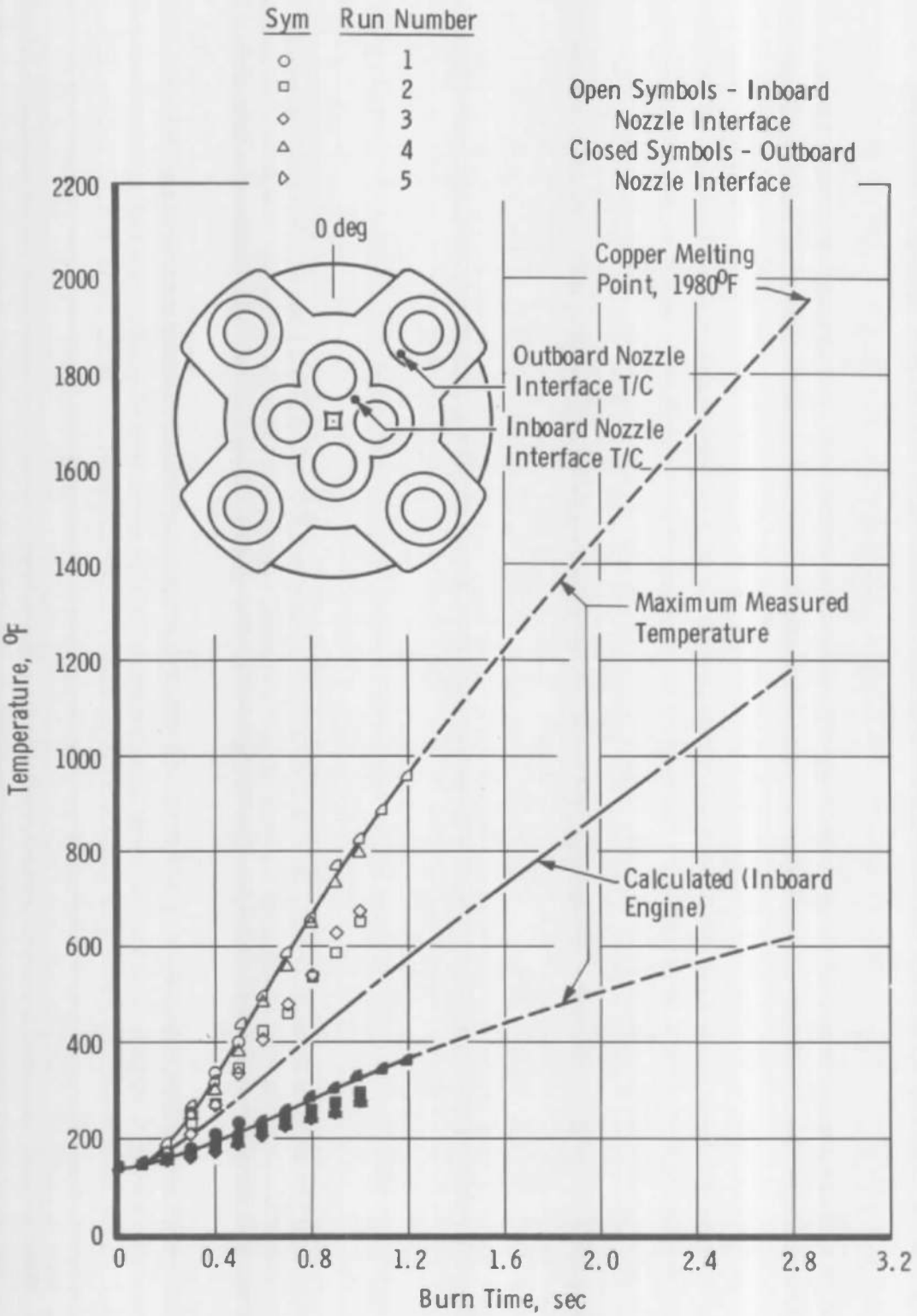

Fig. 19 Temperatures Measured on Combustor Surface at Nozzle Interface

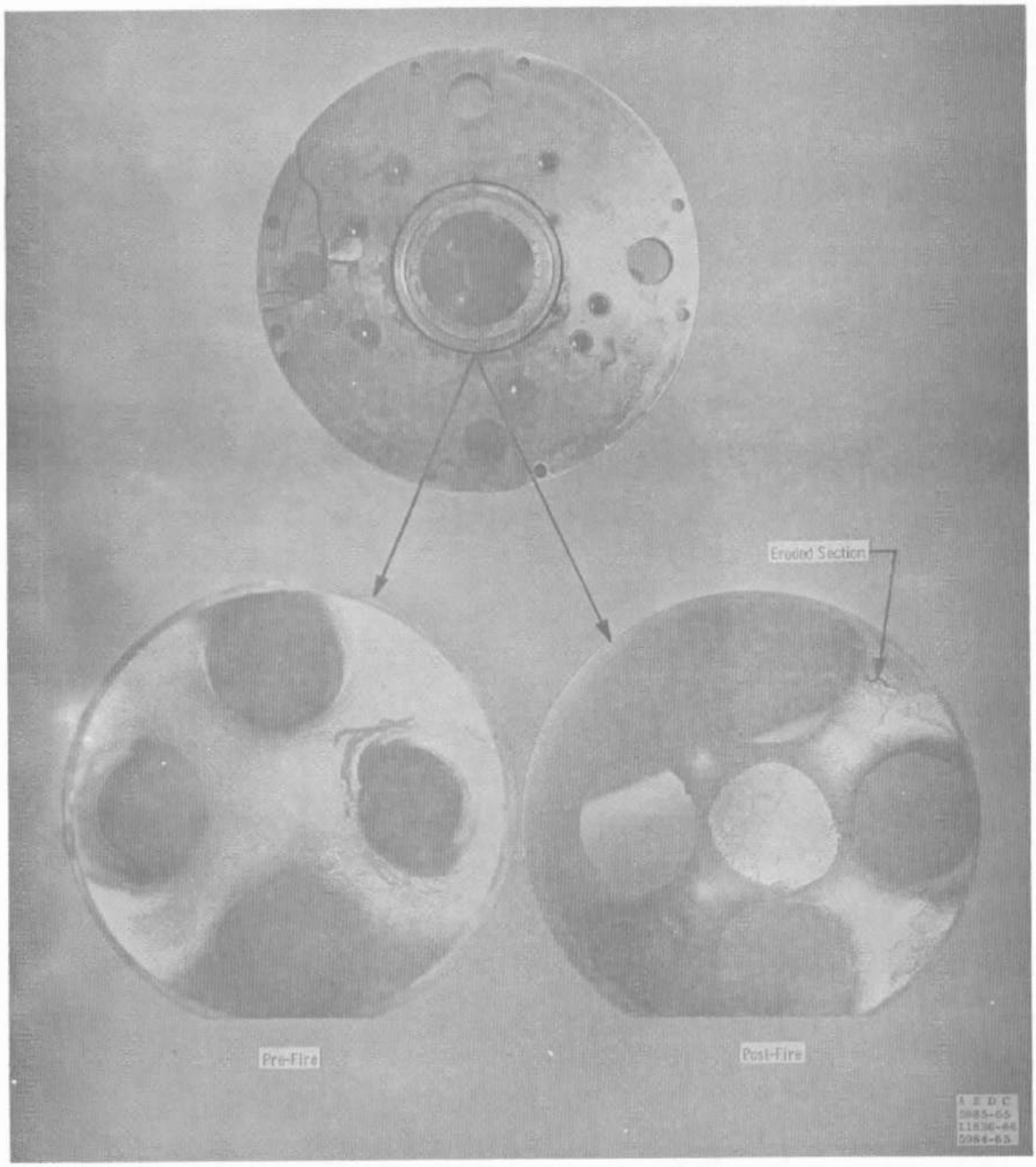

Fig. 20 Photograph of Combustor Interior Showing Erosion on Center Section

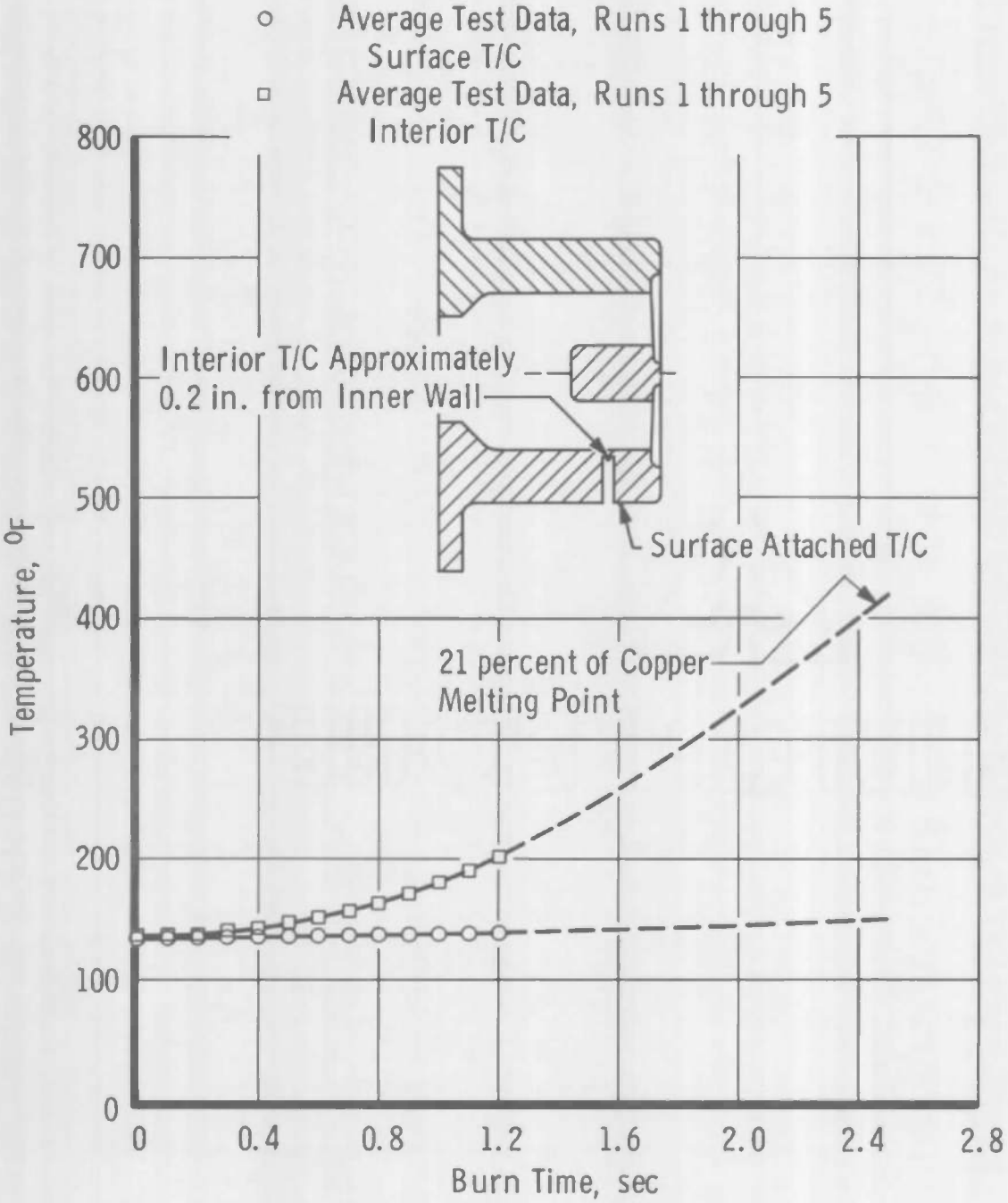

Fig. 21 Combustor Wall Temperature-Time Histories

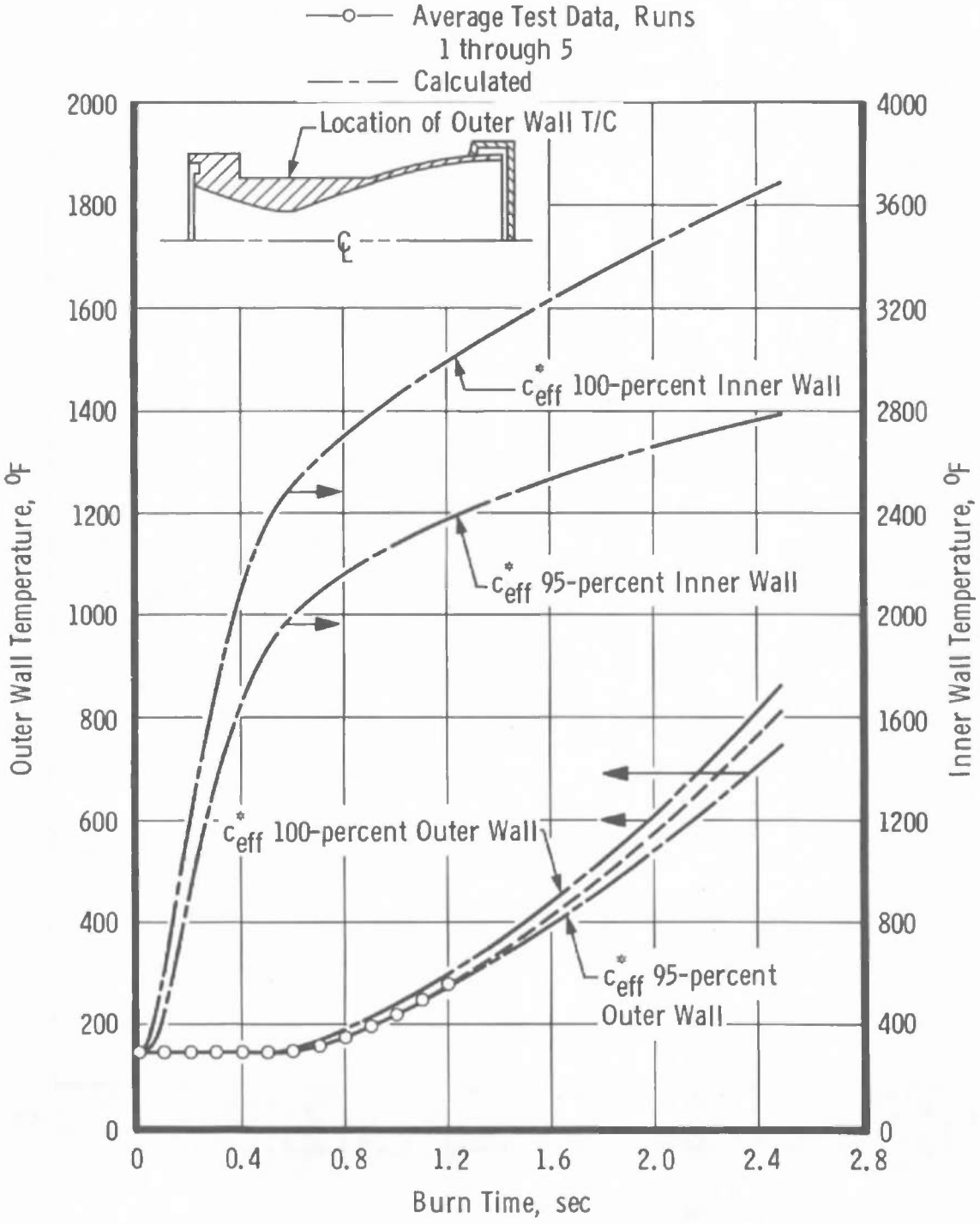

Fig. 22 Comparison of Measured with Calculated Outboard Nozzle Throat Wall Temperatures

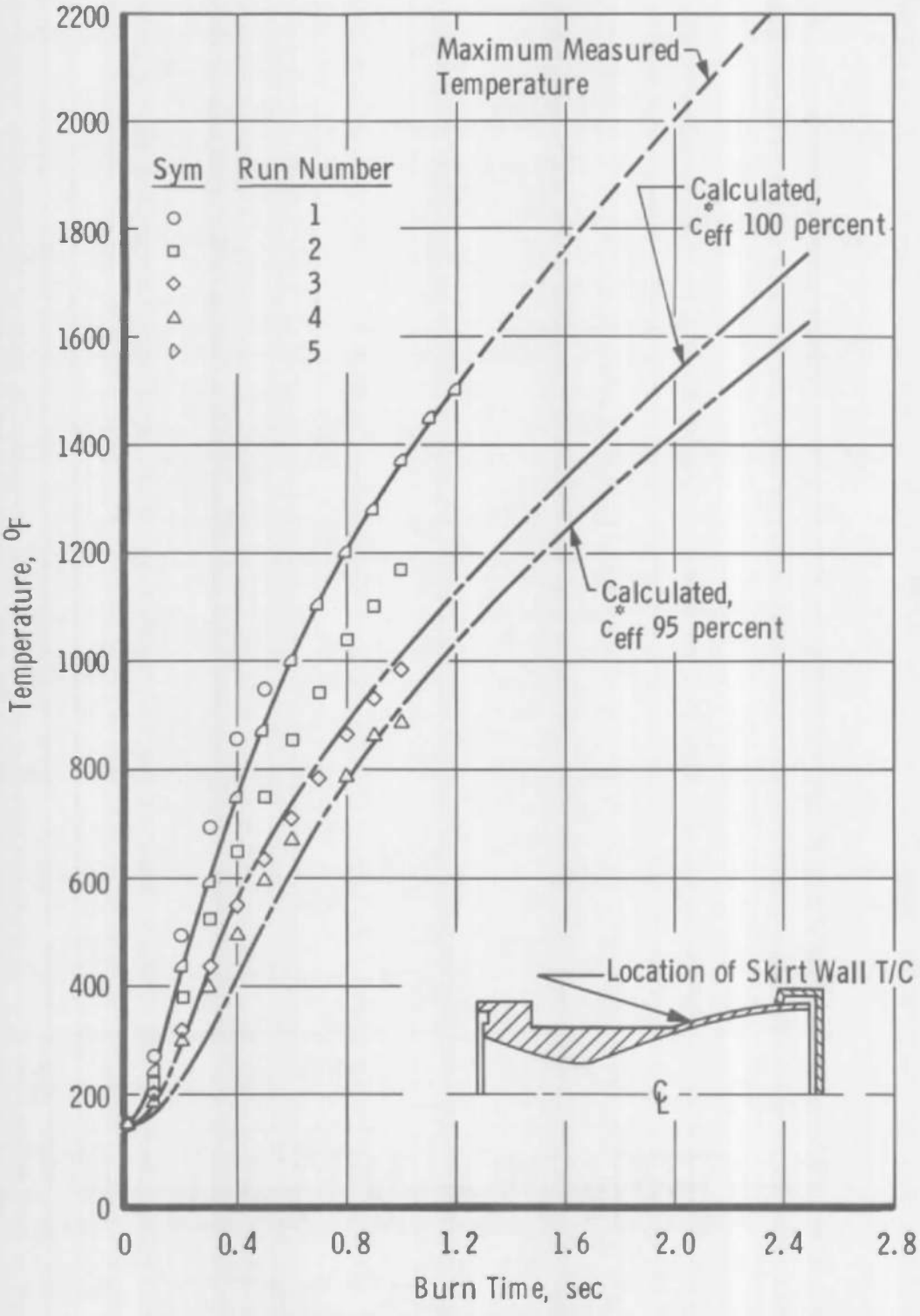

o. Outboard Nozzle

Fig. 23 Comporison of Measured with Colculated Nozzle Skirt Wall Temperoture

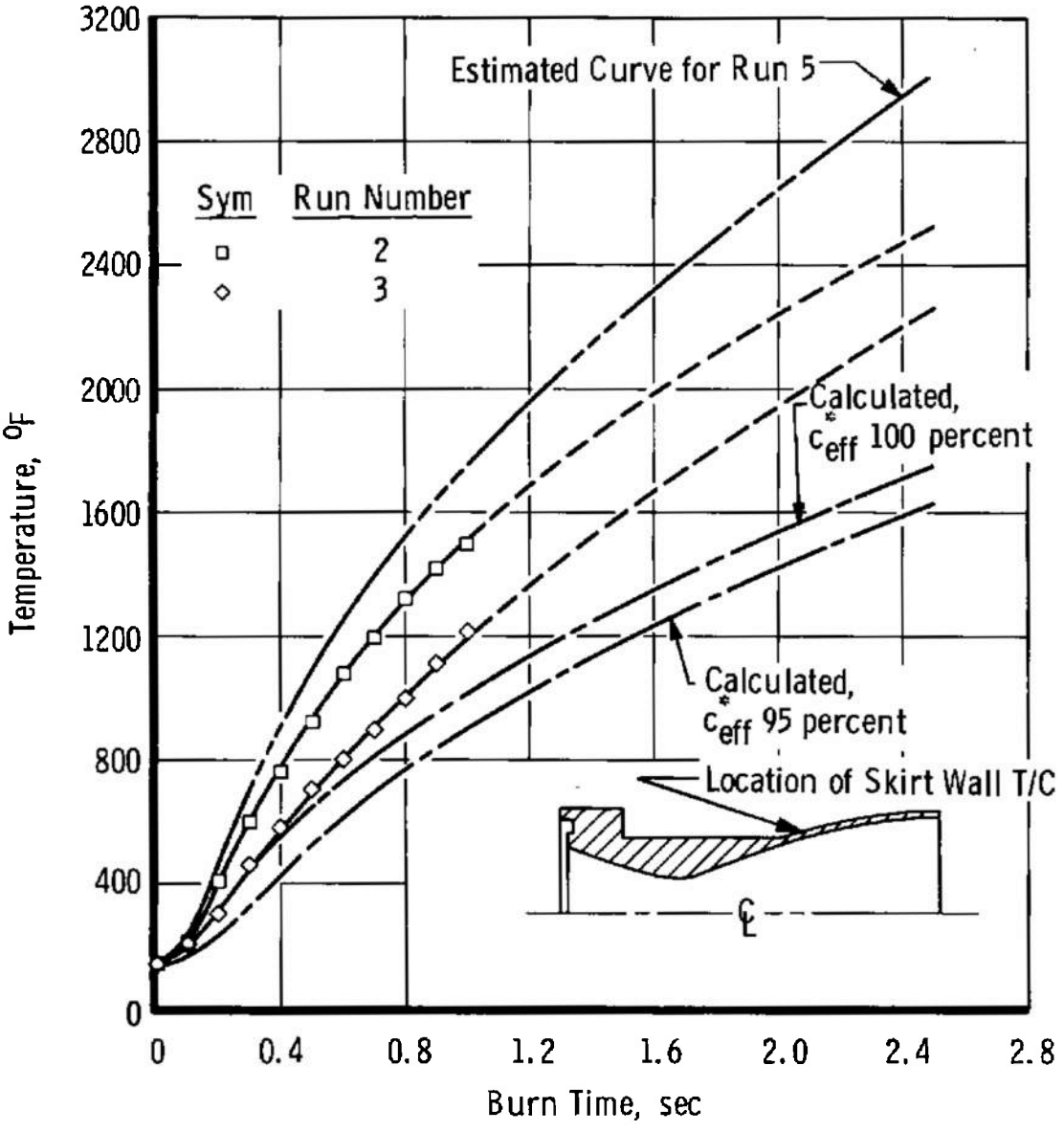

b. Inboard Nozzle

Fig. 23 Concluded

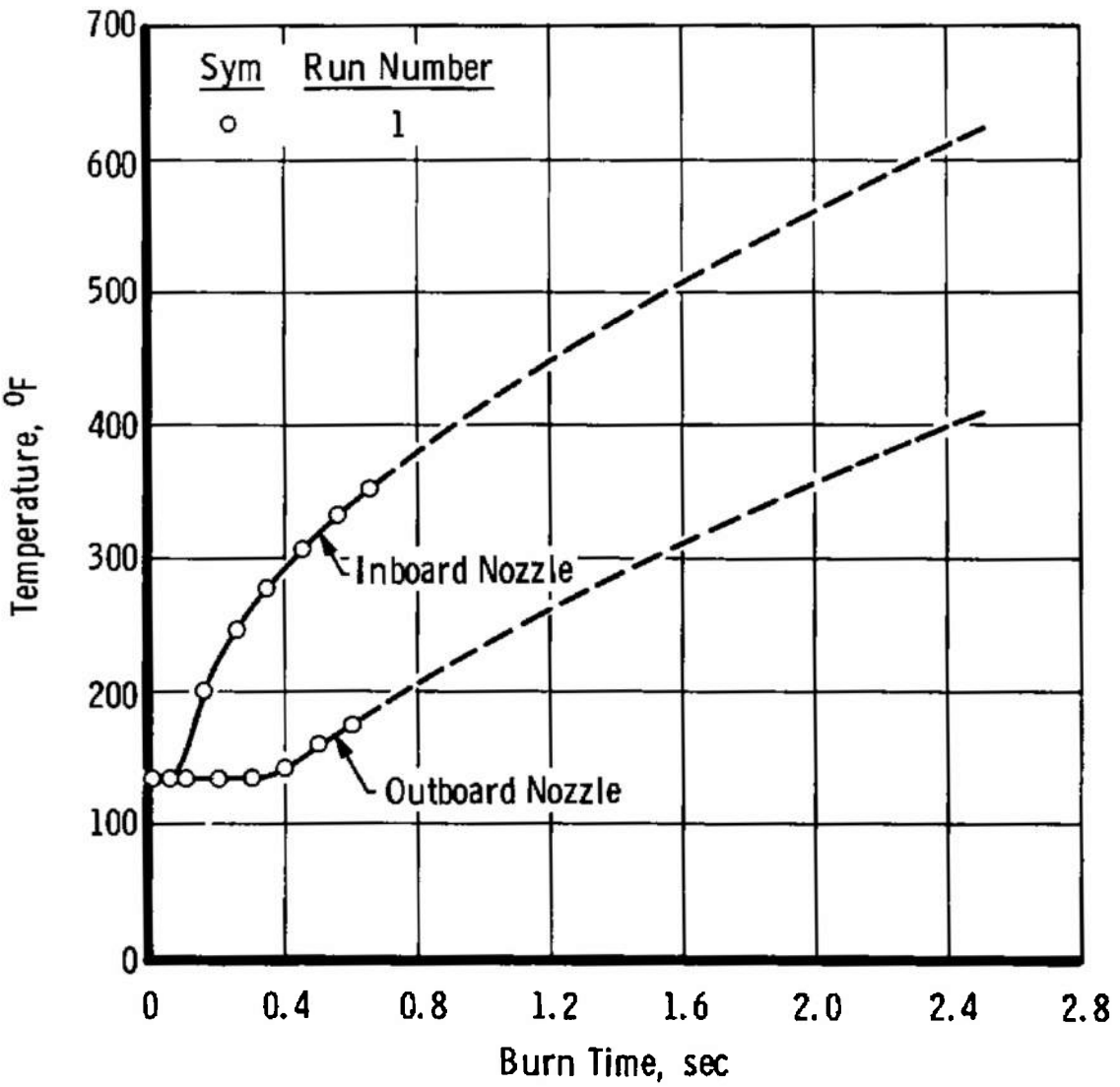

Fig. 24 Temperatures Measured on Nozzle Flange at Combustor Interface

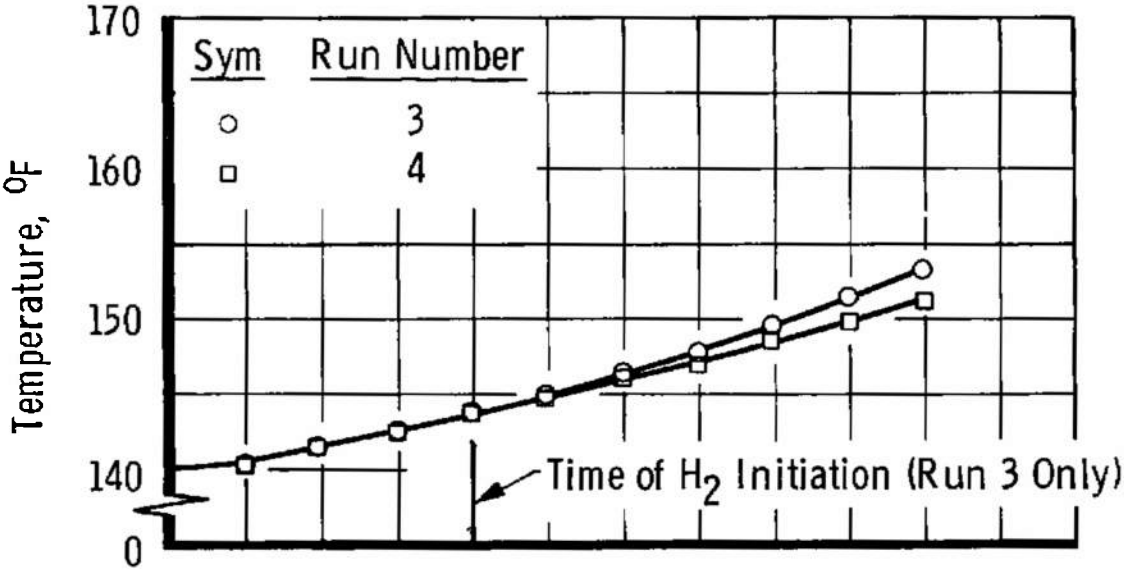

a. Temperature

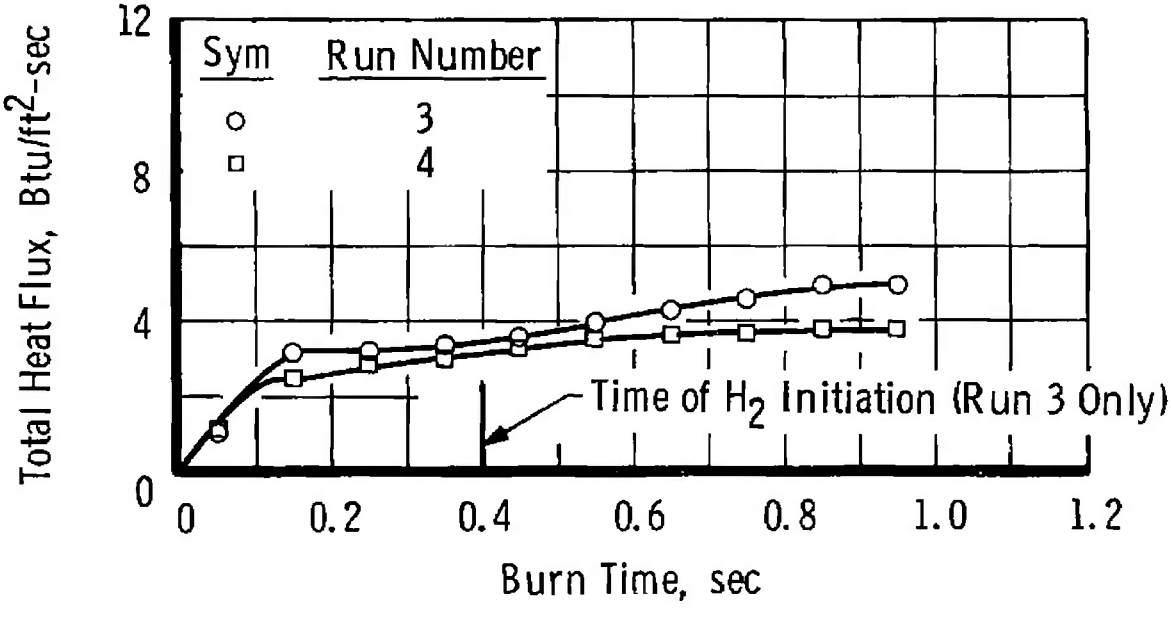

b. Heat Flux

Fig. 25 Typical Temperature and Heat Flux Histories for Base Heat Shield Slug Calorimeters

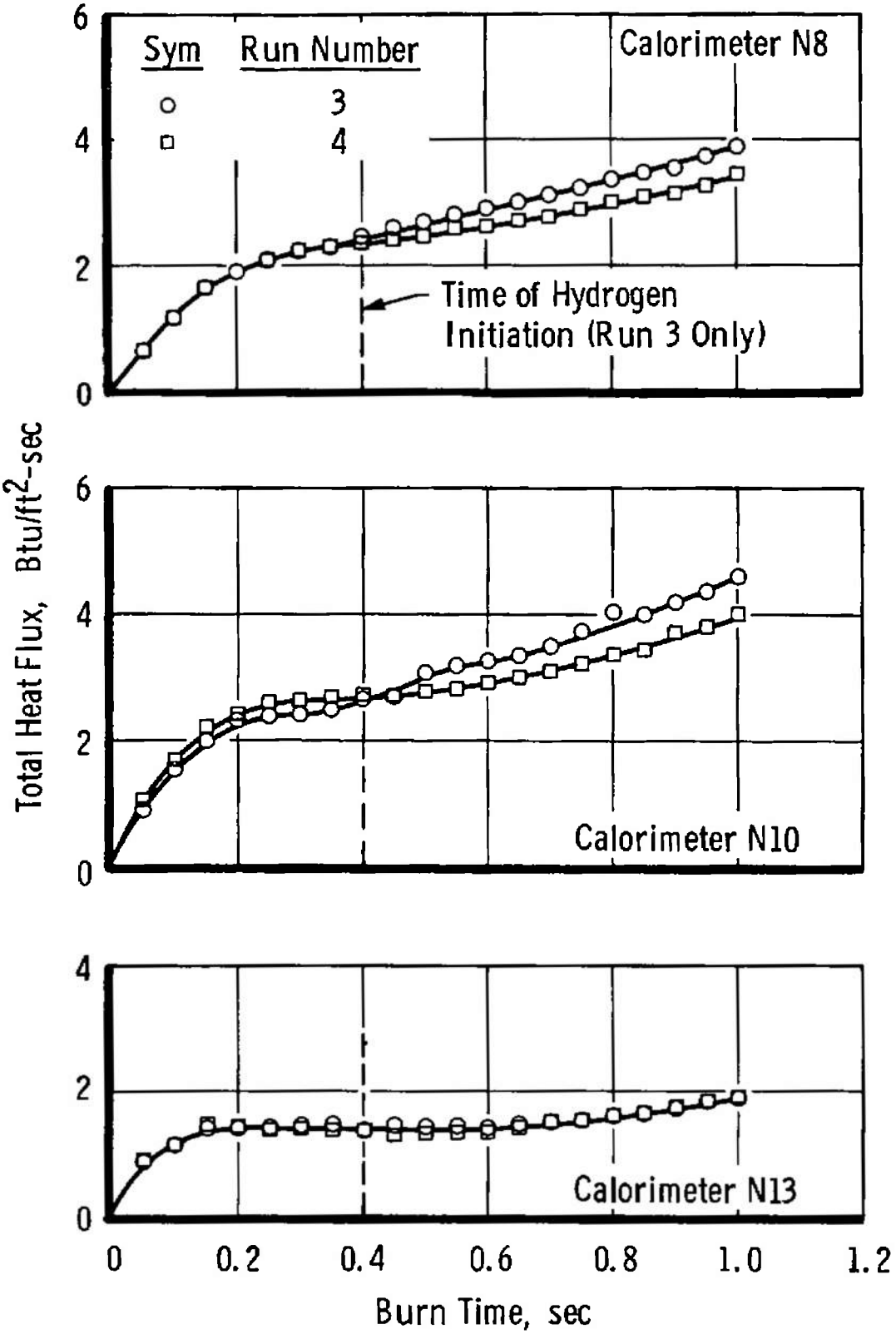

Fig. 26 Typical Heat Flux Histories for Membrane-Type Calorimeter

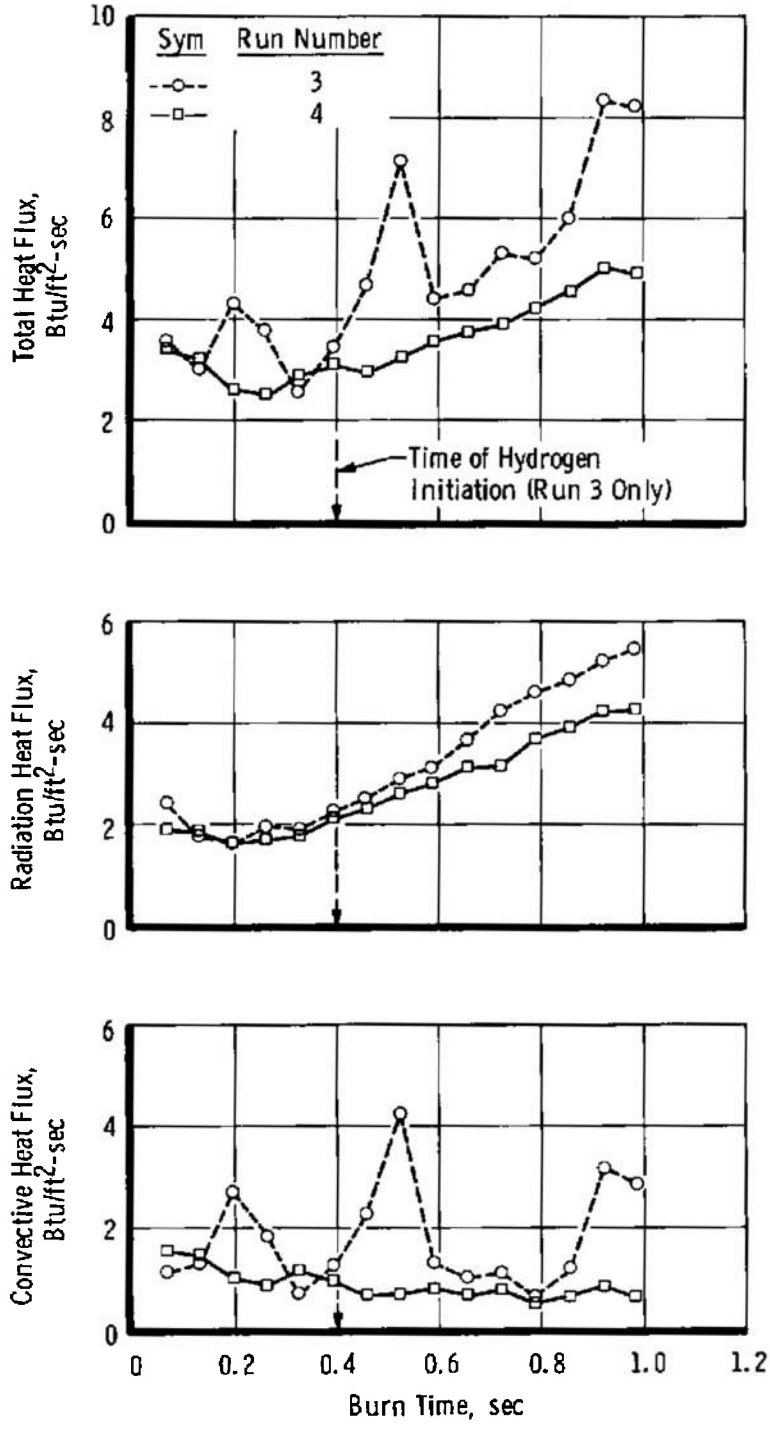

a. Outer Region Calorimeter N12

Fig. 27 Heat Flux Histories for Dual-Element Thin-Film Heat Gages

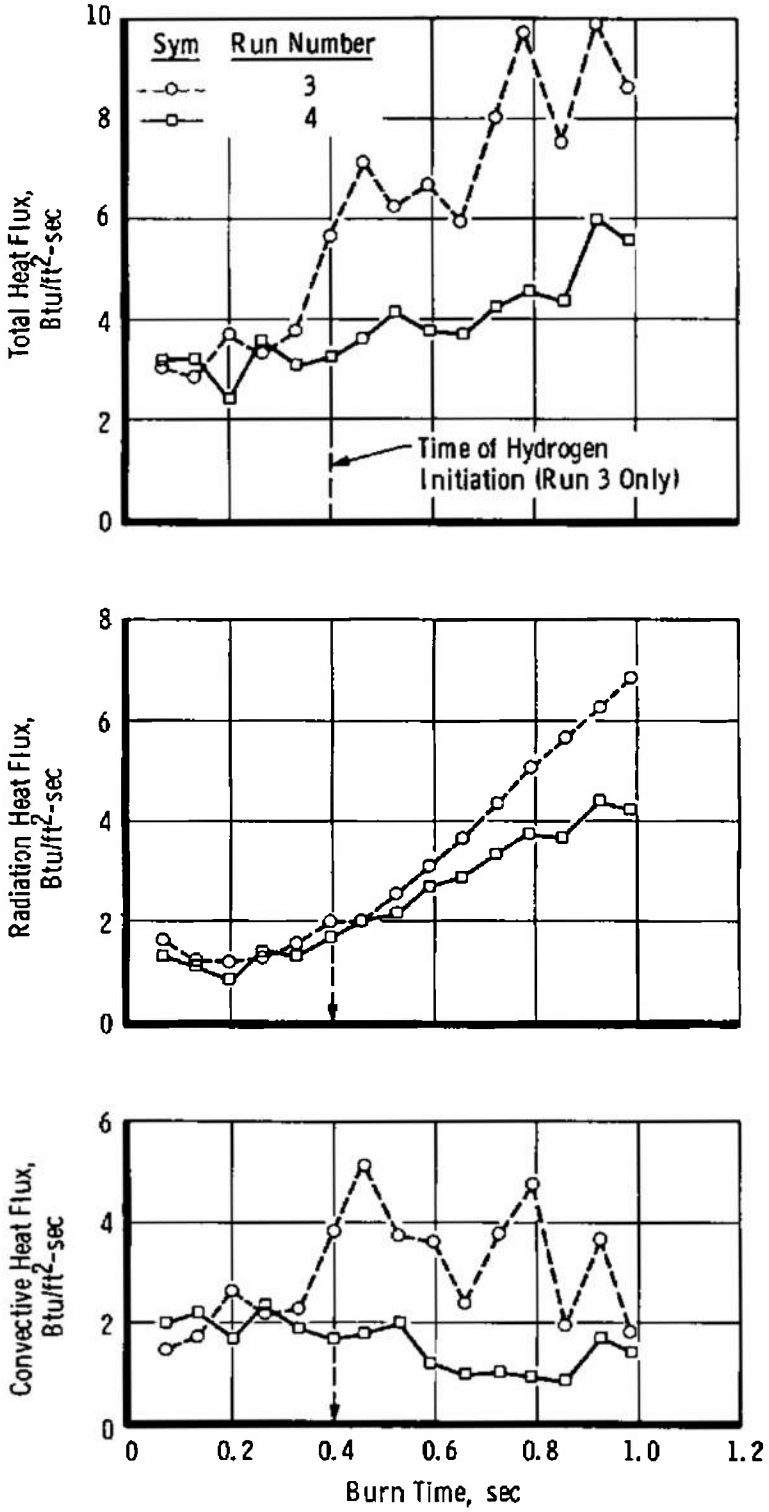

b. Inner Region Calorimeter N16

Fig. 27 Concluded

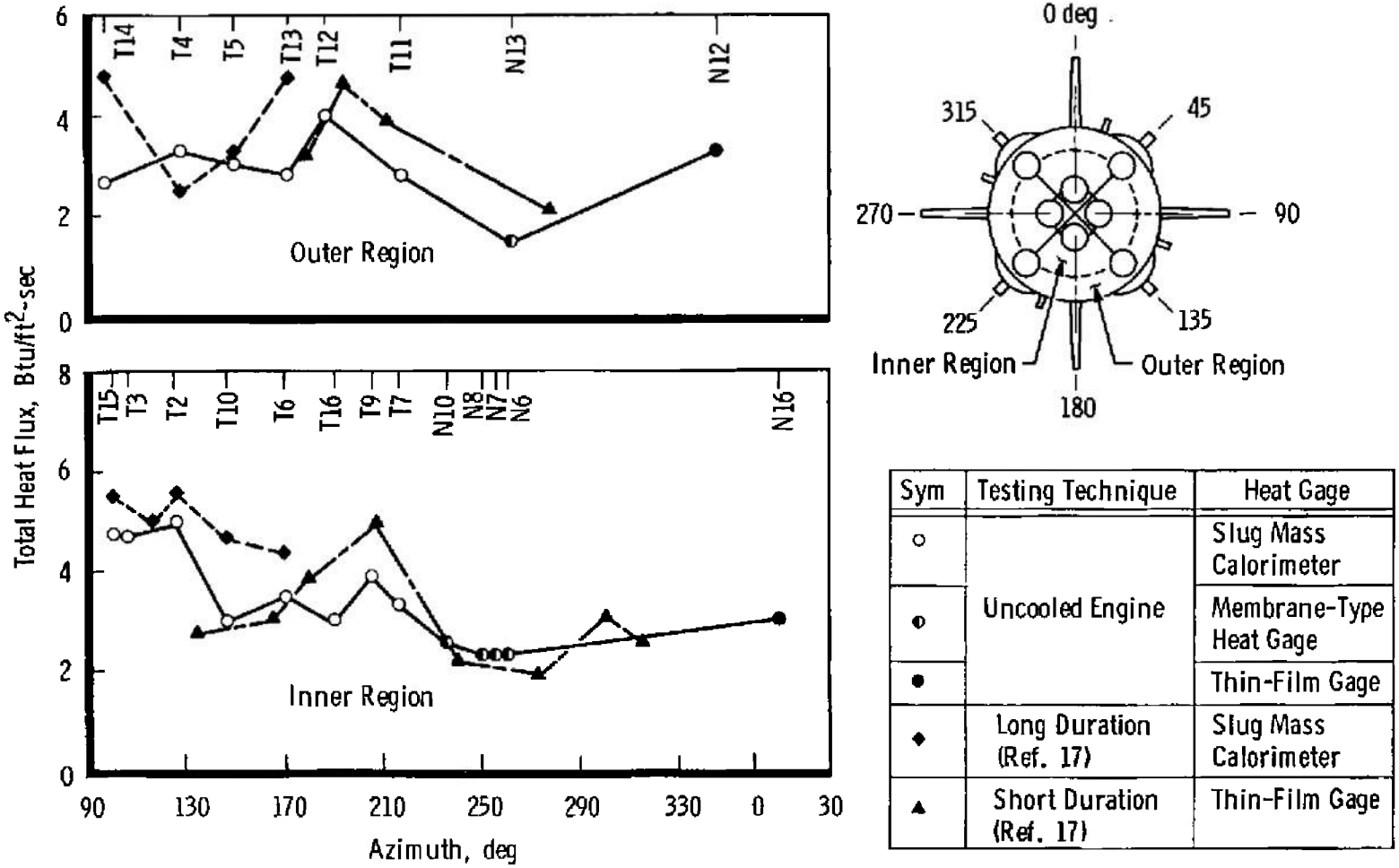

Sym	Testing Technique	Heat Gage
○	Uncooled Engine	Slug Mass Calorimeter
◐		Membrane-Type Heat Gage
●		Thin-Film Gage
◆	Long Duration (Ref. 17)	Slug Mass Calorimeter
▲	Short Duration (Ref. 17)	Thin-Film Gage

a. Without Turbine Exhaust Simulation

Fig. 28 Comparison of Uncooled Engine Model Base Heating Data with Long- and Short-Duration Data

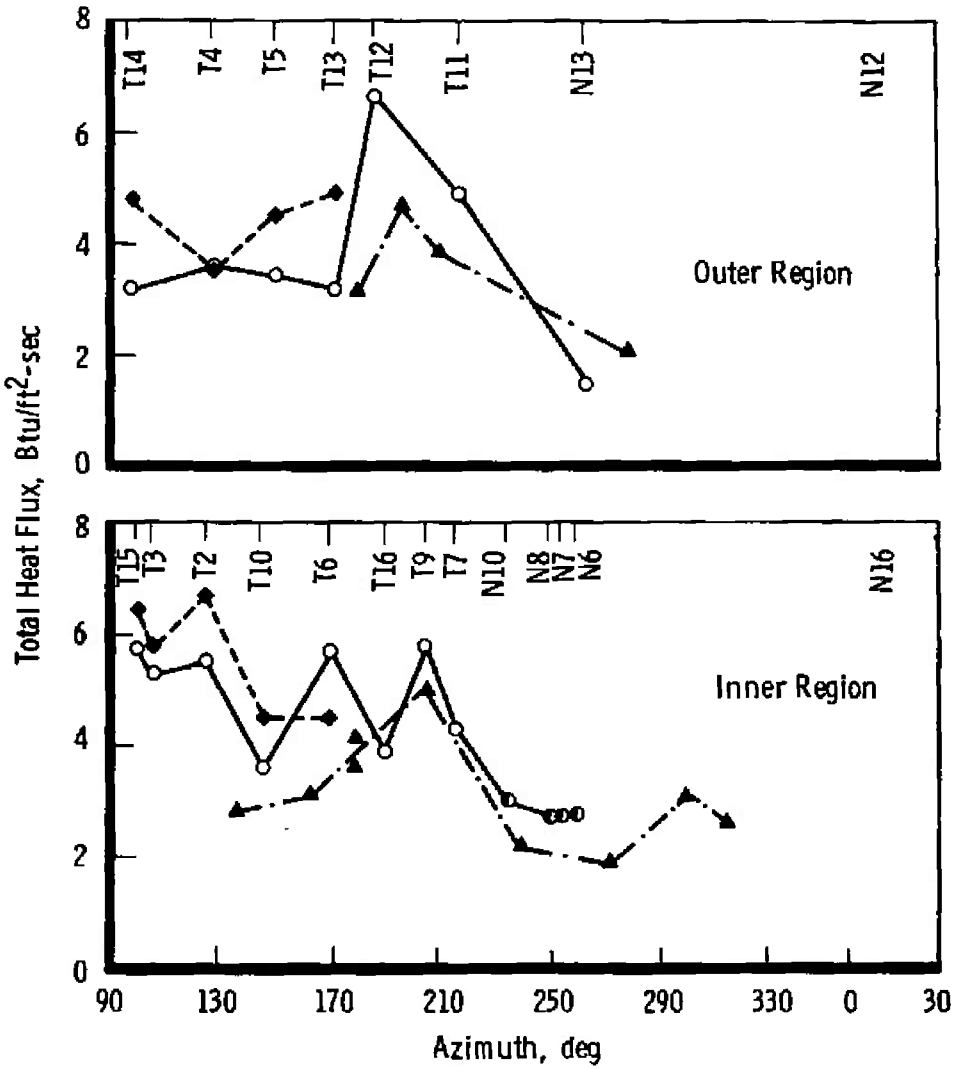

Sym	Testing Technique	Heat Gage
○	Uncooled Engine	Slug Mass Calorimeter
◐		Membrane-Type Heat Gage
●		Thin-Film Gage
◆	Long Duration (Ref. 17)	Slug Mass Calorimeter
▲	Short Duration (Ref. 17)	Thin-Film Gage

b. With Turbine Exhaust Simulation

Fig. 28 Concluded

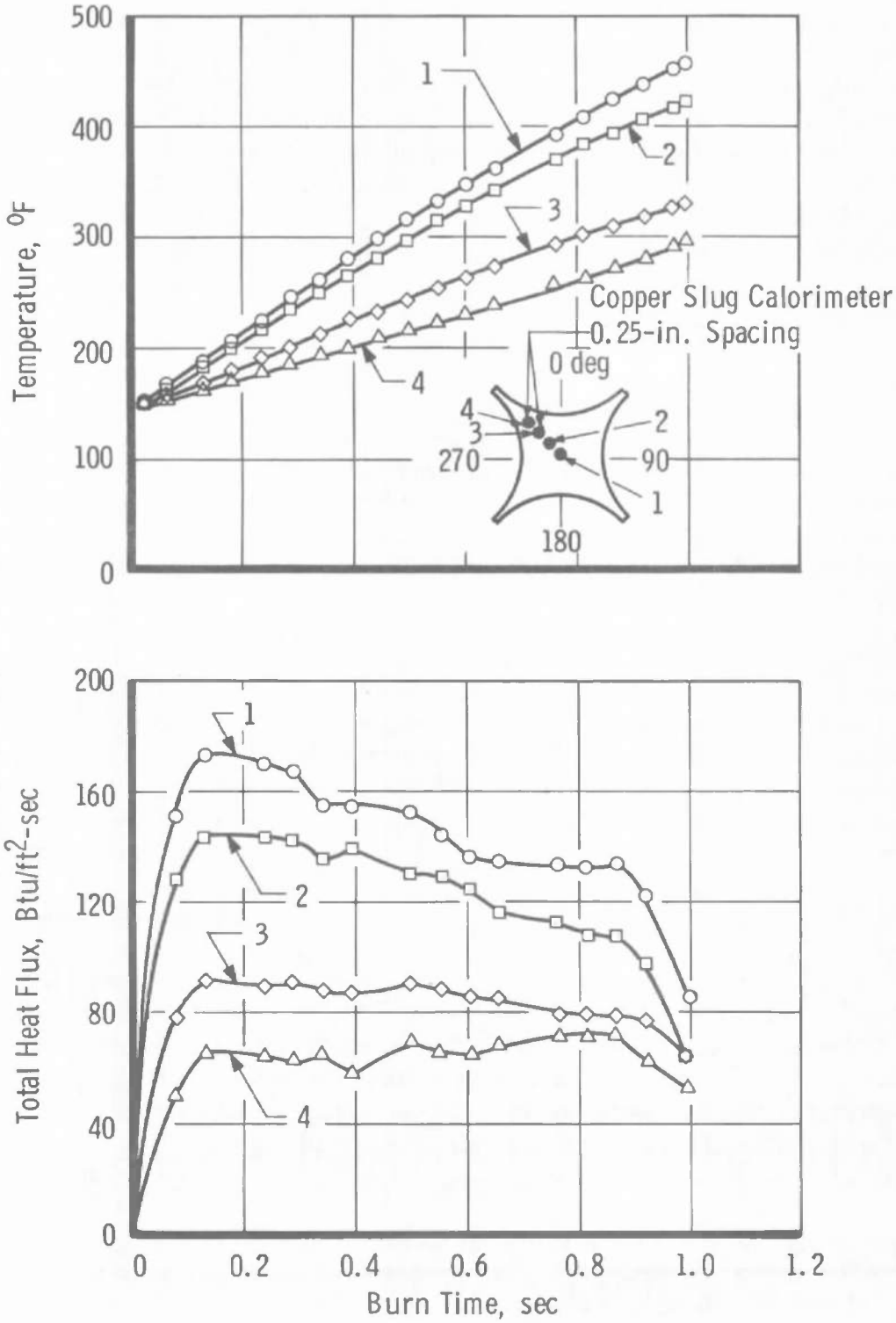

Fig. 29 Typical Temperature and Heat Flux Histories for Uncooled Engine Model Flame Shield Slug Calorimeters

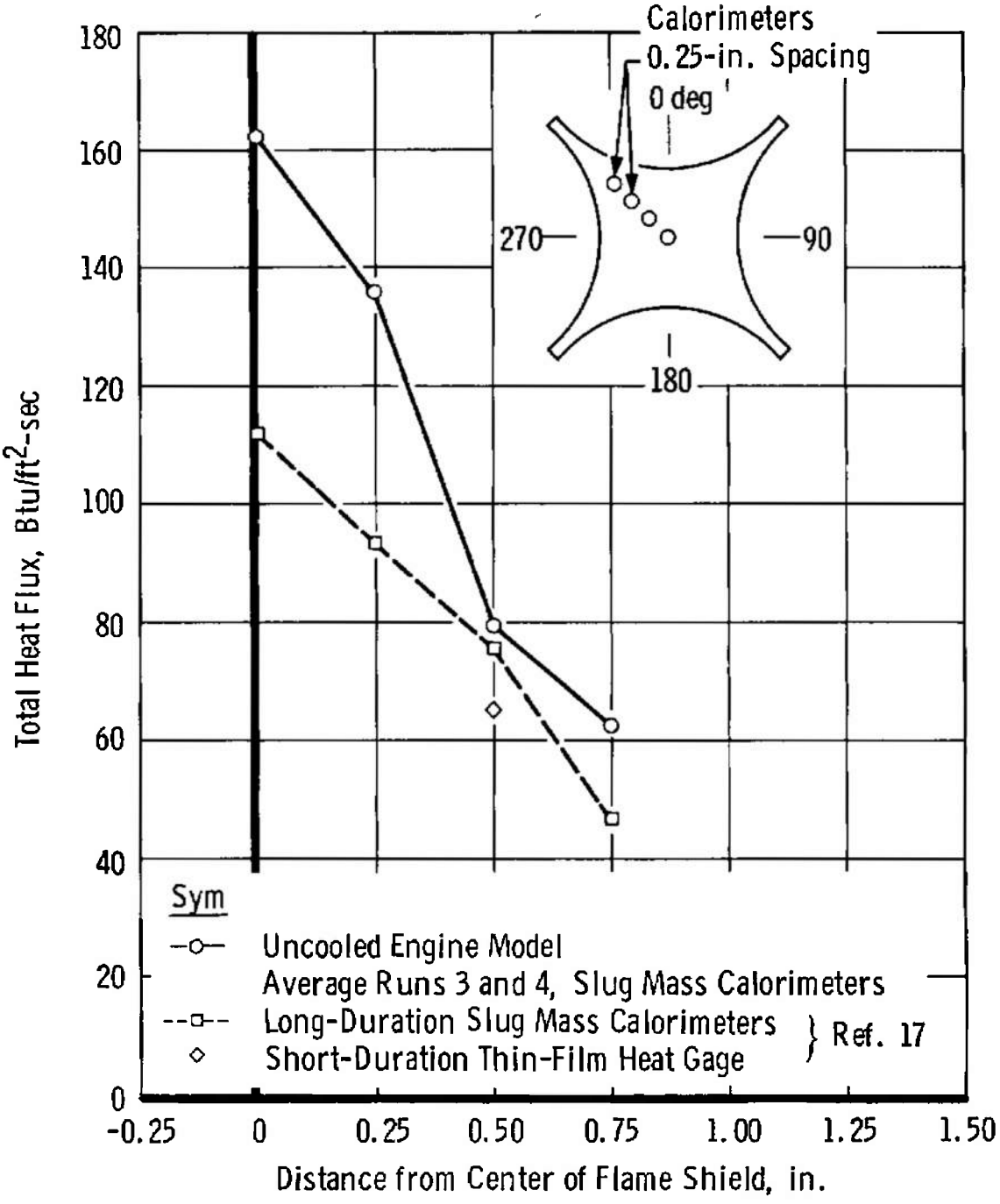

Fig. 30 Comparison of Uncooled Engine Model Flame Shield Heat Flux with Long- and Short-Duration Data

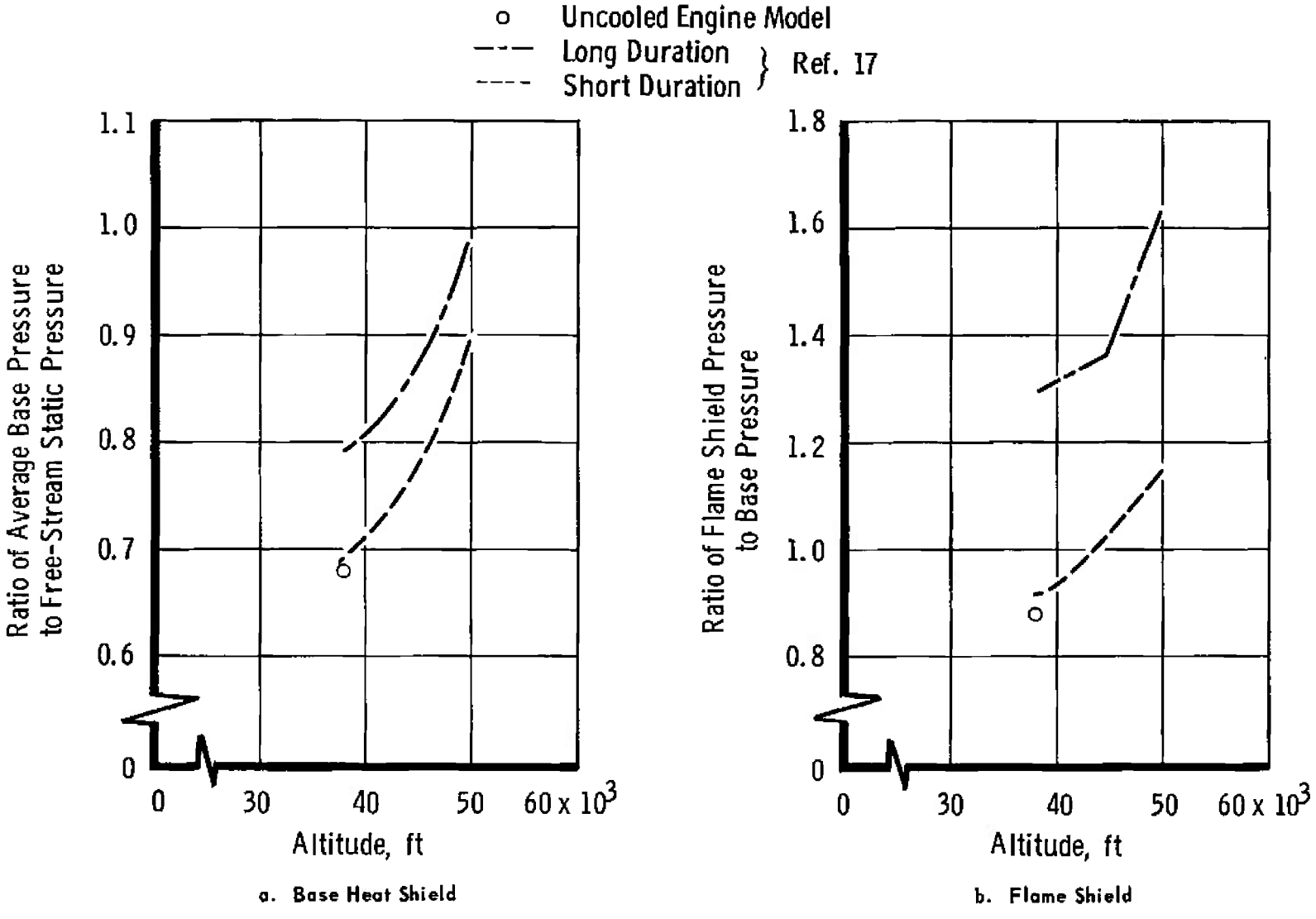

a. Base Heat Shield

b. Flame Shield

Fig. 31 Comparison of Uncooled Engine Model Base Heat Shield and Flame Shield Pressure Data with Short- and Long-Duration Data

TABLE I
COMPARISON OF MODEL DESIGN PARAMETERS

Parameter	Model			Saturn SI-Block II Flight Vehicle
	Short Duration	Uncooled Engine	Long Duration	
Afterbody diameter, in.	14.8	14.8	14.8	277
Nozzle throat diameter, in.	0.884	0.884	0.9	16.50
Nozzle exit diameter, in.	2.5	2.5	2.5	46.74
Nozzle shape	Contoured	Contoured	Contoured	Contoured
Nozzle exit angle, deg	3	3	4	0
Nozzle expansion ratio	8.0:1	8.0:1	7.71:1	8.0:1
Combustion chamber design	Single	Single	Multiple	Multiple
Operating chamber pressure, psia	500	500	500	600
Center engine cant angle, deg	3	3	0	3
Outer engine gimbal angle, deg	6 (fixed)	6 (fixed)	6 (fixed)	6 (neutral)
Oxidizer	Gaseous O_2	Gaseous O_2	Liquid O_2	Liquid O_2
Fuel	Gaseous Ethylene	Gaseous Ethylene	RP-1	RP-1
Coolant	None	None	Water (3 lb/sec)	Fuel
Oxidizer flow rate, lb_m/sec/eng	1.08	1.08	1.5	504
Fuel flow rate, lb_m/sec/eng	0.492	0.492	0.7	212
Operating O/F ratio	2.2	2.2	2.2	2.38
Characteristic velocity, c*, ft/sec	6200	6200	4590	5537
c* Efficiency, percent	100	100	79	96
[1]Isentropic exponent, γ	1.19	1.19	1.25	1.22
[1]Exhaust gas Mach number	2.98	2.98	3.02	2.98
[1]Exhaust gas temperature, °F	3740	3740	1760	3140
Burn time, sec (nominal)	0.050	3.0	20	165

[1]These parameters obtained from Fig. 4.

TABLE II

HIGH-TEMPERATURE PROPERTIES OF 90-PERCENT TANTALUM, 10-PERCENT TUNGSTEN ALLOY, AND OHFC COPPER

High Temperature Properties of 90-percent Tantalum 10-percent Tungsten

Melting Point: 5495°F

Density: 0.608 lb/in.^{3}

Specific Heat: 0.051 Btu/lb-°R

Elevated Temperature Tensile Properties, 0.060-in.-thick sheet (Ref. 33)

	Slow Strain Rate		
Temperature, °F	Ultimate Tensile Strength, psi	Yield Strength, psi	Elongation, percent
1500	103×10^3	98×10^3	11
1800	94×10^3	80×10^3	4
2200	67×10^3	55×10^3	4
2500	22×10^3	20×10^3	22
2600	21×10^3	14×10^3	17
3000	12×10^3	12×10^3	33
3500	7.5×10^3	7.2×10^3	37
4000	4.3×10^3	4.3×10^3	35
4500	2.1×10^3	2.0×10^3	30
5000	0.6×10^3	0.6×10^3	20

Thermal Conductivity, K (Ref. 33)

Temperature, °F	K, Btu/ft^2-sec-°F/ft
2600	0.00907
3140	0.00834
3500	0.00786
4040	0.00719
4400	0.00672
4940	0.00598
5300	0.00551

High Temperature Properties of OFHC Copper

Melting Point: 1980°F

Density: 0.323 lb/in.^{3}

Specific Heat: 0.092 Btu/lb-°R

Thermal Conductivity: 0.0625 Btu/ft^2-sec-°F/ft

Short Time Elevated Temperature Tensile Properties (Ref. 34)

Temperature, °F	Tensile Strength, 1000 psi
Room Temperature	34.4
250	29.8
450	24.8
650	19.9
1000	8.6
1300	3.4

TABLE III
INSTRUMENTATION

Parameter	Estimated System Accuracy Assumes Steady-State Signal at Operating Level	Measuring Device	Range of Measuring Device	Recording Device
Base Heat Flux	±5°F	CA Thermocouple Attached to Copper Slug	0-600°F	Multi-Channel Analog-to-Digital Converter
Base Heat Flux	±1.5 mv	Membrane Calorimeter	0-10 mv	Multi-Channel Analog-to-Digital Converter
Base Heat Flux	Unknown	CAL Thin-Film Heat Gage	0-300 Btu/ft^2-sec	Multi-Channel Analog-to-Digital Converter
Base Pressures	±3 percent	Strain-Gage-Type Pressure Transducer	0-10 psia	Oscillograph
Combustor Chamber Pressure	±2 percent	Strain-Gage-Type Pressure Transducer	0-1000 psia	Direct Print Oscillograph
Combustor and Nozzle Wall Temperatures	±10°F	CA Thermocouple	0-2500°F	Multi-Channel Analog-to-Digital Converter Strip Chart Oscillograph
Propellant System Pressures	±2 percent	Kistler Crystal Transducer and Charge Amplifiers	0-2000 psia	Direct Print Oscillograph
	±2 percent	Strain-Gage-Type Pressure Transducer		
Propellant System Temperatures	±10°F	CA Thermocouples	0-500°F	Strip Charts
Test Cell Pressures	±0.05 in. Hg	Mercury Manometers	0-16 psia	Photographic
	±3 percent	Strain-Gage-Type Pressure Transducer	0-25 psia	Oscillograph

TABLE IV
SUMMARY OF THE INTERMEDIATE-DURATION ENGINE OPERATING CHARACTERISTICS

Sym	Parameter \ Run Number	1	2	3	4	5
PRO	O_2 Reservoir Pressure, psia	1522	1432	1429	1425	1409
PLO	O_2 Line Pressure, psia	1398	1266	1267	1267	1228
PVO	O_2 Venturi Pressure, psia	Void	377	446	438	426
PIJI	O_2 Injector Pressure, psia	Void	Void	818	810	828
TLO	O_2 Temperature, °F	80	91	104	90	100
PRCH	C_2H_4 Reservoir Pressure, psia	1547	1332	1412	1384	1384
PLCH	C_2H_4 Line Pressure, psia	1425	1240	1338	1327	1327
PVCH	C_2H_4 Venturi Pressure, psia	Void	691	751	723	723
PIJ2	C_2H_4 Injector Pressure, psia	Void	Void	Void	Void	Void
TLCH	C_2H_4 Temperature, °F	250	192	182	183	192
$\dot{w}_O$	O_2 Flow Rate, lb_m/sec	8.80	7.92	7.85	7.92	7.60
$\dot{w}_C$	C_2H_4 Flow Rate, lb_m/sec	3.80	3.60	4.00	3.95	3.90
$\dot{w}_T$	Total Flow Rate, lb_m/sec	12.6	11.52	11.85	11.87	11.50
O/F	Oxidizer/Fuel Ratio	2.3	2.2	2.0	2.0	2.0
PC	Chamber Pressure, psia	505	454	495	495	478
c*	Characteristic Velocity, ft/sec	6323	6208	6573	6578	6573
t	Run Time, sec	0.5	1.0	1.0	1.0	1.2

APPENDIX I
NOZZLE HEAT TRANSFER CALCULATIONS

Determination of the minimum nozzle throat wall thickness required for a given burn duration consisted of (1) calculating a gas side film coefficient and (2) specifying a maximum allowable throat inner wall temperature, then calculating the wall thickness corresponding to the desired burn duration using an analytical solution for transient, one-dimensional heat conduction in a cylindrical section subjected to sudden internal heating. The method and charts used for this calculation can be found in Temperature Response Charts by Schneider (Ref. 27).

The following equation (Ref. 28) was used for calculating the film coefficient at the nozzle throat:

$$h_g = 0.026 \frac{K}{D} \left(\frac{DV\rho}{\mu g}\right)^{0.8} \left(\frac{\mu g C_p}{K}\right)^{0.4}$$

where

D = throat diameter, ft

V = velocity, ft/sec

g = dimensional constant, $32.174 \frac{lb_m\text{-ft}}{lb_f\text{-sec}^2}$

The gas viscosity (μ), density (ρ), specific heat (c_p), and gas conductivity (K) were assumed constant and were obtained from Ref. 29.

The chamber gas temperature was calculated from

$$T_{c_m} = T_{c_T} \left(\frac{c^*_m}{c^*_T}\right)^2$$

where

T_{c_m} = chamber temperature calculated for model, °R

T_{c_T} = theoretical chamber temperature = 6700°R (Fig. 4)

c^*_m = characteristic velocity for model engines, ft/sec

c^*_T = theoretical characteristic velocity, ft/sec

A combustion efficiency $\left(\frac{c^*_m}{c^*_T}\right)$ of 95 percent was assumed in computing T_{cm}. The static temperature and pressure at the nozzle throat used in the calculation of h_g were obtained from isentropic flow relationships given in Ref. 30 for $\gamma = 1.22$.

The results of the transient heat conduction calculations are plotted in Fig. I-1, which shows wall thickness as a function of burn time required for the throat inner wall temperature to reach 4120°F (75 percent of the throat material melting point) with chamber pressures of 300, 500, and 1000 psia and assuming a c* efficiency of 95 and 100 percent. In the actual nozzle design, the throat section wall thickness was made twice as thick as the calculations indicated was required in order to provide an adequate safety factor and ensure that local melting did not occur at the nozzle throat.

By using essentially the same calculation procedure described above, but holding the wall thickness constant and varying burn time, the nozzle throat inner and outer wall temperature histories were calculated and are presented in Fig. I-2. Actual nozzle throat wall thickness of 0.528 in. was used in these calculations.

p_c, psia	h_g, Btu/ft^2-sec/^{o}F	c^*_{eff}	T_{c_T}, ^{o}R	T_{c_m}, ^{o}R	T_{s_T}, ^{o}R
300	0.322	100	6700	6700	6080
500	0.50	95	6700	6050	5500
1000	1.16	100	6700	6700	6080

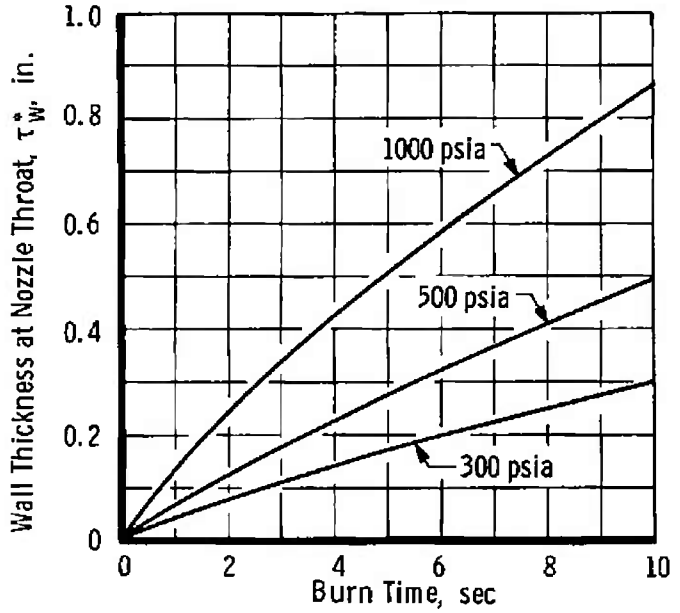

Fig. I-1 Minimum Throat Wall Thickness as a Function of Burn Time for Inner Wall Temperature to Reach 75 percent of TA-10W Melting Point (4120°F)

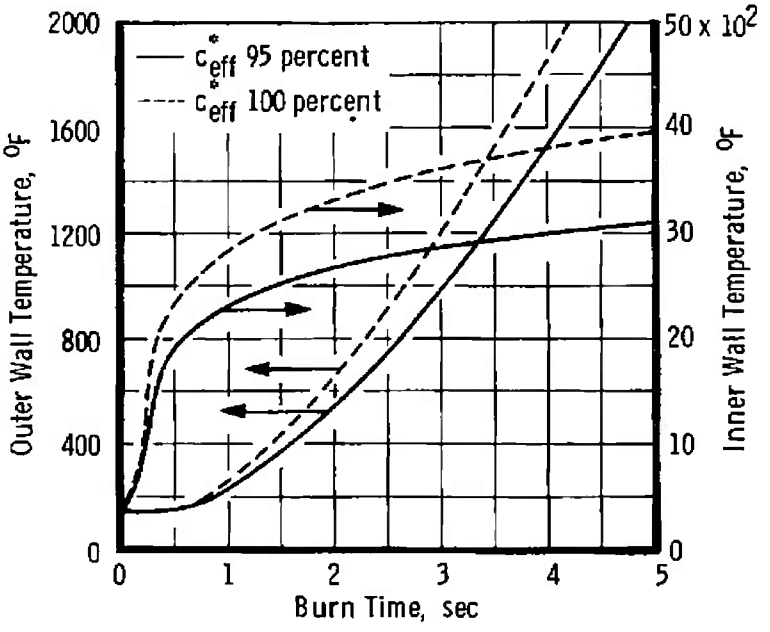

Fig. I-2 Theoretical Temperature of Nozzle Throat Inner and Outer Walls

APPENDIX II
METHOD OF CALCULATING PROPELLANT FLOW RATES

Oxygen is assumed a perfect gas at the conditions prevailing throughout the propellant supply system and did not pose any specific flow measuring problems. The flow rate of oxygen through the sonic venturi was calculated at the venturi throat using the continuity equation written in the following form:

$$\dot{w} = C_D A(P) \frac{\dot{m}(P/P_T)}{\sqrt{T_t}}$$

where

$\dot{m}$ = mass flow function

$$\dot{m} = M \left[\frac{\gamma g_c}{R}\right]^{1/2} \left[1 + \frac{\gamma - 1}{2} M^2\right]^{1/2}$$

M = Mach number (M = 1 at venturi throat)

γ = ratio of specific heats = 1.4

q_c = unit conversion factor, 32.174 lb_m-ft/lb_f-sec^2

R = gas constant, 48.31 lb_f-ft/lb_m-°R

A = venturi throat area, $in.^2$

P = oxygen line pressure, psia

P/P_T = static to total pressure ratio = $\left(1 + \frac{\gamma - 1}{2} M^2\right)^{-\frac{\gamma}{\gamma - 1}}$

T_t = absolute gas temperature, °R

Ethylene, on the other hand, is a highly imperfect gas and must be treated differently to avoid serious flow calculation errors. To ensure steady and predictable flow, the gas must be heated to prevent two-phase flow during expansions encountered in the flow process.

The ethylene flow rate was determined from Mollier diagram data and by using the following procedure:

$$\text{Flow rate, } \dot{w} = C_D A \rho V$$

where

C_D = 0.99

A = venturi throat area, ft^2

ρ = gas density, lb_m/ft^3

V = gas velocity = $(\Delta h 2 g_c J)^{1/2}$, ft/sec

Δh = enthalpy change, Btu/lb_m

$$g_c = 32.174 \frac{lb_m\text{-}ft}{lb_f\text{-}sec}$$

$$J = 778.2 \frac{ft\text{-}lbf}{Btu}$$

A starting point was established on the Mollier diagram at the intersection of constant pressure-temperature lines corresponding to conditions just upstream of the flow measuring venturi. The enthalpy, h_1, at this point was noted and, by moving along a constant entropy line to an arbitrary new h_2, the velocity was calculated using $(\Delta h 2 g_c J)^{1/2}$ where $\Delta h = h_2 - h_1$. The average gas density (ρ) between h_1 and h_2 was obtained from the specific volume line, and the product ρV was calculated. The process was continued on to a new h_3, h_4, h_5, . . . etc., until ρV reached a maximum value. This maximum value of ρV occurs at the venturi throat; therefore, it can be substituted into the continuity equation and the maximum ethylene flow rate calculated which corresponds to the initial upstream pressure-temperature conditions.

These procedures were used to construct the family of propellant flow curves shown in Fig. II-1. These curves were then used to determine propellant flow rates for the tests reported herein.

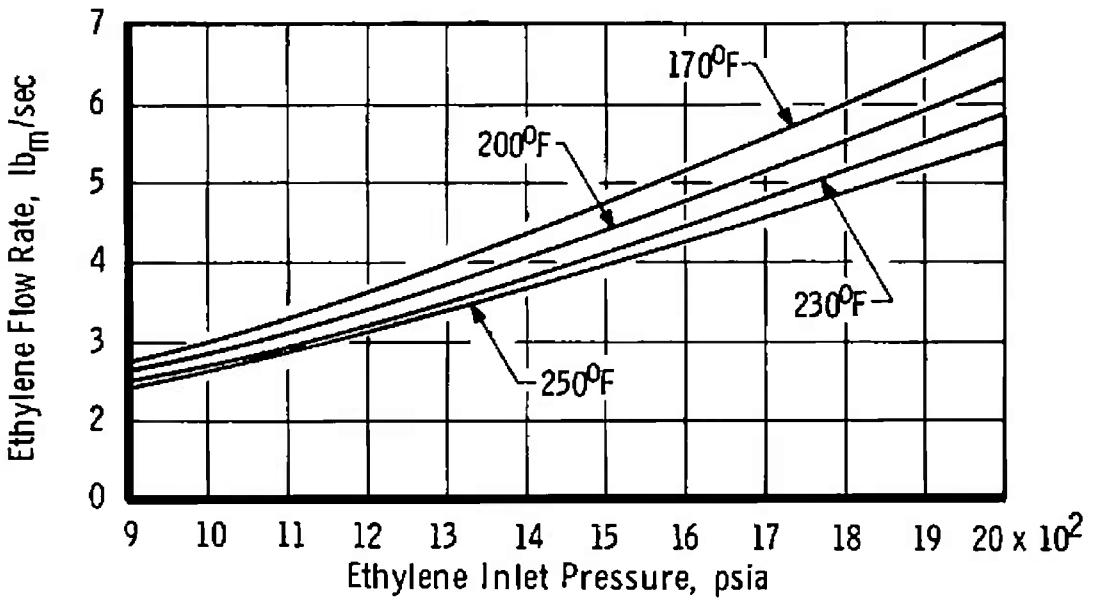

a. Ethylene

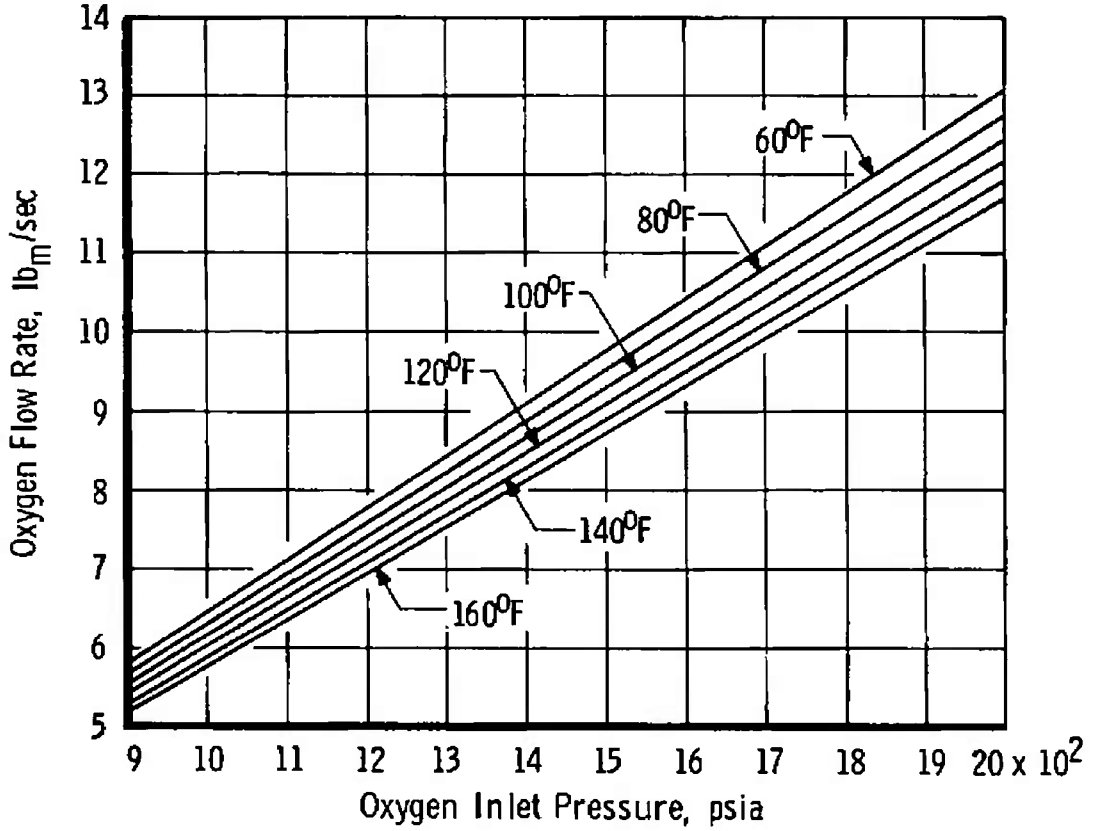

b. Oxygen

Fig. II-1 Propellant Flow Rates for Various Venturi Inlet Pressures and Temperatures

APPENDIX III
DETAILS OF MODEL BASE HEAT FLUX INSTRUMENTATION

Slug Mass Calorimeters

The method of data reduction for the slug mass calorimeters consisted of evaluating the slope of the slug temperature history at 0.10-sec intervals and applying the appropriate slug constant according to the following equation:

$$q = K \frac{dT}{dt}$$

where

$K = \frac{c_p m}{A}$ = 0.2786 for calorimeters T2 through T16 and 0.4503 for T17 through T20

c_p = specific heat of copper slug, $Btu/lb_m-°F$

m = mass of slug, lb_m

A = exposed surface area of slug, ft

dT/dt = slope of slug temperature history

Most of the errors associated with slug mass calorimeters, which are exposed to a heat input for relatively long periods of time and consequently attain high temperatures, were probably not encountered in these tests because of the small slug temperature rise (nominally 15°F). Some advantages and disadvantages of using slug mass calorimeters for model base heat flux measurements are presented in Ref. 31.

Membrane-Type Heat Gages

Instruments of this type consisted of a thin, blackened constantan sensor disc connected at its edges to a larger copper heat sink. These two materials have a combination of physical properties which provide a linear relation between the instrument output and incident heat flux. One end of a fine copper wire is butt-welded to the center of the constantan disk; another copper wire is connected to the heat sink. The potential (E) between these two wires was measured, and the heat flux (q) was evaluated from q = K x E, where K is a constant determined during calibration of the instrument at the factory.

Dual-Element Thin-Film Heat Gages

The thin-film heat gages consisted of two platinum resistance thermometer strips mounted at right angles on the top and bottom of a

1/16-in.-thick, 3/8-in.-diam quartz substrate. The substrate served as a semi-infinite solid which permitted the rear face gage to sense only radiant heating for burn times up to 100 msec, whereas the front face gage sensed both convective and radiant heating. Each heat gage was placed in an electrical circuit as an active arm of a Wheatstone bridge, which was balanced just prior to firing. As the heat gage temperatures increased, their resistances changed and unbalanced the bridge to produce a millivolt signal proportional to the temperature rise sensed by the gages. The heat gage signals were recorded on magnetic tape with a multi-channel analog-to-digital converter system. Playback of this tape on a computer gave a digital printout of temperature rise during firing. Heat transfer rates were then calculated using the following modified semi-infinite solid heat conduction equation (Ref. 32):

$$\dot{Q}(t)_{gage} = \left[1 + 0.00033\Delta T(t)\right] \sqrt{\frac{\pi \rho C_p K}{4t}} \left\{\Delta T(t) + \frac{1}{\pi} \int_0^t \left[\frac{\lambda \Delta T(t) - t\Delta T(\lambda)}{(t-\lambda)^{3/2}}\right] d\lambda \right\}$$

where

$$\Delta T(t) = \left[1 - \sqrt{(1 - 5.18 \times 10^{-4}\, \Delta T_{meas})}\right] / 2.59 \times 10^{-4}$$

The equation for $\Delta T(t)$ is an empirical correction to account for the nonlinearity of the sensor resistance with temperature.

The term $0.00033\Delta T(t)$ is an empirical correction to match this solution to an exact solution by CAL of the nonlinear heat conduction equation with substrate properties given as individual functions of temperature, using numerical techniques and a digital computer. λ is a dummy integration variable with units of time, and the integral is a correction for nonconstant heating rate. The physical properties are those of the substrate evaluated at the engine-off base heat shield temperature.

Derivation and limitations of this equation are given in Ref. 15.

Actual heating rates were obtained from the measured gage heating rates by applying the following constants determined from known-heat-source radiation calibrations and obtained from Ref. 32:

$$\dot{Q}_{rear\ face\ gage} = 0.32\, \dot{Q}_{radiation}$$

$$\dot{Q}_{convection} = \dot{Q}_{front\ face\ gage} - 0.43\, \dot{Q}_{radiation}$$

$$\dot{Q}_{total} = \dot{Q}_{radiation} + \dot{Q}_{convection}$$

Security Classification

DOCUMENT CONTROL DATA - R&D

(Security classification of title, body of abstract and indexing annotation must be entered when the overall report is classified)

1. ORIGINATING ACTIVITY (Corporate author) Arnold Engineering Development Center ARO, Inc., Operating Contractor Arnold Air Force Station, Tennessee	2a. REPORT SECURITY CLASSIFICATION UNCLASSIFIED 2b. GROUP N/A

3. REPORT TITLE

EVALUATION OF AN UNCOOLED ROCKET ENGINE OPERATING TECHNIQUE APPLICABLE TO THE EXPERIMENTAL STUDY OF MISSILE BASE HEATING

4. DESCRIPTIVE NOTES (Type of report and inclusive dates)

N/A

5. AUTHOR(S) (Last name, first name, initial)

Parker, J. R. and Christenson, R. J., ARO, Inc.

6. REPORT DATE	7a. TOTAL NO. OF PAGES	7b. NO. OF REFS
June 1966	96	34

8a. CONTRACT OR GRANT NO. AF40(600)-1200 b. PROJECT NO. c. System 921A d.	9a. ORIGINATOR'S REPORT NUMBER(S) AEDC-TR-66-104 9b. OTHER REPORT NO(S) (Any other numbers that may be assigned this report) N/A

10. AVAILABILITY/LIMITATION NOTICES

~~Qualified requesters may obtain copies of this report from DDC and transmittal to foreign governments and foreign nationals must have prior approval of AEDC.~~

11. SUPPLEMENTARY NOTES N/A	12. SPONSORING MILITARY ACTIVITY Arnold Engineering Development Center (AEDC) Air Force Systems Command (AFSC) Arnold Air Force Station, Tenn.

13. ABSTRACT

A description is given of an uncooled rocket engine operating technique applicable to the experimental study of missile base heating. The primary advantage offered by this technique over those in current use is that it retains the single combustion chamber, uncooled engine concept of the short-duration test technique while providing burn durations of sufficient time to permit use of conventional, steady-state instrumentation. This technique also eliminates the usually complex propellant and control systems associated with conventional liquid-cooled long-duration engines. Uncooled engine operating characteristics are reported for burn durations of 1.2 sec; extrapolation of these data indicate engine burn duration can be extended to 2.5 sec. Base heating data obtained with a 5.47-percent-scale Saturn I-Block II model utilizing the uncooled engine test technique are compared with data from a Saturn I-Block II model which utilized short- and long-duration test techniques.

Per AF letter dtd 23 January 75, signed William A. Cole.

DD FORM 1 JAN 64 1473

Security Classification

Security Classification

14 KEY WORDS	LINK A		LINK B		LINK C	
	ROLE	WT	ROLE	WT	ROLE	WT
1 missiles -- ↖ Saturn I 2 rocket engines -- ↖ 16. 3. base heating liquid propellants 3. missiles -- Base heating 4 Base heating						

INSTRUCTIONS

1. ORIGINATING ACTIVITY: Enter the name and address of the contractor, subcontractor, grantee, Department of Defense activity or other organization *(corporate author)* issuing the report.

2a. REPORT SECURITY CLASSIFICATION: Enter the overall security classification of the report. Indicate whether "Restricted Data" is included. Marking is to be in accordance with appropriate security regulations.

2b. GROUP: Automatic downgrading is specified in DoD Directive 5200.10 and Armed Forces Industrial Manual. Enter the group number. Also, when applicable, show that optional markings have been used for Group 3 and Group 4 as authorized.

3. REPORT TITLE: Enter the complete report title in all capital letters. Titles in all cases should be unclassified. If a meaningful title cannot be selected without classification, show title classification in all capitals in parenthesis immediately following the title.

4. DESCRIPTIVE NOTES: If appropriate, enter the type of report, e.g., interim, progress, summary, annual, or final. Give the inclusive dates when a specific reporting period is covered.

5. AUTHOR(S): Enter the name(s) of author(s) as shown on or in the report. Enter last name, first name, middle initial. If military, show rank and branch of service. The name of the principal author is an absolute minimum requirement.

6. REPORT DATE: Enter the date of the report as day, month, year; or month, year. If more than one date appears on the report, use date of publication.

7a. TOTAL NUMBER OF PAGES: The total page count should follow normal pagination procedures, i.e., enter the number of pages containing information.

7b. NUMBER OF REFERENCES: Enter the total number of references cited in the report.

8a. CONTRACT OR GRANT NUMBER: If appropriate, enter the applicable number of the contract or grant under which the report was written.

8b, 8c, & 8d. PROJECT NUMBER: Enter the appropriate military department identification, such as project number, subproject number, system numbers, task number, etc.

9a. ORIGINATOR'S REPORT NUMBER(S): Enter the official report number by which the document will be identified and controlled by the originating activity. This number must be unique to this report.

9b. OTHER REPORT NUMBER(S): If the report has been assigned any other report numbers *(either by the originator or by the sponsor)*, also enter this number(s).

10. AVAILABILITY/LIMITATION NOTICES: Enter any limitations on further dissemination of the report, other than those imposed by security classification, using standard statements such as:

(1) "Qualified requesters may obtain copies of this report from DDC."

(2) "Foreign announcement and dissemination of this report by DDC is not authorized."

(3) "U. S. Government agencies may obtain copies of this report directly from DDC. Other qualified DDC users shall request through _____."

(4) "U. S. military agencies may obtain copies of this report directly from DDC. Other qualified users shall request through _____."

(5) "All distribution of this report is controlled. Qualified DDC users shall request through _____."

If the report has been furnished to the Office of Technical Services, Department of Commerce, for sale to the public, indicate this fact and enter the price, if known.

11. SUPPLEMENTARY NOTES: Use for additional explanatory notes.

12. SPONSORING MILITARY ACTIVITY: Enter the name of the departmental project office or laboratory sponsoring *(paying for)* the research and development. Include address.

13. ABSTRACT: Enter an abstract giving a brief and factual summary of the document indicative of the report, even though it may also appear elsewhere in the body of the technical report. If additional space is required, a continuation sheet shall be attached.

It is highly desirable that the abstract of classified reports be unclassified. Each paragraph of the abstract shall end with an indication of the military security classification of the information in the paragraph, represented as *(TS)*, *(S)*, *(C)*, or *(U)*.

There is no limitation on the length of the abstract. However, the suggested length is from 150 to 225 words.

14. KEY WORDS: Key words are technically meaningful terms or short phrases that characterize a report and may be used as index entries for cataloging the report. Key words must be selected so that no security classification is required. Identifiers, such as equipment model designation, trade name, military project code name, geographic location, may be used as key words but will be followed by an indication of technical context. The assignment of links, rules, and weights is optional.